# UNIVERSITAT POLITÈCNICA DE VALÈNCIA

**DEPARTAMENT DE QUÍMICA**



# Functional silica materials for controlled release, sensing and elimination of target molecules.

## PhD. THESIS

Submitted by


**Inmaculada C. Candel Busquets**

PhD. Supervisors:

**Prof. Ramón Martínez Máñez**
**Prof. Félix Sancenón Galarza**


**Valencia Junio 2014**

Instituto Interuniversitario de Reconocimiento Molecular y Desarrollo Tecnológico

RAMÓN MARTÍNEZ MÁÑEZ, PhD in Chemistry and Professor at the Universitat Politècnica de València, and FÉLIX SANCENÓN GALARZA, PhD in Chemistry and Lecturer at the *Universitat Politècnica de València*.

CERTIFY:

That the work *"Functional silica materials for controlled release, sensing and elimination of target molecules."* has been developed by Inmaculada C. Candel Busquets under their supervision in the Centro de Reconocimiento Molecular y Desarrollo Tecnológico de la *Universitat Politècnica de València*, as a thesis Project in order to obtain the degree of PhD in Chemistry at the *Universitat Politècnica de València.*

Valencia, April 29th 2014.

Prof. Ramón Martínez Máñez Dr. Félix Sancenón Galarza

*A la memoria de mi abuelo.*

*“Porque no hay nada imposible para Dios” (Lc 1, 37)*

# *Acknowledgements.*

## *Agradecimientos*

Llegados a este punto es momento de echar la vista atrás. Desde que entré en el laboratorio, allá por 2008, hasta hoy han pasado muchas cosas y hay muchas cosas que agradecer.

Quisiera agradecer, en primer lugar, a mis directores de tesis la oportunidad que me han dado de vivir la experiencia de la investigación.
A todos los profesores del departamento de Química que me han dado consejo en algún momento o con los que he compartido charlas agradables. A los profesores del departamento de Química Orgánica de Burjassot por acogerme en su laboratorio, aconsejarme y guiarme en la última etapa experimental.

A mis compañeros de laboratorio, tanto del politécnico como de Burjassot, por su compañía, ayuda y apoyo. Me quedaré con los recuerdos buenos y borraré de mi memoria los malos. A todas/os las que habéis acabado convirtiéndoos en mis amigas/os, con las que compartir este largo camino que es la tesis, que habéis aguantado (y disfrutado, confesadlo) 5 años de candeladas, y los que os quedan; que estáis y estaréis a mi lado, con esta locura mía, si Dios quiere, muchos años.

A las personas ajenas al mundo químico pero muy presentes en mi vida.
A mi familia, que ha ido creciendo a lo largo de estos 5 años, por estar ahí conmigo, apoyarme y aguantarme en mis días malos y compartir la alegría de los buenos. A mis amigas, que aunque no entendíais muy bien de qué hablaba estábais ahí para escucharme, dejarme desahogarme y apoyarme. A mis hermanos/as de comunidad, por no dejarme olvidar lo verdaderamente importante.
Y por supuesto, a Marcos. ¿Qué puedo decir? Nadie como tú…Has estado conmigo toda la tesis, la has vivido conmigo. Imposible enumerar todo lo que te he de agradecer. Tendré que darte un trocito del título.

# Resumen

La presente tesis doctoral titulada “Materiales de sílice funcionales para la liberación controlada, detección y eliminación de moléculas de interés” se centra en el diseño y desarrollo de materiales híbridos orgánico-inorgánicos mediante la aplicación de los conceptos de Química Supramolecular. Durante el desarrollo de la presente tesis doctoral se han preparado y caracterizado diferentes materiales de base silícea para distintas aplicaciones.

La primera parte de la tesis se centra en el desarrollo de materiales de base silícea capaces de variar su comportamiento fluorescente en función de la presencia o ausencia de un cierto analito en el medio. Estos materiales emplean como soporte nanopartículas de sílice que se funcionalizan superficialmente con dos unidades diferentes, una coordinante y una indicadora (un fluoróforo). La interacción del analito de interés (en nuestro caso aniones) con la unidad coordinante modificará las propiedades emisivas del fluoróforo. Así, se han preparado dos materiales en los cuales el grupo fluorescente es rodamina mientras que el grupo coordinante es un imidazolato o una sal de guanidinio respectivamente. Una vez caracterizados ambos materiales se estudió su comportamiento frente a diferentes especies aniónicas a diferentes concentraciones resultando selectivos a la presencia de benzoato (el material funcionalizado con imidazolatos), dihidrógeno fosfato e hidrógeno sulfato (el material funcionalizado con sales de guanidinio).

El tercer capítulo de la tesis se centra en la aplicación de materiales híbridos orgánico-inorgánicos para la detección y eliminación de especies altamente tóxicas como son los agentes neurotóxicos. Estos son compuestos organofosforados capaces de causar graves lesiones en el sistema nervioso central. En una primera aproximación se emplea el concepto de puerta molecular para la detección de agentes neurotóxicos. Para ello, se utiliza como soporte inorgánico un material mesoporoso de sílice (MCM-41) cuyos poros se cargan con un colorante que actúa de indicador mientras que la superficie externa del mismo

se funcionaliza con una molécula capaz de reaccionar con dichos agentes neurotóxicos. Dicha molécula es capaz de interaccionar entre sí (mediante enlaces de hidrógeno) formando una red que mantiene bloqueada la salida de los poros. En presencia de DCP (dietilclorofosfato, un simulante de agente neurotóxico), y después de que este reaccione con dicha molécula, se produce una reorganización espacial que permite la liberación del colorante. De este modo, la presencia de los agentes neurotóxicos está señalizada mediante un cambio de color. En una segunda aproximación se aborda el uso de soportes inorgánicos de tipo MCM-41 como materiales para la eliminación de agentes neurotóxicos. Para ello se modificaron químicamente las superficies de estos materiales silíceos mediante tratamiento con distintas bases. Como consecuencia de este tratamiento básico los silanoles de la superficie se desprotonan dando lugar a los correspondientes silanolatos (nucleófilos fuertes). Estos silanolatos son capaces de reaccionar con los agentes neurotóxicos descomponiéndolos y favoreciendo su eliminación de un medio contaminado.

Por último, se estudia la aplicación de materiales híbridos orgánico-inorgánicos funcionalizados con puertas moleculares en aplicaciones de liberación controlada, concretamente, en liberación controlada intracelular de fármacos de interés. El material híbrido consta de un soporte de sílice mesoporosa cuyos poros se cargan con un compuesto citotóxico (camptotecina) y su superficie externa se funcionaliza con una gluconamida. La presencia de una monocapa densa de gluconamidas por el exterior del material inhibe la liberación del compuesto citotóxico. Al añadir enzimas con capacidad para hidrolizar enlaces amida (amidasa y pronasa) se produce la liberación de la camptotecina. El correcto funcionamiento del material se comprobó *in vitro* e *in vivo* (en células HeLa).

# Resum

La present tesi doctoral titulada “Materials de sílice funcionals per a l’alliberament controlat, detecció i eliminació de molècules d’interés” es centra en el disseny i desenvolupament de materials híbrids orgànico-inorgànics per aplicació dels conceptes de Química Supramolecular. Durant el desenvolupament de la present tesi doctoral es prepararen i caracteritzaren diferents materials de base de sílice per a diferents aplicacions.

La primera part de la tesi es centra en el desenvolupament de materials basats en sílice capaços de variar el seu comportament fluorescent en funció de la presència o absència d’un analit al medi. Aquestos materials utilitzen com a suport nanopartícules de sílice que es funcionalitzen superficialment amb dues unitats diferents, una de coordinació i una d’indicació (un fluoròfor). La interacció de l’analit d’interés (en aquest cas, anions) amb la unitat de coordinació modificarà les propietats d’emissió del fluoròfor. Així, es prepararen dos materials als quals el grup fluorescent és rodamina mentre que el grup coordinant és un imidazolat o una sal de guanidini respectivament. Després de caracteritzar ambdós materials, es va estudiar el seu comportament davant diferents espècies aniòniques a diferents concentracions. Resultaren selectius a la presència de benzoat (el material funcionalitzat amb imidazolats), dihidròg en fosfat i hidròg en sulfat (el material funcionalitzat amb sals de guanidini).

El tercer capítol de la tesi es centra en l’aplicació de materials híbrids orgànico-inorgànics per a la detecció i eliminació d’espècies altament tòxiques com els agents neurotòxics. Aquestos són compostos organofosforats capaços de causar greus lesions al sistema nerviós central. En una primera aproximació, s’utilitza el concepte de porta molecular per a la detecció d’agents neurotòxics. Així, s’utilitza com a suport inorgànic un material mesoporós de sílice (MCM-41) al qual els porus es carreguen amb un colorant que actua com a indicador mentre que la superfície externa d’aquest sòlid es funcionalitza amb una molècula capaç de reaccionar amb els agents neurotòxics. Aquesta molècula és capaç de interaccionar entre sí (mitjançant enllaços d’hidrogen) per a formar una xarxa que

bloqueja l'eixida dels porus. En presència de DCP (dietilclorofosfat, un simulant d'agent neurotòxic), i després de la reacció entre el simulant i aquesta molècula, es produeix una reorganització espacial que permet l'alliberament del colorant. Així, la presència dels agents neurotòxics està senyalitzada per un canvi de color. En una segona aproximació, s'estudia l'utilització de suports inorgànics del tipus MCM-41 com a materials per a l'eliminació d'agents neurotòxics. Per això, es van modificar químicament les superfícies d'aquestos materials de silice per tractament amb diferents bases. Com a conseqüència d'aquest tractament bàsic, els silanols de la superfície es desprotonen originant els correspondents silanolats (nucleòfils forts). Aquestos silanolats són capaços de reaccionar amb els agents neurotòxics per a descompondre-los i afavorir la seua eliminació d'un medi contaminat.

Per últim, s'estudia l'aplicació dels materials híbrids orgànico-inorgànics funcionalizats amb portes moleculars en aplicacions d'alliberament controlat, concretament, en alliberament controlat intracel·luar de fàrmacs d'interés. El material híbrid està compost per un suport de sílice mesoporosa al qual els porus es carreguen amb un compost citotòxic (camptotecina) i la seua superfície externa es funcionalitza amb una gluconamida. La presència d'una monocapa densa de gluconamides a l'exterior del material inhibeix l'alliberament del compost citotòxic. Al afegir enzims amb capacitat d'hidrolitzar els enllaços amida (amidasa i pronasa) es produeix l'alliberament de la camptotecina. El comportament adequat del material es va comprovar *in vitro* i *in vivo* (en cèl·lules HeLa).

## Abstract

The present PhD thesis entitled “Functional silica materials for controlled release, sensing and elimination of target molecules” is centred in the design and development of organic-inorganic hybrid materials through the application of supramolecular chemistry concepts. Several materials based on silica have been prepared and characterized for different applications and were presented on this thesis.

The first part of the thesis is centred on the development of materials based on silica being able to modify their fluorescent behaviour depending on the presence or absence of a target analyte on the media. These materials are based on silica nanoparticles acting as inorganic scaffolding, the surface of which is functionalized with two different units: a coordination and a signalling unit (a fluorophore molecule). The interaction between the target analyte (in this case, anions) and the coordination unit will modulate the fluorescent emission properties of the fluorophore. Thus, different materials have been prepared wherein the fluorescent moiety is rhodamine whereas the coordination moiety is imidazolate or a guanidinium salt, respectively. Once both materials have been characterized, their behaviour upon different anionic species at different concentrations was studied, these materials being selective to benzoate (imidazolate functionalized material), dihydrogen phosphate and hydrogen sulphate (guanidinium functionalized material).

The third chapter of the thesis is focused on the application of organic-inorganic hybrid materials for the sensing and elimination of highly toxic species such as neurotoxic agents. These are organophosphorous compounds able to affect seriously the central nerve system. On a first approximation, the molecular gate concept is used for sensing neurotoxic agents. To do that, an inorganic mesoporous silica scaffold is used (MCM-41), whose pores are loaded with a dye acting as signalling molecule whereas the external surface of said scaffolding is functionalized with a molecule being able to react with those neurotoxic agents. That molecule forms a hydrogen bonding network that blocks the pore outlets. In

the presence of DCP (diethylchlorophosphate, a neurotoxic agent mimics), and after it has reacted with that molecule, a spatial rearrangement takes place, thus allowing the release of the dye. This way, the presence of neurotoxic agents is signalized with a colour change. In a second approximation, the use of inorganic supports such as MCM-41 for the elimination of neurotoxic agents is studied. To do that, this siliceous material was treated with different bases. As a consequence of this basic treatment, the silanols on the silica surface are deprotonated originating the corresponding silanolates (strong nucleofiles). These silanolates are able to react with the neurotoxic agents yielding to their decomposition and thus, enhancing their elimination from a polluted medium.

Finally, the use of organic-inorganic hybrid materials being functionalized with molecular gates for controlled release applications was studied. The hybrid materials consists on a mesoporous scaffolding based on silica whose pores are loaded with a cytotoxic compound (camptothecin) and its external surface is functionalized with a gluconamide derivative. The presence of a dense monolayer of gluconamides in the outer surface of the material inhibits the release of the cytotoxic compound. Upon addition of enzymes being able to hydrolyse amide bonds (amidase and pronase) the release of camptothecin takes place. The behaviour of the material was proved *in vitro* and *in vivo* using HeLa cells.

PUBLICACIONES

1. Inmaculada Candel, Pilar Calero, Ramón Martínez-Máñez, Félix Sancenón, M. Dolores Marcos, Teresa Pardo, J. Soto. *Sensing properties of silica nanoparticles functionalized with anion binding sites and sulforhodamine B as fluorogenic signalling unit*. Inorganica Chimica Acta, 2012, 381, 188–194

2. Inmaculada Candel, Andrea Bernardos, Estela Climent, M. Dolores Marcos, Ramón Martínez-Máñez, Félix Sancenón, Juan Soto, Ana Costero, Salvador Gil, Margarita Parra. *Selective opening of nanoscopic capped mesoporous inorganic materials with nerve agent simulants; an application to design chromo-fluorogenic probes.* Chem. Commun., 2011, 47, 8313–831.

3. Inmaculada Candel, Elena Aznar, L.aura Mondragón, Cristina de la Torre, Ramón Martínez-Máñez, Félix Sancenón, M. Dolores Marcos, Pedro Amorós, Carmen Guillem, Enrique Pérez-Payá, Ana Costero, Salvador Gil, Margarita Parra. *Antitumoral drug amidase-responsive controlled release on intracellular media using gluconamide-capped mesoporous silica nanoparticles.* Nanoscale, 2012, 4, 7237–7245

4. Inmaculada Candel, María D. Marcos, Ramón Martínez-Máñez,Félix Sancenón, Ana M. Costero, Margartita Parra, Salvador Gil, Carmen Guillem,Francisco Pérez-Plá and Pedro Amorós. *Hydrolysis of DCNP (a Tabun mimic) catalysed by mesoporous silica nanoparticles*. Submitted

# Abbreviations

| | |
|---|---|
| **α-CD** | α-cyclodextrin |
| **Ann V** | Annexin V |
| **ATP** | Adenosine Triphosphate |
| **BET** | Brunauer, Emmett and Teller Model |
| **BJH** | Barret, Joyner and Halenda Model |
| **CBPQT$^{4+}$** | Cyclobis-(paraquat-p-phenylene) |
| **CPT** | Camptothecin |
| **CTABr** | Hexadecyltrimethylammonium bromide |
| **CWA** | Chemical Warfare Agents |
| **DABCO** | 1,4-Diazabicyclo[2.2.2]octane |
| **DCNP** | Diethyl cyanophosphonate |
| **DCP** | Diethyl chlorophosphate |
| **DCPP** | Diethyl(2-cyanoethyl)phosphonate |
| **DCTP** | Dimethyl chlorothiophosphate |
| **DFP** | Diisopropyl fluorophosphate |
| **DLS** | Dinamic light scattering |
| **DMSO** | Dimethyl sulfoxide |
| **DMTMPP** | Diethyl(methylthiomethyl)phosphate |
| **DNA** | Deoxyribonucleic acid |
| **DNPD** | 1,5-dioxynaphthalene derivative |
| **DOPPP** | Diethyl(2-oxopropyl)phosphonate |
| **DOX** | Doxorubicin |
| **DPEPP** | Diethyl 1-phenylethyl phosphonate |
| **EDX** | Energy Dispersive X-Ray Spectroscopy |
| **FCS** | Fetal Calf Serum |
| **FH** | Fluorescein Hydrazide |
| **G1.5 PAMAM** | Generation 1.5 polyamido(amine) |
| **GA** | Tabun |
| **GB** | Sarin |
| **GD** | Soman |
| **GF** | Cyclosarin |
| **HET** | 3-[Bis(2-hidroxyethyl)amino]propyltriethoxysilane |
| **MCM** | Mobile Crystalline Material |
| **MLCT** | Metal to Ligand Charge Transfer |

| | |
|---|---|
| **MOFs** | Metal-Organic Frameworks |
| **MSN** | Mesoporous Silica Nanoparticles |
| **NBD** | Nitrobenzoxadiazole |
| **NMR** | Nuclear Magnetic Resonance |
| **PESG** | Proteolytic Enzymes Obtained from Streptomyces griseus |
| **PET** | Photoinduced Electron Transfer |
| **PI** | Propidium Iodide |
| **PLE** | Porcine Liver Esterase |
| **POPs** | Porous Organic Polymers |
| **QDA** | Quencher Displacement Assay |
| **$Ru(bipy)_3^{2+}$** | tris(2,2'bipyridyl)Ruthenium(II) |
| **SAW** | Surface Acoustic Wave |
| **SDTA** | Single Differential Thermal Analysis |
| **SEM** | Scanning Electron Microscopy |
| **STZ** | Sulfotiazole |
| **$TEAH_3$/$TEAH_2$/TEA** | Triethanolamine |
| **TEM** | Transmission Electron Microscopy |
| **TEOS** | Tetraethylorthosilicate |
| **TGA** | Thermogravimetric Analysis |
| **TLCT** | True Liquid-Crystal Templating |
| **TNT** | Trinitrotoluene |
| **TSNPs** | Terpyridine-Sulforhodamine-Functionalised Nanoparticles |
| **UV** | Ultraviolet |
| **WGA** | Wheat Germ Agglutinin |
| **XRD** | X-ray diffraction |

# Content


**1. GENERAL INTRODUCTION..... 3**

1.1 Supramolecular Chemistry..... 3

1.1.1 Molecular recognition. ..... 4

1.2 Organic-inorganic hybrid materials. ..... 7

1.2.1 Silica nanoparticles. ..... 8

1.2.2 Mesoporous materials..... 12

1.2.2.1 Synthesis of mesoporous materials. ..... 13

1.2.2.2 Functionalization of the MCM-41 siliceous surface. ..... 15

1.2.3 Applications of Organic-Inorganic Mesoporous Hybrid Materials. ..... 17

1.2.3.1 Molecular Gates: Definition ..... 17

1.2.3.2 Light-Driven Molecular Gates ..... 20

1.2.3.3 pH-Driven Molecular Gates. ..... 22

1.2.3.4 Temperature-Driven Molecular Gates ..... 24

1.2.3.5 Redox-Driven Molecular Gates ..... 25

1.2.3.6 Molecular Interaction-Driven Molecular Gates ..... 26

**2. FUNCTIONALIZED SILICA NANOPARTICLES FOR ANIONS RECOGNITION. 29**

2.1 Introduction ..... 31

2.1.1 Fluorogenic probes for sensing of anions. ..... 31

2.1.2 Silica nanoparticles as sensing materials. ..... 33

2.2 Objectives ..... 35

2.3 Design of the system ..... 36

**Sensing properties of silica nanoparticles functionalized with anion binding sites and sulforhodamine B as fluorogenic signalling unit.....37**

**3. SENSING AND REMEDIATION OF NEUROTOXIC AGENTS ..... 59**

3.1 Introduction. ..... 61

3.1.1 Neurotoxic Agents. ..... 61

3.1.2 Chromogenic detection of nerve agents. ..... 63

3.1.3 Remediation and elimination of neurotoxic agents ..... 65

3.1.4 Gated materials as sensors ..... 66

3.2 Objectives ..... 68

3.3 Design of the systems ..... 69
3.3.1 Design of neurotoxic agents responsive gated material ..... 69
3.3.2 Design of the hydrolyzing material ..... 69

***Selective opening of nanoscopic capped mesoporous inorganic materials with nerve agent simulants; an application to design chromo-fluorogenic probes.....71***

***Hydrolysis of DCNP (a Tabun mimic) catalysed by mesoporous silica nanoparticles.....95***

**4. HYBRID MATERIALS FOR DRUG RELEASE .....121**
4.1 Introduction. ..... 123
4.1.1 Biomolecules as capping/uncapping agents. ..... 123
4.1.2 Drug release ..... 126
4.2 Objectives ..... 127
4.3 Design of the system ..... 127

***Antitumoral drug amidase-responsive controlled release on intracellular media using gluconamide-capped mesoporous silica nanoparticles.....129***

**5. CONCLUSIONS.....157**

# 1. GENERAL INTRODUCTION

## 1.1 **Supramolecular Chemistry.**

Whitin all branches of chemistry science, supramolecular chemistry has become one of the most interesting research areas in the last years. Supramolecular chemistry[1] studies the interactions exisiting between molecules beyond covalent bonding. It is defined as the science that examines the weak and reversible noncovalent interactions between molecules such as hydrogen bonding, metal coordination, hydrophobic forces, van der Waals forces, $\pi$-$\pi$ interactions and electrostatic effects and which deals with the design and the study of unique complex nanostructured supermolecules joined by intermolecular interactions.

The term *Supramolecular Chemistry* was defined during the decade of 1960 by Pedersen, Cram and Lehn, who received the Nobel Prize in 1987 for their contributions to the development of this new area inside chemistry. According to Dr. Lehn, "a *supermolecule* is an organized complex entity that is created from the association of two or more chemical species held together by intermolecular forces, supermolecules structures are the result of not only additive but also cooperative interactions, including, hydrogen bonding, hydrophobic interactions and coordination, and their properties are different (often better) than the sum of the properties of each individual component".[2]

Since it appeared, the objective of this area of chemistry has been the design of nanostructures which mimic the ability of biologic macromolecules to form supramolecules by intermolecular interactions. Molecular recognition processes (such as enzymatic reactions, protein-protein complexes assembling, immunological antigen-antibody association, intermolecular reading, or

[1] Taylor & Francis Group, Encyclopedia of Supramolecular Chemistry, Vols. 1, 2 (Ed.: Atwood, J.L.; Steed, J.W.), LLC, New York, 2004.

[2] J. -M. Lehn, Supramolecular Chemistry, Ed. VCH, 1995; J.-M. Lehn, Nobel lecture, **1987**

translation and transcription of the genetic code) are key elements to numerous biochemical processes.

### *1.1.1 Molecular recognition.*

Molecular recognition is the basis of supramolecular chemistry and it can be defined as the selective interaction between a host or receptor molecule and a guest or substrate through non-covalent interactions.

At the end of the 19th century, Emil Fisher defined the main principle in which molecular recognition is based: *The lock and key principle*. According to this principle, there is a selective interaction between the receptor/host and the guest/substrate in the same way that there is just one key that matches a specific lock (See Figure 1).[3]

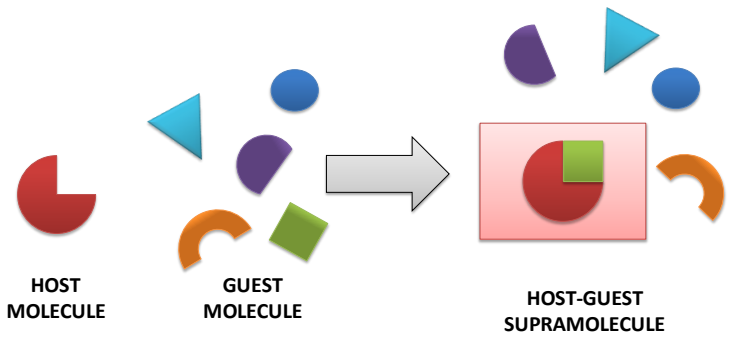


**Figure 1.** Scheme of the lock and key principle, the molecular recognition process to form supramolecules.

In the last decades, many advances have been achieved on this area, resulting in the synthesis and development of new molecular receptors. Among all receptors, the ones specifically designed for sensing purposes are generally called

[3] J.P. Behr, *The Lock-and-Key Principle, The State of the Art--100 Years On*, **2008**, Ed. John Wiley & Sons.

*chemosensors*. In the sensing process, a molecular interaction is transformed into a macroscopic signal. The interaction of these chemosensors with cations, anions or neutral molecules and their chemical modifications with selected moieties have been extensively studied.[4]

Chemosensors are normally composed of two subunits that have specific functions:

- The *binding site* subunit is able to recognize and interact selectively with the target molecule, usally via non-covalent interactions.
- The *signalling subunit* is able to translate chemical information (taking place at the molecular level) into a signal, such as modulations in colour or fluorescence.

Bearing in mind the different possibilities of arranging the binding site and the signalling subunits, three main approaches in the development of chemosensors have been described. Binding sites and signaling units can be covalently linked (binding site-signaling subunit and chemodosimeter approaches) or not (displacement approach).

- *Binding site-signaling subunit approach*: In this paradignm, both subunits are covalently linked, the colour (in case of chromogenic chemosensors) or fluorescence (in case of fluorogenic chemosensors) of the signaling subunit is modified when the target molecule coordinates with the binding site.[5] (See Figure 2)

[4] (a) R. Martínez-Máñez, F. Sancenón, *Chem. Rev*., **2003**, *103*, 4419. (b) P. D. Beer, P. A. Gale, *Angew. Chem. Int. Ed.* **2001**, *40*, 486. (c) C.R. Bondy, S. Loeb, *J. Coord. Chem. Rev*. **2003**, *240*, 77-99. (d) J. F. Callan, A. P. de Silva, D. C. Magri, *Tetrahedron,* **2005**, *61*, 8551. (e) G. J. Mohr, *Sens. Actuators B,* **2005**, *107*, 2. (f) E. Climent, M.D. Marcos, R. Martínez-Máñez, F. Sancenón, J. Soto, K. Rurack, P. Amorós *Angew. Chem. Int. Ed.;* **2009**, *48*, 8519.

[5] (a) R. A. Bissell, P. de Silva, H. Q. N. Gunaratne, P. L. M. Lynch, G. E. M. Maguire, K. R. A. S. Sandanayake, *Chem. Soc.Rev.* **1992**, 187. (b) T. Gunnlaugsson, M. Glynn, G. M. Tocci, P. E. Kruger, F. M. Pfeffer, *Coord. Chem. Rev*., **2006**, *250*, 3094. (c) V. Amendola, D. Esteban-Gómez, L. Fabbrizzi, M. Lichelli, *Acc. Chem. Res*., **2006**, *39*, 343. (d) T. Gunnlaugsson, H. D. P. Ali, M. Glynn, P. E. Kruger, G. M. Hussey, F. M. Pfeffer, C. M. G. Dos Santos, J. Tierney, J. *Fluoresc*., **2005**, *15,* 287.

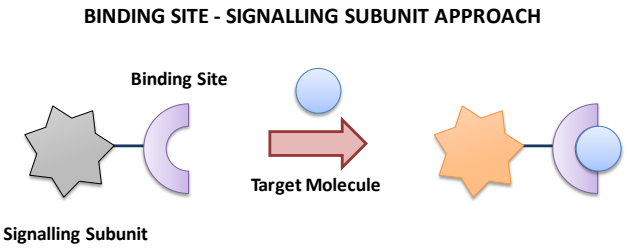


**Figure 2.** Illustrative scheme of the binding site-signalling subunit approach.

- *Displacement approach*: The binding site and the signalling subunit form a non-covalently attached supramolecular ensemble. In the presence of the target molecule, a displacement reaction is induced. If the colour or fluorescence of the signalling subunit depends on its coordination state, the displacement reaction will induce a signalling event. This phenomenon will not occur unless the stability constant of the "binding site – signalling unit" complex is lower than the stability constant of the "binding site – target molecule" complex.[6] (See Figure 3)

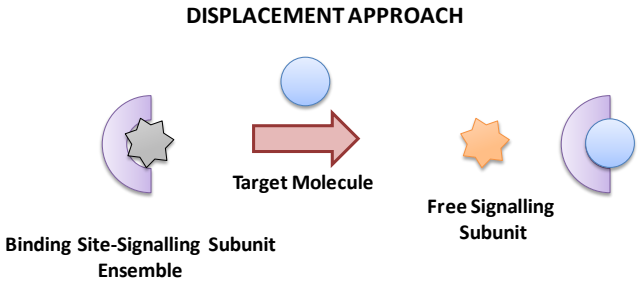


**Figure 3.** Illustrative scheme of the displacement approach.

[6] S. L. Wiskur, H. Aït-Haddou, J.J. Lavigne, E. V. Anslyn, *Acc. Chem. Res.* **2001**, *34*, 963.

- *Chemodosimeter approach:* In this approach, specific chemical reactions (usually irreversible) triggered by the presence of target anions that are coupled to a color or emission variation are involved, thus, inducing an optical change.[7] (see Figure 4)

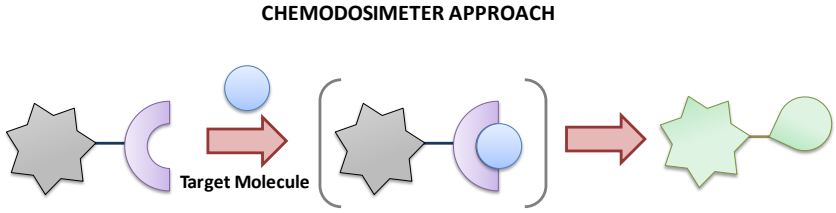


**Figure 4.** Illustrative scheme of the chemodosimeter approach.

## 1.2 **Organic-inorganic hybrid materials.**

A hybrid material is composed of an intimate mixture of inorganic, organic or both components, where, at least, the domain of one of them has a dimension ranging from a few angstroms to several nanometers. Consequently, the properties of hybrid materials are usually not only the sum of the individual contributions of both phases, but often the role of their inner interfaces becomes predominant.[8]

[7] (a) M.-Y. Chae, A. W. Czarnik, *J. Am. Chem. Soc.* **1992**, *114*, 9704. (b) V. Dujols, F. Ford, A. W. Czarnik, *J. Am. Chem. Soc.* **1997**, *119*, 7386. (c) Z. Xu, X. Chen, H. N. Kim, J. Yoon, *Chem. Soc. Rev.*, **2010**, *39*, 127.

[8] (a) J. Alemán, A. V. Chadwick, J. He, M. Hess, K. Horie, R. G. Jones, P. Kratochvíl, I. Meisel, I. Mita, G. Moad, S. Penczek, R. F. T. Stepto, *Pure and Appl. Chem.* **2007**, *79*, 1. (b) C. Sánchez, *J. Mater. Chem.*, **2005**, 15, 3557.

### *1.2.1 Silica nanoparticles.*

In 1956, Kolbe[9] first reported the possibility of producing monodisperse suspensions of silica spheres in the colloidal range of size. He observed that the reaction between tetraethylsilicate in alcoholic solutions, in the presence of certain bases, resulted in the formation of silica spheres. The detailed parameters on the obtention procedures of silica particles were later exthensively studied and described by Stöber.[10]

Silica spheres up to 2 μm diameter can be synthetized by hydrolysis and condensation of tetraesters of sililic acid in basic alcoholic solutions. Time reaction, base concentration and water content on the reaction mixture influence the condensation rate and, therefore, the size of the resulting particles. Nevertheless, the particles obtained by applying this method tend to coagulate and aggregate.[11] The earliest attempts to avoid this phenomenon consisted on the adsorption of several surfactants or electrolytes on the silica surface. The first examples of covalent coating of alcoxysilane derivatives onto the surface of silica nanoparticles were also reported with the aim of improving the inertness of this material.[12] This fact introduced the possibility of obtaining functional hybrid supports by covalently anchoring certain receptors to the silica surface.

Among reported applications of these materials (such as catalytic, environmental and biomedical applications) these hybrid organic–inorganic materials have been reported to display novel signalling properties that are hardly achievable by the individual components alone or when using analogous molecular-based systems.

---

[9] G. Kolbe, "*Das* komplexehemische Verhalten der Kieselsure," Dissertation, Jena (**1956**).
[10] W. Stober, A. Fink, *J. of Colloid Interface Sci.* **1968**, *26,* 62.
[11] (a) S. Barany, M. A. C. Stuart, G. J. Fleer, *Colloids and Surfaces A: Physieochemical and Engineering Aspects* **1996**, *106*, 213. (b) M. Kobayashi, M. Skarba, P. Galletto, D. Cakara , M. Borkovec, *J. Colloid Interface Sci.* **2005**, *292* 139.
[12] (a) A. P. Philipse, A. J. Vrij, *J. Colloid. Interface Sci*. **1983**, *128*, 121 (b) G. Petzold, A. Nebel, H.-M. Buchhammer, K. Lunkwitz*, Colloid Polym. Sci*. **1998**, *276*, 125. (c) C. Beck, W. Härtl, R. Hempelmann, *Angew. Chem. Int. Ed.* **1999***, 38,* 1297.

The ability of these materials to recognize target molecules is in most cases improved compared to the free receptor in solution. This phenomenon is observed because of the preorganization of the receptor molecules onto the surface of the silica nanoparticles, which results in the formation of a dense monolayer of binding sites where every moiety is placed in a specific location, asuring the maximum response.[13] Although these cooperative effects could be also observed when using other materials as scaffoldings,[14] silica nanoparticles are particularly suitable for the study of the influence of cooperative effects on optical chemosensors since they are transparent and photophysically inert. In fact, it is possible to find in the literature many examples where cooperative effects in silica nanoparticles have been used in different sensing protocols.[15]

For instance, *Cheng et al.*[16] prepared a chemodosimeter system to detect Cu(II) ions in a partially aqueous media by grafting a fluorescein hydrazide (FH) onto the surface of silica nanoparticles. Upon coordination of Cu(II) to the ligand molecule, a ring-opening reaction takes place resulting in a significant fluorescence enhancement. (see figure 5)

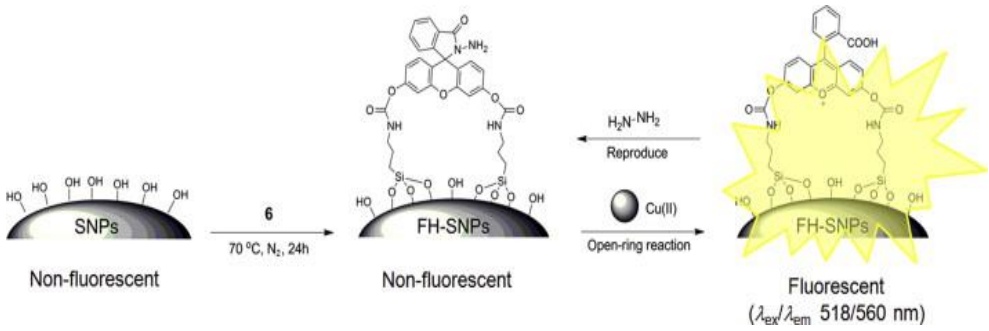


**Figure 5**. The grafting procedure of FH molecules onto the surface of SNPs. *Reprinted from Dyes and Pigments, 95 , X. Chen, A. Tong,, Modification of silica nanoparticles with fluorescein hydrozide for Cu(II) sensing, 775, Copyright (2012), with permission fromElsevier.*

[13] M. Arduini, E. Rampazzo, F. Mancin, P. Tecilla, U.Tonellato, *Inorg. Chim. Acta* **2007**, *360*, 721.
[14] (a) E. L. Doyle, C. A. Hunter, H.C. Phillips, S.J. Webb, N. H. Williams, *J. Am. Chem. Soc*. **2003**, *125*, 4593. (b) R. Simon, M. E. Collins, D. A. Spivak, *Anal. Chim. Acta* **2007**, *591*, 7.
[15] (a) T. Doussineau, S. Trupp, G. J. Mohr, *J. Colloid Interface Sci.* **2009**, *339*, 266. (b) M. Montalti, L. Prodi, N. Zaccheroni, J. Fallini*, J. Am. Chem. Soc.,* **2002**, *124*, 13540. (c) Z. Song, C. Xiao, Y.Dai, Q. Fei, Y. Huan, Guodong Feng, *Nanotechnology,* **2012**, *23*, 425501.
[16] X. Chen, A. Tong, *Dyes Pigments* **2012**, 95, 776.

Several researchers noticed that these additional cooperative effects also occurred when the surface of silica nanoparticles was functionalized with separated binding sites and signaling subunits. In 2003, *Brasola* and co-workers[17] reported the first example of bifunctionalized silica nanoparticles as a probe to $Cu^{2+}$ ions via fluorescence changes. They studied the sensing behaviour of silica nanoparticles whose surface had been functionalized with different ratios of trimetoxysilane derivatized dansylamide (acting as signalling subunit) and picolinamide (as binding site subunit). The communication between both subunits is achieved thanks to the spatial proximity assured by its grafting onto the silica surface. Thus, not only the binding of the $Cu^{2+}$ ions to the nanoparticles induces the fluorescence quenching of dansyl moieties, but also cooperative effects are observed. The authors pointed out that silica nanoparticles functionalized with a higher proportion of binding site subunit showed the best efficiency as sensors of the metal ion. This observation can be explained by the fact that $Cu^{2+}$ affinity towards the binding subunit improves by increasing its ratio on silica surface, due to the surface organization of picolinamide moieties that may induce the formation of multivalent binding sites.

Another example of this kind of materials was reported by *Montalti* and co-workers.[18] The authors functionalized the surface of silica nanoparticles with dansyl moieties, which play the role of luminescent unit, and polyamine chains in order to make them able to bind certain ions. In the presence of copper, cobalt and nickel ions, an important quenching of the fluorescence is observed suggesting that each ion is able to quench up to 13 dansyls moieties, thanks to the spatial organization of said fluorophores on the silica surface.

Nevertheless, not only metal ions but other species can also be detected by taking advantage of pre-organization effects on silica surfaces.[19] As an example, *Han* and

[17] E. Brasola, F. Mancin, E. Rampazzo, P. Tecilla, U. Tonellato, C*hem. Commun.*, **2003**, 3026.
[18] M. Montalti, L. Prodi, N. Zaccheroni, *J. Mater. Chem.,* **2005**, *15*, 2810.
[19] (a) M. Arduini, F. Mancin, P. Tecilla, U. Tonellato, *Langmuir*, **2007**, *23*, 8632 (b) D. Gao, Z. Wang, B. Liu, L. Ni, M. Wu, Z. Zhang, *Anal. Chem*., **2008,** *80*, 8545. (c) A. J. Moro, J. Schmidt, T. Doussineau, A. Lapesta-Fernandez, J. Wegener, G. J. Mohr, *Chem. Commun.*, **2011**, *47*, 6066

co-workers[20] developed an ON-OFF fluorescent system to detect both proton ions and TNT molecules by bifunctionalizating the surface of silica nanoparticles with fluorescent nintrobenzoxadiazole (NBD) acting as signaling unit and amino moieties that play the role of binding site. Amines, thanks to their nitrogen lone-pair electrons, are able to partially quench the fluorophore through a nitrogen-to-fluorophore photoinduced electron transfer (PET). The binding of the proton to the amino group stops the PET phenomenon and, therefore, an enhacement of the fluorescence is observed (fluorescence ON) (see figure 6). On the contrary, in the presence of TNT, fluorescence resonance energy transfer processes (FRET) are predominant over PET. The binding of TNT to the nitrogen atom quenches the initial fluorescence of the material (fluorescence OFF) because of the formation of strong charge-transfer interactions between NBD and the formed TNT-amino complexes (see figure 7).

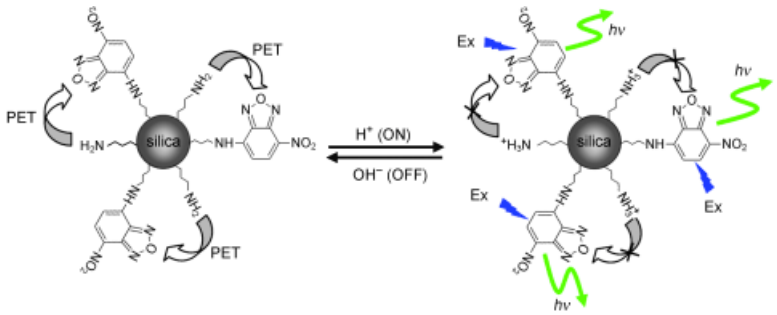


**Figure 6**. Schematic diagram of the reversible fluorescence switch by sequential titration of HCl and NaOH into the suspension of NBD–($NH_2$)–silica nanoparticles. *Adapted from Chem. Eur. J. 2010, 16, 3720. Copyright © 2010 Wiley.*

[20] J. Geng, P. Liu, B. Liu, G. Guan, Z. Zhang, M.-Y. Han, *Chem. Eur. J*. **2010**, *16*, 3720.

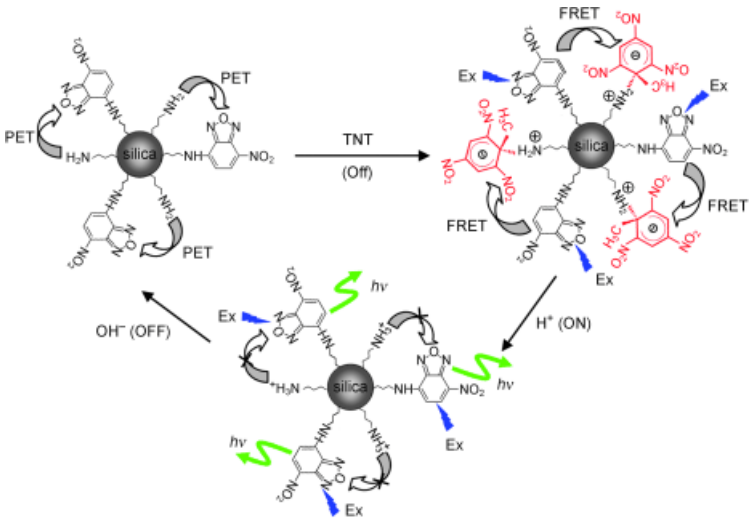


**Figure 7.** Schematic diagram of the fluorescence cycle through the addition of TNT, HCl, and NaOH based on the PET and FRET mechanisms at the surface of the silica nanoparticles. *Adapted from Chem. Eur. J. 2010, 16, 3720. Copyright © 2010 Wiley.*

### *1.2.2 Mesoporous materials.*

In 1992, researchers of the Mobil Company reported the synthesis of new mesoporous silica family, known as M41S phases.[21] This group of materials consists of three different phases, which can be easily distinguished thanks to their specific X-Ray pattern: MCM-41 (Mobile Crystalline Material having an hexagonal mesoporosity), MCM-48 (cubic porosity) and MCM-50 (lamellar phase).

Mesoporous materials are one of the most used scaffoldings to prepare hybrid organic-inorganic materials. Due to their particular properties, such as ordered porosity (the pore diameter is *ca*. 2-10 nm), high pore volume (*ca*. 1 $cm^3/g$) and high specific surface area (*ca*. 1000 $m^2/g$), mesoporous materials are usally used in processes involving the adsorption of high amounts of molecules.

[21] C. T. Kresge, M. E. Leonowicz, W. J. Roth, J. C. Vartuli, J. S. Beck, *Nature*, **1992**, *359*, 710.

### 1.2.2.1 *Synthesis of mesoporous materials.*

The synthesis of ordered mesoporous materials involves the use of structure-directing surfactants able to form micelles in aquous media. The condensation of the silica precursors around these micelles, in basic conditions, leads to the mesoporous composite. The mesoporous materials are obtained by subsequent removal of the surfactant by extraction or calcination.

Particularly, the surfactant used on the synthesis of MCM-41 materials is hexadecyltrimethylammonium bromide (CTAB).

Two different mechanisms take place in this process: On the one hand, in true liquid-crystal templating (TLCT), the concentration of the CTAB is so high that, under the prevailing conditions (temperature, pH), a lyotropic liquid-crystalline phase is formed without requiring the presence of the precursor inorganic framework materials (normally, tetraethylorthosilicate, TEOS). On the other hand, it is also possible that this phase forms even at lower concentrations of surfactant molecules, for example, when there is cooperative self-assembly of the SDA and the already added inorganic species, in which case a liquid-crystal phase with hexagonal, cubic, or laminar arrangement can develop. In a second step, TEOS condensate around the template micelles resulting in a siliceous mesoporous material having surfactant molecules inside the pores. Finally, the hexagonal mesoporous scaffolding is obtained after the elimination of the surfactant, either by high temperature calcinations procedures or by solvent extraction methods.[22] (See figure 8)

[22] (a) J. S. Beck, J. C. Vartuli, W. J. Roth, M. E. Leonowicz, C. T. Kresge, K. D. Schmitt, C. T. W. Chu, D. H. Olson, E. W. Sheppard, *J. Am. Chem. Soc.*, **1992**, *114*, 10834. (b) G. S. Attard, J. C. Glyde, C. G. Göltner, *Nature,* **1995**, *378*, 366. (c) F. Hoffmann, M. Cornelius, J. Morell, M. Fröba *Angew. Chem. Int. Ed.* **2006**, *45*, 3216 .

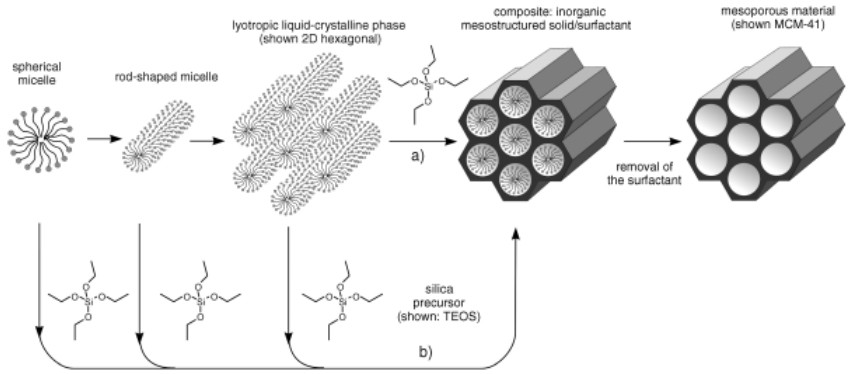


**Figure 8**. Formation of mesoporous materials by structure-directing agents: a) true liquid-crystal template mechanism, b) cooperative liquid-crystal template mechanism. *Adapted from Angew. Chem. Int. Ed. 2006, 45, 3216. Copyright © 2006 Wiley.*

The materials obtained using this procedure show several advantages such as versatility (it is possible to modify their final properties by changing small features of the synthetic process) and homogeneus porosity (not only in size but also in form).

Besides, they show some other advantages that make them suitable to act as scaffolding for the preparation of hybrid organic-inorganic materials: The regular, homogeneus, fair-sized pore system can be loaded with different size molecules and the inner and outer surface of the pores can be easily functionalized using appropriate organic molecules.

Silicon chemistry has been extensively studied and, nowadays, it is almost possible to control the amount and density of the organic moieties incorporated to the solid as well as their arrangement on the siliceous surface since these materials show a high silanol groups density (Si-OH) being able to react covalently with molecules having trialkoxysilane moieties. Being able to functionalize the siliceous surface of MCM-41 materials with organic molecules, it is possible to control its surface properties.

### 1.2.2.2 *Functionalization of the MCM-41 siliceous surface.*

The functionalization process can be achieved by following two different procedures:[23] Grafting (post-functionalization) and co-condensation (direct synthesis) procedures. In the first case, the synthesis of the inorganic scaffolding and the modification of its surface are two different and independent processes. Once the mesoporous material is obtained (having previously eliminated the surfactant template by a calcination process); a covalent bond is formed between an organic alkoxysilane derivative and the siliceous surface of the former inorganic scaffolding. The condensation reaction between silanol moieties of the silica matrix and the alkoxysilane moiety of the organic molecule yields a covalent O-Si bond that makes the organic molecule remain attached to the silica surface (see figure 9).

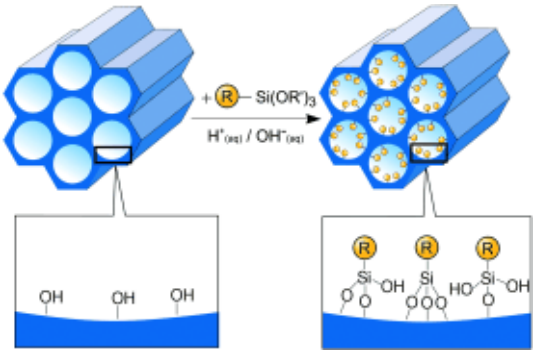


**Figure 9.** Grafting (postsynthetic functionalization) for organic modification of mesoporous pure silica phases with terminal organosilanes of the type $(R'O)_3SiR$. R=organic functional group. *Adapted from Angew. Chem. Int. Ed. 2006, 45, 3216. Copyright © 2006 Wiley.*

When using this method, the siliceous surface is not uniformly functionalized. Distribution and concentration of organic moieties depend on the reactivity and size of the alkoxysilane moiety, as steric hindrance factors would avoid the organic molecule to approach the inorganic surface. Although condensation

[23] (a) A. Stein, , B. J. Melde, R.C. Schroden, *Adv. Mater.* **2000**, *19*, 1403. (b) A. Vinu, , K. Z. Hossain, K. Ariga, *Nanosci. Nanotech.,* **2005**, *5*, 347.

process takes place, preferently, on the outer surface and on the pores openings, the inner functionalization can also be achieved by using higher reaction times. As the mesoporous structure of MCM-41 is preserved troughout the process, this procedure can be applied repetidly into the same surface if a higher functionalization degree is needed.

In contrast to the first process, in the co-condensation procedure, the polymerization of the silicon precursor (TEOS) and the incorporation of the organic moiety, an alkoxysilane derivative, into the inorganic scaffolding take place on a single step. In this way, it is posible to achieve an homogeneous distribution of the organic moieties in the mesoporous structure, not only in the external but also in the inner surface of the pores (see figure 10).

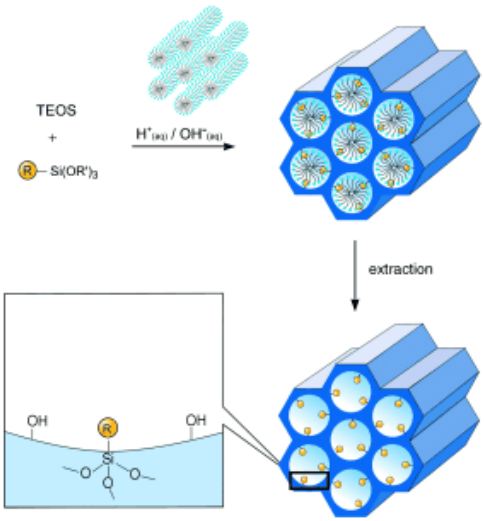


**Figure 10**. Co-condensation method (direct synthesis) for the organic modification of mesoporous pure silica phases. R=organic functional group. *Adapted from Angew. Chem. Int. Ed. 2006, 45, 3216. Copyright © 2006 Wiley.*

It is important to point out that, in this case, it is not possible to remove the surfactant template by calcination since the organic molecules attached to the

structure would also be eliminated as a consecuence of the high temperature treatment.

### *1.2.3 Applications of Organic-Inorganic Mesoporous Hybrid Materials.*

Mesoporous silica materials have been used as effective scaffoldings in a number of applications due to their properties, such as chemical inertness, three dimensional structure, high external surface, high load capacity, biocompatibility etc.[24] In particular, mesoporous solids have been employed in catalysis processes, in controlled release, environmental remediation materials, sensing applications etc.[25] Among these uses we are specially interested in the design of gated mesoporous materials for delivery applications (vide infra).

#### 1.2.3.1 *Molecular Gates: Definition*

Molecular or supramolecular gates can be defined as nanoscopic supramolecular-based devices, attached to certain solid supports, in which mass transport can be triggered by a target external stimulus that can control the state of the gate (closed or open) at will.[26] That is, a *molecular-gate* is the ensemble with which the external surface of mesoporous scaffoldings can be functionalized, thereby forming an organic-inorganic hybrid material. This molecule must be able to change some of their properties in response to target external stimuli thus

[24] a) M. Vallet-Regi, A. Rámila, R. P. del Real, J. Pérez-Pariente, *J. Chem. Mater.* **2001**, *13*, 308. b) B. Muñoz, A. Rámila, J. Pérez-Pariente, I. Díaz, M. Vallet-Regi, *Chem. Mater.* **2003**, *15*, 500.

[25] (a) K. Sarkar, Y. Salinas, I. Campos, R. Martínez-Máñez, M. D. Marcos, F. Sancenón, P. Amorós, *ChemPlusChem*, **2013**, *78*, 684. (b) A.M. Ewlad-Ahmed, M. A. Morris , S. V. Patwardhan, L. T. Gibson, *Environ. Sci. Technol.*, **2012**, *46* , 13354.

[26] A. B. Descalzo, R. Martínez-Máñez, F. Sancenón, K. Hoffmann, K. Rurack, *Angew. Chem. Int. Ed.,* **2006**, *45*, 5924.

avoiding (closed gate) or allowing (open gate) the release of the entrapped cargo into the solution (see figure 11).

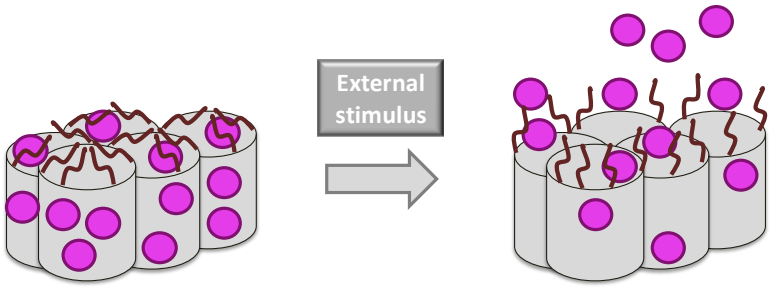


**Figure 11**. Schematic representation of the behaviour of gated mesoporous materials.

Since the first example of molecular gate reported by Fujiwara and coworkers in 2003,[27] many different molecular gated organic–inorganic hybrid materials using a wide range of different chemistries have been reported.[28] A large number of both physical and chemical stimuli have been reported to be able to trigger the opening/closing mechanism: light,[29] pH,[30] temperature,[31] redox potential[32] or the presence of certain chemical species.[33]

[27] (a) N. K. Mal, M. Fujiwara, Y. Tanaka, Y. *Nature,* **2003**, *421*, 350. (b) N. K. Mal, M. Fujiwara, Y. Tanaka, T. Taguchi, M. Matsukata, *Chem. Mater.* **2003**, *15*, 3385-3394.

[28] (a) E. Aznar, R. Martínez-Máñez, F. Sancenón, *Expert Opin. Drug Delivery*, **2009**, 6, 643; (b) K. Cotí, M. E. Belowich, M. Liong, M. W. Ambrogio, Y. A. Lau, H. A. Khatib, J. I. Zink, N. M. Khashab and J. F. Stoddart, *Nanoscale*, **2009**, 1, 16.

[29] (a) E. Aznar, R. Casasús, B. García-Acosta, M. D. Marcos, R. Martínez-Máñez, F. Sancenón, J. Soto and P. Amorós, *Adv. Mater.,* **2007**, *19*, 2228 (b) N. G. Liu, Z. Chen, D. R. Dunphy,Y.-B. Jiang, R. A. Assink and C. J. Brinker, *Angew. Chem., Int. Ed*., **2003**, *42*, 1731; (c) J. Lu, E. Choi, F. Tamanoi and J. I. Zink, *Small*, **2008**, *4*, 421 (d) E. Aznar, M. D. Marcos, R. Martínez-Máñez, F. Sancenón, J. Soto, P. Amorós and C. Guillem*, J. Am. Chem. Soc.*, **2009**, *131*, 6833 (e) J. Lai, X. Mu, Y. Xu, X. Wu, C. Wu, C. Li, J. Chen, Y. Zhao, *Chem. Commun.,* **2010**, *46*, 7370 (f) X. Yang, X. Liu, Z. Liu, F. Pu, J. Ren and X. Qu, *Adv. Mater.,* **2012**, *24*, 2890.

[30] (a) R. Casasus, M. D. Marcos, R.Martínez-Máñez, J. V. Ros-Lis, J. Soto, L. A. Villaescusa, P. Amorós, D. Beltrán, C. Guillem, J. Latorre, *J. Am. Chem. Soc.,* **2004**, *126*, 8612. (b) Q.Yang, S. Wang, P. Fan, L. Wang, Y. Di, K. Lin, F. –S. Xiao, *Chem. Mater.,* **2005**, *17*, 5999. (c) A. Bernardos, E. Aznar, C. Coll, R.

We will show below some selected exemples according to the external stimulus that induces the release of the cargo.

---

Martínez-Máñez, J. M. Barat, M. D. Marcos, F. Sancenón, J. Soto, *J. Control. Rel.*, **2008**, *131*, 181. (d) T. D. Nguyen, K. C.-F. Leung, M. Liong, C. D. Pentecost, J. F. Stoddart and J. I. Zink, *Org. Lett*., **2006**, *8*, 3363; (e) C. Park, K. Oh, S. C. Lee,C. Kim, *Angew. Chem., Int. Ed*., **2007**, *46*, 1455; (f) S. Angelos, Y. –W. Yang, K. Patel, J. F. Stoddart, J. I. Zink, *Angew. Chem. Int. Ed.*, **2008**, *47*, 2222. (g) R. Casasús, E. Climent, M. D. Marcos, R. Martínez-Máñez, F. Sancenón, J. Soto, P. Amorós, J. Cano, E. Ruiz, *J. Am. Chem. Soc.,* **2008**, *130*, 1903; (h) H. Meng, M. Xue, T. Xia, Y. –L. Zhao, F. Tamanoi, J. F. Stoddart, J. I. Zink, E. A. Nel, *J. Am. Chem. Soc.*, **2010**, *132*, 12690 (i) Y. Klichko, N. M. Khashab, Y. –W. Yang, S. Angelos, J. F. Stoddart, J. I. Zink, *Micropor. Mesopor. Mater.*, **2010**, *132*, 435. (j) V. Cauda, C. Argyo, A. Schlossbauer, T. J. Bein, *J. Mater. Chem.*, **2010**, *20*, 4305. (k) J. Liu, X. Du, *J. Mat. Chem.*, **2010**, *20*, 3642. (l) W. Guo, J. Wang, S. -J. Lee, F. Dong, S. S. Park, C. –S. Ha, *Chem. Eur. J.*, **2010**, *16*, 8641. (m) F. Muhammad, M. Guo, W. Qi, F. Sun, A. Wang, Y. Guo, G. Zhu, *J. Am. Chem. Soc*., **2011**, *133*, 8778 (n) A. Popat, J. Liu, G. Q. Lu, S. Z. Qiao, *J. Mater. Chem.,* **2012**, *22*, 11173. (o) K. Zhou, Y. Wang, X. Huang, K. Luby-Phelps, B. D. Sumer and J. Gao, *Angew. Chem., Int. Ed*., **2011**, *50*, 6109

[31] (a) Q. Fu, G. V. R. Rao, L. K. Ista, Y. Wu, B. P. Andrzejewski, L. A. Sklar, T. L. Ward and G. P. López, *Adv. Mater.,* **2003**, *15*, 1262; (b) C. R. Thomas, D. P. Ferris, J.-H. Lee, E. Choi, M. H. Cho, E. S. Kim, J. F. Stoddart, J.-S. Shin, J. Cheon and J. I. Zink, J. *Am. Chem. Soc.,* **2010**, *132*, 10623; (c) E. Ruiz-Hernández, A. Baeza, M. Vallet-Regí, *ACS Nano*, **2011**, *5*, 1259 (d) A. Baeza, E. Guisasola, E. Ruiz-Hernández and M. Vallet-Regí, *Chem. Mater.*, **2012**, *24*, 517; (e) J. Croissant and J. I. Zink, *J. Am. Chem. Soc.,* **2012**, *134*, 7628.

[32] (a) R. Hernandez, H. –R. Tseng, J. W. Wong, J. F. Stoddart, J. I. Zink, *J. Am. Chem. Soc.*, **2004**, *126*, 3370. (b) B. G. Trewyn, S. Giri, I. I. Slowing and V. S.-Y. Lin, *Chem. Commun.,* **2007**, 3236; (c) R. Mortera, J. Vivero-Escoto, I. I. Slowing, E. Garrone, B. Onida, V. S.-Y. Lin, *Chem. Commun.,* **2009***,* 3219 (d) R. Liu, Y. Zhang and P. Feng, *J. Am. Chem. Soc.*, **2009**, *131*, 15128; (e) F. Porta, G. E. M. Lamers, J. I. Zink and A. Kros, J. *Phys. Chem. C,* **2011**, *13*, 9982; (f) Z. Luo, K. Cai, Y. Hu, L. Zhao, P. Liu, L. Duan, W. Yang, *Angew. Chem., Int. Ed.*, **2011**, *50*, 640.

[33] (a) C. Coll, R. Casasús, E. Aznar, M. D. Marcos, R. Martínez-Máñez, F. Sancenón, J. Soto and P. Amorós, *Chem. Commun*., **2007**, 1957; (b) E. Aznar, C. Coll, M. D. Marcos, R. Martínez-Máñez, F. Sancenón, J. Soto, P. Amorós, J. Cano and E. Ruiz, *Chem.–Eur. J.,* **2009**, *15*, 6877; (c) E. Climent, M. D. Marcos, R. Martínez-Máñez, F. Sancenón, J. Soto, K. Rurack and P. Amorós, *Angew. Chem., Int. Ed.,* **2009**, *48*, 8519 (d) J. Lee, J. Lee, S. Kim, C.-J. Kim, S. Lee, B. Min, Y. Shin and C. Kim, Bull. *Korean Chem. Soc.,* **2011**, *32*, 1357.

### 1.2.3.2 *Light-Driven Molecular Gates*

Light is a powerful tool to control opening-closing processes involving molecular gate systems. To desing such a system, it is necessary to anchor a photosensitive molecule onto the surface of the siliceous scaffolding.

In this case it is possible to achieve a fine control of the released cargo by selecting the area and the time of exposure to the light stimulus.

*Fujiwara* and co-workers developed a light driven reversible system by functionalizing the outer surface of the mesopores of a MCM-41 siliceous scaffolding with an alcoxisilane coumarine derivative.[27b] When irradiating this material with ultraviolet light (λ>310nm) the intramolecular photodimerization of the coumarine takes place inducing the formation of a dimer molecule having a ciclobutante ring. This bulky molecule blocks the pores and avoids the release of the cargo from the material to the solution. To monitorize the reaction, the pores were previously loaded with phenantrene molecules. If the dimer molecule is formed the pores are blocked and, thus, the gate is closed, whereas, when the system is irradiated at λ=250nm, the photodimerization is reverted, the coumarine monomers are obtained and, therefore, the gate is opened, allowing the release of the entrapped phenantrene molecules (see figure 12).

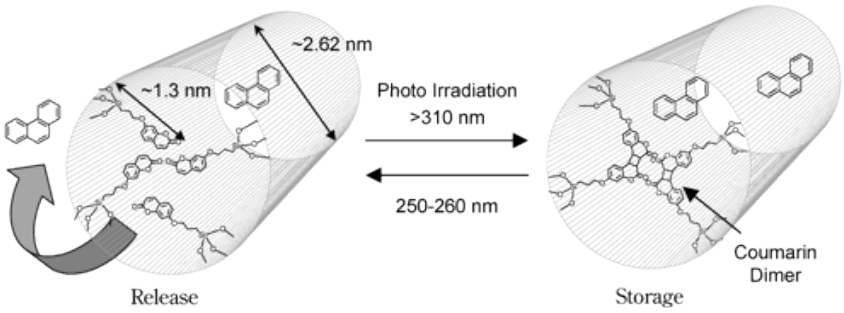


**Figure 12**. Schematic representation of light triggered dimerization reaction of the coumarine at λ>310nm and dimer cleaveage and subsequent gate opening and cargo release at λ= 250nm. *Reprinted (adapted) with permission from (Chem. Mater. 2003, 15, 3385-3394). Copyright (2003) American Chemical Society.*

More recently, another example of this kind of photochemical devices was studied by *Aznar, Martínez-Máñez* and co-workers.[29a] They designed the first two-input gated hybrid system based on photoswitchable molecules anchored on a mesoporous silica support. The system consisted of a mesoporous silica material whose external surface was functionalized with an alcoxysilane derivative of spiropyrian photochrome. This molecule is able to isomerize to its ionic merocyanine form (at darkness or when irradiated with UV light) and to revert to its neutral closed spiropyran form upon irradiation with visible light. In this case, the pores of the mesoprous structure were previously loaded with a dye that plays the role of indicator on the gating process. In order to achive said gating process, it was necessary to incorporate an additional component into the system: generation 1.5 polyamido(amine) (G1.5 PAMAM) dendrimers acting as molecular stoppers. In darkness the spiropyran is in its merocyanine form being able to interact electrostatically with the PAMAM. This interaction blocks the pores and avoids the cargo to be released. On the contrary, when the system is irradiated with visible light, the molecular gate changes to its neutral form so the interaction with the dendrimer is no longer possible and the pores are unblocked. The gate is now open allowing the release of the dye to the solution (see figure 13).

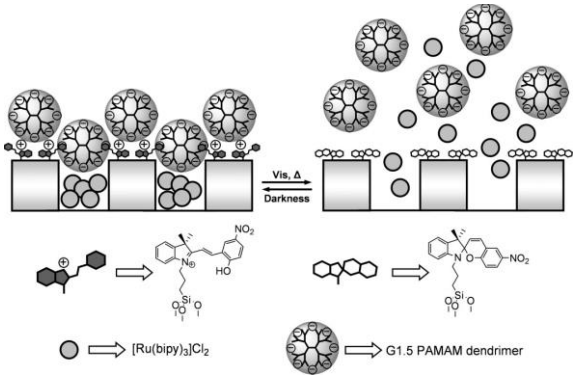


**Figure 13**. Schematic representation of the photochemical opening-closing paradigm. The gate can be open by deprotonation of the capping molecule or by irradiation with visible light. *Adapted from Adv. Mater., 2007, 19, 2228. Copyright © 2007 Wiley.*

In this case, the gate can be also controlled by protonation-deprotonation processes due to pH variations. Upon protonation of the PAMAM it remains positively charged and, thus, the electrostatic interaction with the spiropyran is no longer possible. Some other examples of pH-controlled systems will be explained in the following section.

#### 1.2.3.3 *pH-Driven Molecular Gates.*

pH changes leading to pronotonation/deprotonation processes have been also used to control molecular gate opening processes. *Casasús, Martínez-Máñez* and co-workers developed the first pH-driven molecular gated system.[30a] They functionalized the external surface of a MCM-41 material with pH-responsive groups, polyamines; thus, forming a monolayer of amines in the outer surface of the pores. When protonated, two different effects avoid the release of the cargo: the coulombic repulsion between the ammonium moieties and the interaction with anions present on the aqueous media. In this state, the gate is closed. On the contrary, if the polyamines are deprotonated, in their neutral form, the interactions are not possible and the polyamines adopt a flexible conformation around the pore entrance allowing the release of the cargo (See figure 14).

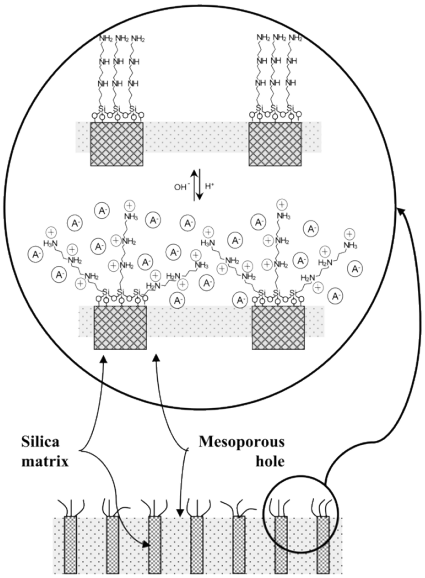


**Figure 14.** Schematic respresentation of the opening-closing paradigm of the gated materials depending on the pH of the aqueous media. *Reprinted (adapted) with permission from (J. Am. Chem. Soc., 2004, 126, 8612). Copyright (2004) American Chemical Society*.

This kind of control shows many practical advantages as it would allow, for example, the desing of delivery devices able to protect the cargo in acidic pH (i.e. on the stomach conditions) and its subsequent release at basic pH (i.e. intestinal conditions).

Based in this concept, *Bernardos, Martínez-Máñez et al*. developed a pH-responsive device to control the release of riboflavin (vitamin $B_2$). [30c] In order to achieve this goal, the rivoblafin was loaded on the mesopores and the derivative 3-[2-(2-aminoethylamino)ethylamino]propyl-trimethoxysilane was covalently anchored onto the pore outlets. Based on the same paradigm as the previous example, the riboflavin can only be released in basic conditions; otherwise, the polyamines being protonated, cargo release is inhibited.

### 1.2.3.4 Temperature-Driven Molecular Gates

Although there are several reported exemples, tailor-made temperature-responsive gated mesoporous materials have not been extensively studied.

One of these exemples was reported by *Aznar, Martínez-Máñez et al.* in 2011.[34] In this case, the gated device is based on the use of paraffins as capping agents, since they can be melted at a particular temperature. After having loaded the mesopores with the dye molecules that would act as indicators of the process, the external surface of MCM-41 nanoparticles is functionalized with molecules (octadecyltrimethoxysilane) not being able to block the pores by themselves, but able to interact with paraffins. Thus, a paraffins hydrophobic layer is formed avoiding the guest molecules to be released. Upon increasing the temperature above the melting point of said paraffins, they melt and, therefore, the pores are uncapped. The release of the dye from the pores to the solution is translated into a color change (see figure 15).

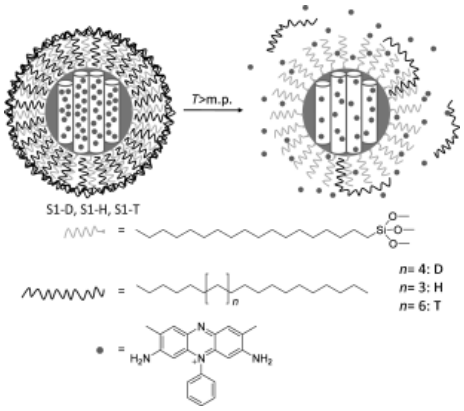


**Figure 15.** Representation of the gated materials functionalized with octadecyltrimethoxysilane and capped with different paraffins. The delivery of the entrapped guest (Safranine O) is triggered when temperature rises above the paraffin melting point. *Adapted from Angew. Chem. Int. Ed. 2011, 50, 11172. Copyright © 2011 Wiley.*

[34] E. Aznar, L. Mondragón, J. V. Ros-Lis, F. Sancenón, M. D. Marcos, R. Martínez-Máñez, J. Soto, E. Pérez-Payà and P.Amorós. *Angew. Chem. Int. Ed*. **2011**, *50*, 11172.

### 1.2.3.5 *Redox-Driven Molecular Gates*

Redox reactions have also been widely used for the development of gated mesoporous hybrid materials. *Stoddart, Zink* and co-workers described redox-responsive silica nanovalves that can be uncapped on demand.[32a] These devices are based on the use of [2]pseudorotaxanes as capping agents The pores of the silica material were loaded with an Iridium complex and, then, the external surface was functionalized with a 1,5-dioxynaphthalene derivative (DNPD). Upon addition of cyclobis-(paraquat-*p*-phenylene) ($CBPQT^{4+}$), a pseudorotaxane is formed between $CBPQT^{4+}$ and DNPD blocking, thus, the pore entrances. In the presence of a reducing agent, the pseudorotaxane dethreading takes place inducing the release of the iridium complex into the solution (see figure 16).

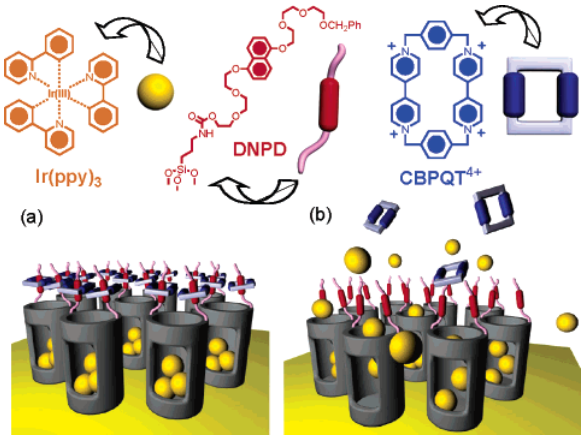


**Figure 16.** Graphical representations of operation of the gated system. (a) The orifices of the nanopores (diameter 2 nm) are covered with pseudorotaxanes (formed between DNPD and $CBPQT^{4+}$) which trap the luminescent Ir-$(ppy)_3$ molecules inside the nanopores. (b) Upon the reduction of the pseudorotaxane, the $CBPQT^{2+}$ bisradical dications are released and so, the $Ir(ppy)_3$ is allowed to escape. *Reprinted (adapted) with permission from (J. Am. Chem. Soc. 2004, 126, 3370). Copyright (2004) American Chemical Society*.

Another example of this kind of mechanism was reported by *Fujiwara et al*. in 2006.[35] In this case, the study was not based on the entrapped guest release but on the access of the solution to the pores of the material. The external surface of the material was functionalized with disilane–disulfide derivative which is cleaved in the presence of dithiothreitol. In such conditions *a*-methylstyrene is able to enter the pores inducing its dimerization reaction. The whole process is monitorized by controlling the amount of dimer species formed.

#### 1.2.3.6 *Molecular Interaction-Driven Molecular Gates*

One of the first examples of this opening/closing mechanism was reported by *Coll, Martínez-Máñez* and co-workers.[33a] They designed a material for the selective sensing of long-chain carboxylates based on a polarity change protocol. The pores of the MCM-41 scaffolding were filled with a ruthenium complex acting as indicator dye, and the outer surface was functionalized with an imidazolium derivative. In the absence of carboxylates the gate is open and the dye can easily diffuse to the solution whereas, in the presence of long-alkyl chain carboxylates, the pores are blocked and the release is not possible (see figure 17). Thus, the presence of the target molecules (long-chain carboxilates) can be noticed by a color change. The chromogenic response is related with the ability of the positively charged imidazolium groups to form complexes with carboxylates.

[35] M. Fujiwara, S. Terashima, Y. Endo, K. Shiokawa, H. Ohue *Chem. Commun*., **2006**, 4635.

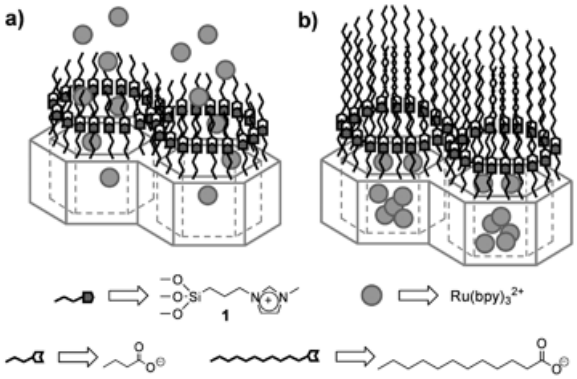


**Figure 17.** A representation of the sensory hybrid material **MS-Im** and the interaction of the gate-like ensemble with (a) butanoate (the ''gate''remains ''open'') and with (b) dodecanoate (the ''gate'' is ''closed''). *Adapted from Chem. Commun., 2007, 1957. Copyright © 2007 Royal Society of Chemistry*.

# 2. FUNCTIONALIZED SILICA NANOPARTICLES FOR ANIONS RECOGNITION

## 2.1 **Introduction**

### *2.1.1 Fluorogenic probes for sensing of anions.*

The development of fluorogenic chemosensors for anions has received growing interest during the past years due to the fundamental roles that anions play in chemical and biological processes.[1] Bearing in mind supramolecular concepts, many responsive fluorescent sensors for the detection of anions have been developed.[2] All these luminescent sensors have been designed attending to the three different approaches used in chemosensing design. Certain selected examples will be explained below.

*Veale, Gunnlaugsson et al.* designed thiourea based 4-amino-1,8-naphthalimide molecules as fluorescent receptors for anions taking into account the *binding site-signalling subunit approach*.[3] The fluorescence of these receptors in DMSO media suffered a several degrees quenching upon addition of basic anions such as $F^-$ and $H_2PO_4^-$. This phenomenon is due to a PET process from the coordinated anion (that forms hydrogen bonding interactions with the thiourea protons) to the photoexcited fluorophore. Moreover, other anions, for instance $Cl^-$ and $Br^-$, induced no effect on the receptor's fluorescence (see figure 1).

[1] F. P. Schmidtchen, M. Berger, *Chem. Rev*. **1997**, *97*,1609

[2] (a) M.E. Moragues, R.Martínez-Máñez, F. Sancenón, *Chem. Soc. Rev.,* 2011, **40**, 2593. (b) L.E. Santos-Figueroa, M.E. Moragues, E. Climent, A. Agostini, R. Martínez-Máñez, F. Sancenón *Chem. Soc. Rev.,* **2013**, *42*, 3489.

[3] E.B.Veale, G.M. Tocci, F.M. Pfeffer, P.E. Kruger*a,* T. Gunnlaugsson *Org. Biomol. Chem.*, **2009**, *7*, 3447.

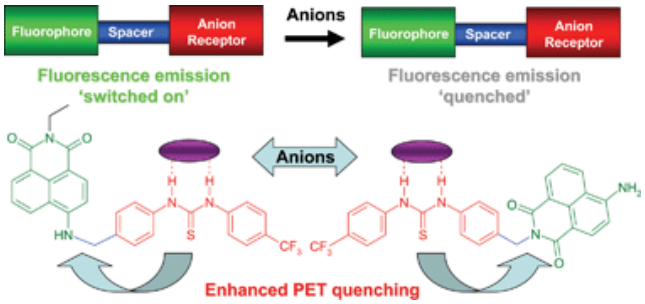


**Figure 1**. Graphical representation of the fluorescence quenching of the thiourea based supramolecular receptors upon addition of target anions. *Adapted from Org. Biomol. Chem., 2009, 7, 3447. Copyright © 2009 Royal Society of Chemistry.*

*Tang, Quian et al.* developed a selective and sensitive chemosensing ensemble for the recognition of pyrophosphate in aqueous media.[4] The chemosensing ensemble consists on a dinuclear Zn complex (2,6-bis[(bis(2-benzimidazolylmethyl)amino)methyl]-pcresol) acting as the anions receptor and sodium fluoresceine that plays the role of indicator. Upon addition of different anions to the non-fluorescent receptor-indicator pair, only pyrophosphate is able to displace the indicator from the ensemble and, thus, induce a fluorescence enhancement (see figure 2).

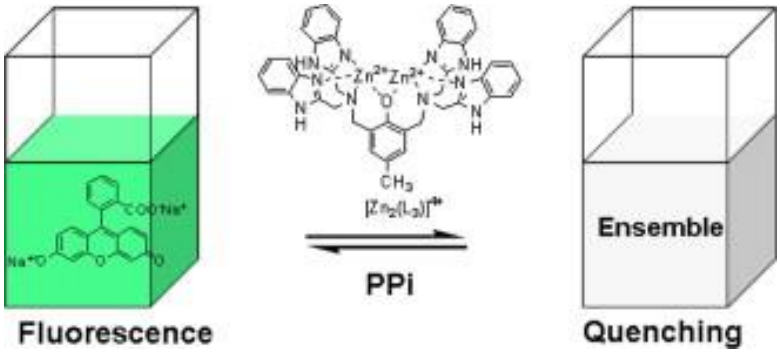


**Figure 2**. Schematic representation of the fluorescence enhancement induced upon addition of pyrophosphate to the non-fluorescent chemosensing ensemble. *Reprinted from Tetrahedron Lett. 2009, 50, L. Tang, Y. Li, H. Zhang, Z. Guo, J. Qian, A new chemosensing ensemble for fluorescent recognition of pyrophosphate in water at physiological pH, 6844, Copyright (2009), with permission from Elsevier*.

[4] L. Tang, Y. Li, H. Zhang, Z. Guo, J. Qian, *Tetrahedron Lett*. **2009**, *50*, 6844.

Taking into account the *chemodosimeter approach*, *Agou, Kawashima et al.* designed a bis(dimesitylboryl)azaborine derivative for $F^-$ signaling.[5] While the charactheristic emission band of this molecule is quenched upon addition of $F^-$, a new emission band appears suggesting the formation of a new derivative. Since the recognition paradigm is based on the reaction of the anion with the boron atoms in the derivative structure, this chemosensor is highly selective for $F^-$ (see figure 3).

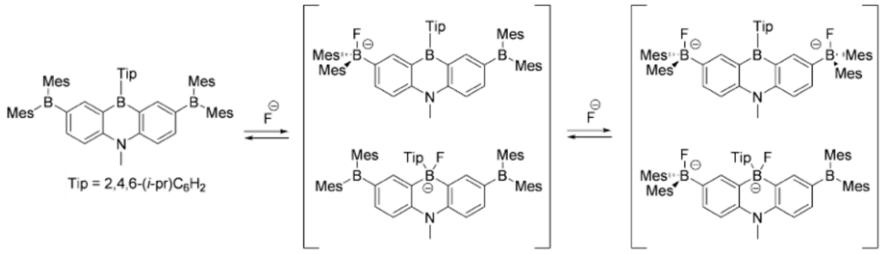


**Figure 3**. Bis(dimesitylboryl)azaborine receptor and the proposed reactions with $F^-$ anion. *Chem. Soc. Rev., 2011, 40, 2593. Copyright © 2011 Royal Society of Chemistry.*

### *2.1.2 Silica nanoparticles as sensing materials.*

Silica nanoparticles have been used in target molecules detection processes due to their ability to induce cooperative phenomena. In particular, it is possible to design sensing materials based on silica nanoparticles by functionalizing them with both binding sites and signalling subunits. In the materials, even if the subunits are not directly linked, the coordination of the target analyte to the binding site will induce a fluorescence change on the signalling subunit.

Although many examples of silica nanoparticles whose surface has been specifically modified for sensing of metal ions have been reported, there are only few examples of the use of these materials for anion recognition.

[5] T. Agou, M. Sekine, J. Kobayashi, T. Kawashima T. Agou, M. Sekine, J. Kobayashi and T. Kawashima, *Chem. Commun.,* **2009**, 1894.

*Calero, Martínez-Máñez et al.* designed a sensing material by functionalizing silica nanoparticles with cation coordination sites and fluorophores for the sensing of anions.[6] The paradigm the authors developed is based in competitive coordination to a metal center. They modified the *displacement approach* since, in this system, the target anion does not induce the release of the signaling subunit but the release of a quencher mediator (*Quencher displacement approach*). Silica nanoparticles are functionalized with sulforhodamine B (fluorophore) and terpyridine coordination sites (receptor subunits able to bind quenching metal ions). The binding of the mediator quenches the sulforhodamine fluorescence. Upon adition of the target anion, the displacement of the mediator takes place and the fluorescence of the fluorophore is restored (see figure 4).

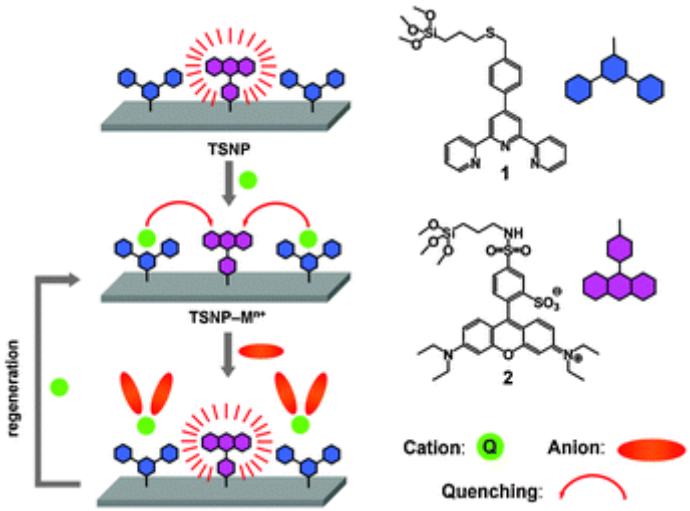


**Figure 4.** Design concept of the quencher displacement assay (QDA) involving terpyridine–sulforhodamine-functionalised nanoparticles (TSNPs) and metal ion quenchers (Q). *Adapted from Chem. Commun., **2011**, 47, 10599. Copyright © 2011 Royal Society of Chemistry.*

[6] P.Calero, M. Hecht, R.Martínez-Máñez, F.Sancenón, J. Soto, J. L. Vivancos, K.Rurack, *Chem. Commun.,* **2011**, *47*, 10599.

## 2.2 **Objectives**

Bearing in mind these examples we considered the possibility of designing a new system able to recognize anions based on the functionalization of silica nanoparticles.

The main objective of this chapter is the design and development of new organic-inorganic hybrid materials that could be able to modulate their emission properties in the presence of target anions in order to obtain sensing materials.

Specially, our aim was:

- The design and synthesis of functionalized silica nanoparticles designed to show fluorescence changes in the presence of target anions.
- The characterization of the new hybrid systems by the usual techniques used in material chemistry for hybrid organic-inorganic solids.
- The evaluation of the sensing behaviour of the prepared hybrid materials in the presence or absence of different anions.

## 2.3 **Design of the system**

Two different hybrid materials were synthesized. Silica nanoparticles were functionalized with sulforhodamine B acting as indicator and positively charged binding sites: imidazolium, in case of material **S1**, or guanidinium moieties, in case of material **S2**.

The system was designed in such a way that, upon coordination of anions with the anchored binding sites (via electrostatic and/or hydrogen bonding interactions), a modulation of the emission behaviour of sulforhodamine groups is induced, via energy or electron transfer process from the anion to the photo-excited fluorophore. It was also expected that the use of different binding sites may result in a different sensing behaviour (see figure 5).

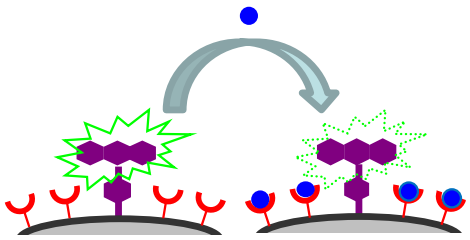

**Figure 5**. Schematic representation of the sensing paradigm. The coordination of the target anion to the binding site induces the fluorescence quenching. *Reprinted from Inorganica Chimica Acta, 381, Inmaculada Candel, Pilar Calero, Ramón Martínez-Máñez Félix Sancenón, M. Dolores Marcos,Teresa Pardo, and Juan Soto., Sensing properties of silica nanoparticles functionalized with anion binding sites and sulforhodamine B as fluorogenic signalling unit, 188–194,Copyright (2012), with permission fromElsevier*

# Sensing properties of silica nanoparticles functionalized with anion binding sites and sulforhodamine B as fluorogenic signalling unit

*Inmaculada Candel,[a,c] Pilar Calero,[a] Ramón Martínez-Máñez,*[a,b,c] Félix Sancenón[a,b,c] M. Dolores Marcos,[a,b,c] Teresa Pardo[a,b,c] and Juan Soto[a,b]*

[a]*Centro de Reconocimiento Molecular y Desarrollo Tecnológico (IDM), Unidad Mixta Universidad Politécnica de Valencia- Universidad de Valencia. Spain.*
[b] *Departamento de Química, Universidad Politécnica de Valencia, Camino de Vera s/n, E-46022 Valencia, Spain.*
[c] *CIBER de Bioingeniería Biomateriales y Nanomedicina (CIBER-BBN).*

***Received 29th June 2011, Accepted 11th Oct 2001***
***First published on the web 20 Oct 2011***

*Inorganica Chimica Acta, 2012, **381**, 188–194*
*(Reproduced with permission of Elsevier)*

**Abstract**

Bi-functionalized hybrid silica nanoparticles have been synthesized, characterized and their optical emission properties in the presence of certain anions studied. The hybrid solid **S1**, coated with sulforhodamine B as fluorogenic signalling unit and imidazolium groups as anion coordination sites, was prepared by the simultaneous grafting of suitable derivatives of these two subunits on silica nanoparticles. For the preparation of the sensing material **S2**, first the surface of silica nanoparticles was grafted with (3-aminopropyl)trimethoxysilane yielding solid $\mathbf{S_N}$. Then, in a second step, the amino groups on the surface were transformed into the corresponding guanidinium binding sites by reaction with pyrazole carboxamidine yielding solid $\mathbf{S_G}$. Finally, the grafting of the sulforhodamine B derivative **1** on $\mathbf{S_G}$ resulted in the hybrid nanoparticles **S2**. Acetonitrile suspensions of **S1** and **S2** showed typical sulforhodamine B absorption bands at ca. 550 nm. Upon excitation, an emission band at 575 nm was observed. Signalling properties of **S1** and **S2**, in acetonitrile and acetonitrile:water 9:1 v/v mixtures, in the presence of organic (acetate, benzoate) and inorganic ($F^-$, $Cl^-$, $Br^-$, $CN^-$, $NO_3^-$, $HSO_4^-$ and $H_2PO_4^-$) anions were studied. **S1** showed a fluorogenic response toward iodide and benzoate, whereas **S2** selectively responds to dihydrogen phosphate and hydrogen sulphate.

**Keywords:** Silica nanoparticles / Molecular recognition / Anions / Fluorescence

**Acknowledgments**

*Financial support from the Spanish Government (project MAT2009-14564-C04-01) and the Generalitat Valenciana (project PROMETEO/2009/016) is gratefully acknowledged.*

## 1. INTRODUCTION

The development of optical chemosensors for ions and neutral species has deserved great attention during the past years.[1] In a classical approach, these chemosensors are formed by the combination of two characteristic groups, i.e.

the “binding site” and the “signalling subunit” which are in general linked through a covalent bond.[2] The binding site is designed bearing in mind the size, shape and nature of the target species to be coordinated, whereas the signalling subunit bears the function of transforming the molecular “binding site”-guest interaction into an easily measurable output signal. Among different possible outputs, light is very useful because allows the use of rather simple and extended instrumentation.[3] Additionally along with different optical chemosensing systems, those based on changes of the emission fluorescence are especially attractive and a large number of fluorogenic probes for the recognition and sensing of metal cations,[4] inorganic and organic anions[5] and neutral species[6] have been described. Very recently, and as alternative to classical fluorogenic chemosensors, self-assembled structures of binding sites and signalling subunits on inorganic surfaces have attracted increasing attention within the field of molecular recognition and sensing.[7] These hybrid organic-inorganic sensing materials have been reported to display novel signalling properties that are hardly achievable by the individual components alone or when using analogous molecular-based systems. Furthermore, from a supramolecular viewpoint, the functionalization of nanostructured solids with certain groups to enhance recognition or switching effects has also been reported and is particularly appealing.[8] Moreover, the functionalization of inorganic supports with binding sites and fluorescent moieties can overcome synthetic problems shown by the classical “biding site–signalling unit” paradigm and provides an efficient strategy for the preparation of fluorogenic sensing systems.[9]

In spite of these interesting features, the organization of fluorescent groups and binding sites in the surface of inorganic materials for the development of fluorogenic probes is still a relatively recent field. Among different available inorganic supports we direct our attention to silica nanoparticles. Silica nanoparticles are versatile supports because they can be synthesized in an easy way (for example using the procedure developed by Stöber)[10] and their surface can be straightforwardly modified by the use of the well-known alcoxysilane chemistry.[11] These features make silica nanoparticles a good choice as inorganic scaffoldings for the covalent grafting of fluorophores and binding sites. Additionally silica is transparent to visible light and inert as far as energy and

electron-transfer processes are concerned. Moreover this approach may induce amplification and cooperative effects. For instance, the close arrangement of binding and signalling units allows intercommunication between both systems without the need of a direct covalent link between them.[12] Also the grafting of the receptor and the fluorophores in surfaces has been reported to induce an enhancement of the coordination ability.[13]

The use of silica nanoparticles as inorganic support in the development of fluorogenic chemosensors for metal cations has successfully been reported recently. At this respect, Tecilla and Tonellato prepared silica nanoparticles in which picolinamides and dansylamides were independently grafted to the surface through covalent bonds.[14] The picolinamide binding sites complexed $Cu^{2+}$ and the bound cation quenched the dansylamide emission in DMSO suspensions. The same authors used a combinatorial approach to functionalize silica nanoparticles with other binding sites and fluorophores in several ratios.[15] The cooperative and collective effects that were achieved are a clear consequence of the pre-organization of the single components on the nanoparticle surface. This pre-organization leaded to the formation of multivalent binding sites which showed increased affinity for $Cu^{2+}$. As additional interesting feature signal amplification was observed and a single metal cation induced the quenching of the emission of up to 10 fluorescent moieties that were surrounding the binding site. Also, in a recently published work, the same authors prepared silica nanoparticles coated with a 6-methoxy-8-(*p*-toluensulfonamido)-quinoline derivative which displayed a selective emission enhancement in the presence of $Zn^{2+}$ cation in ethanol-water 1:1 v/v mixtures.[16] Furthermore, silica nanoparticles functionalized with a fluorescein derivative and suitable coordination sites have been prepared and used for imaging of $Cu^{2+}$ in living cells.[17]

Dealing with the use of functionalized silica nanoparticles as fluorogenic or chromogenic sensory materials for anions, the number of examples described in the literature is very few. The first reported hybrid system was based in the bi-functionalization of silica nanoparticles with a spiropyran photochrome as chromogenic reporter and a thiourea derivative as binding site.[18] The

merocyanine form (yellow) was selectively transformed into the corresponding spyrocyclic structure (red) in the presence long chain carboxylates due to changes in the polarity on the nanoparticle surface. In a second example, the emission behaviour of silica nanoparticles functionalized with an anthracene and several ureas and thioureas moieties was studied in the presence of selected inorganic anions.[19]

Recently bifunctionalized silica nanoparticles have also been used for the chromo-fluorogenic sensing of anions using a different approach consisting in surface functionalization with two different molecules, namely a reactive subunit (an alkyl thiol) and a coordinating subunit. The chromo-fluorogenic response was related with the well known reaction of a blue squaraine dye with thiol moieties that induced bleaching. The control of the accessibility of squaraine (SQ) dye to the nanoparticle surface was achieved by the addition of certain guests that can coordinate the anchored binding site. In the absence of the guest, SQ reacts with the thiol groups leading to a bleaching of the solution. In the presence of the anion the reaction between squaraine and thiol was inhibited and the solution remained blue and highly fluorescent. By using this approach, highly selective and sensitive probes for pyrophosphate,[20] heparin,[21] nerve gases simulants[22] and anionic surfactants[23] have been prepared.

As a continuation of our interest in the design of electrochemical and optical chemosensors and reactants,[24] we report herein the synthesis of silica nanoparticles functionalized with two different units, binding sites (imidazolium or guanidinium groups) and a signalling fluorescent reporter (sulforhodamine B). Moreover, studies of the emission behaviour of suspensions of the prepared nanoparticles in the presence of organic (acetate, benzoate) and inorganic ($F^-$, $Cl^-$, $Br^-$, $CN^-$, $NO_3^-$, $HSO_4^-$ and $H_2PO_4^-$) anions were carried out.

## 2. MATERIAL AND METHODS

### 2.1. General Remarks.

(3-aminopropyl)trimethoxysilane, 1-methylimidazole, (3-chlorooopropyl)triethoxysilane, pyridine, sulforhodamine B acid chloride, pyrazole carboxamidine, *N*,*N*-diisopropylethylamine (DIEA) and 30 % suspension of ludox silica nanoparticles AS-30 Colloidal Silica were purchased from Sigma-Aldrich and were used without any further purification. The solvents were absolute grade and were purchased from Scharlab. The anions were used as tetrabutylammonium salts and were purchased from Aldrich ($Cl^-$, $Br^-$, $AcO^-$, $BzO^-$, $CN^-$, $NO_3^-$, $HSO_4^-$ and $H_2PO_4^-$) and Fluka ($F^-$).

### 2.2 Physical Measurements and instrumentation.

$^1H$ and $^{13}C$ NMR spectra were recorded using a Varian Gemini 300 MHz NMR spectrometer. Chemical shifts are reported relative to residual $CHCl_3$. Multiplicity is given as usual. Thermogravimetric analyses were carried out in a Mettler Toledo TGA/SDTA $851^e$. Transmission Electron Microscopy (TEM) images of the particles were obtained with a Philips CM10 operating at 20 KeV. Samples for TEM were prepared by spreading a drop of nanoparticles solution onto standard carbon-coated copper grids (200 mesh). UV-Vis absorption measurements were measured with a Perkin-Elmer Lambda-35 spectrometer. The fluorescence behaviour was studied with an FS900CDT Steady State T-Geometry Fluorimeter from Edinburgh Analytical Instruments. All solutions for photophysical studies were previously degassed. Anion stock solutions for photophysical studies ($C$ = 1 x $10^{-2}$ mol $dm^{-3}$) were prepared in dry acetonitrile. Fluorescence quantum yields were determined by a standard of quinine sulphate in 0.5 M $H_2SO_4$ ($\phi$ = 0.546).

## 3. EXPERIMENTAL

### 3.1 Synthesis.

The synthesis of the alkoxysilane derivatives **1** and **2** were carried out by reported procedures.[25]

*3.1.1 Synthesis of sulforhodamine B derivative (**1**)*. Sulforhodamine B acid chloride (0.23 g, 0.40 mmol) was dissolved in dichloromethane (20 mL) and cooled in an ice-bath. Then pyridine (100 µL) and (3-aminopropyl)trimethoxysilane (0.17 mL, 1.01 mmol) were added and the mixture stirred at room temperature for 24 hours. The final product was precipitated by adding *t*-butylmethyl ether to the crude reaction (0.250 g, 87 % yield). $^{1}$H-NMR (300 MHz, $CDCl_3$) δ: 0.6 (t, *J* = 6.6 Hz, 2H), 1.1-1.3 (m, 12H), 1.5 (q, *J* = 6.6 and 6.8 Hz, 2H), 2.9 (q, *J* = 7.2 and 7.0 Hz, 4H), 3.3 (s, 9H), 3.4-3.5 (q, *J* = 7.2 Hz, 4H), 6.5-8.5 (m, 9H) ppm.
*3.1.2 Synthesis of imidazolium derivative (**2**)*. 1-methylimidazole (20.5 g, 0.25 mol) and (3-chloropropyl)triethoxysilane (60.2 g, 0.25 mol) were mixed and stirred at 95 ºC for 24 hours. Afterwards, the final product was extracted twice with diethylether and dried at room temperature. The final product was isolated as a yellowish oil (54.8 g, 89 % yield). $^{1}$H-NMR (300 MHz, $CDCl_3$) δ: 0.56 (t, *J* = 6.6 Hz, 2H), 1.85 (q, *J* = 7.1 and 6.6 Hz, 2H), 3.45 (s, 9H), 3.90 (s, 3H), 4.20 (t, *J* = 7,1 Hz, 1H), 7.21 (s, 1H), 7.92 (d, *J* = 1.8 Hz, 1H), 9.6 (s, 1H).

**3.2 Synthesis of functionalized silica nanoparticles:**

Functionalization of silica nanoparticles with signalling subunits and binding sites was carried out by two distinct approaches. The first approach deals with the functionalization of nanoparticles by the grafting of both subunits in only one synthetic step (**S1**). The second approach was based in the consecutive grafting of the two subunits. In the first step nanoparticles functionalized with amine moieties were prepared ($\mathbf{S_N}$), then amine groups were transformed into guanidinium salts ($\mathbf{S_G}$) and, finally, the signalling subunit was incorporated yielding the final material (**S2**).

*3.2.1 Synthesis of nanoparticles functionalized with sulforhodamine B and imidazolium salt (**S1**)*. **1** (0.2 g, 0.28 mmol) and **2** (0.4 g, 1.67 mmol) were placed in a round bottom flask and then dissolved with ethanol (100 mL), water (60 mL) and acetic acid (60 mL). Then a water suspension of silica nanoparticles (12 mL LUDOX AS-30 colloidal silica) was added. The reaction mixture was warmed at 80°C under stirring for 48 hours. After this time, ethanol was evaporated under reduced

pressure and solid $NaHCO_3$ was added to the suspension until a pH value between 5 and 6 was reached. The silica nanoparticles were isolated by centrifugation and washed with water and acetone. The solid was dried at 70 ºC during 16 h. The solid obtained must be stored sheltered from light.

*3.2.2 Synthesis of nanoparticles functionalized with amino groups (**$S_N$**)*. A colloidal dispersion of LUDOX AS-30 silica nanoparticles (12 mL) was added to a solution containing ethanol (100 mL), water (60 mL) and acetic acid (60 mL). Then (3-aminopropyl)trimethoxysilane (0.6 mL, 2.6 mmol) was added to the nanoparticle suspension and the resultant mixture refluxed for 48 hours. Then the ethanol was removed with a rotary evaporator and the pH of the water suspension was lowered to 5 by the addition of sodium hydrogencarbonate. The functionalized **$S_N$** nanoparticles were isolated by centrifugation at 10000 r.p.m., washed with water and acetone and dried at 70 ºC overnight.

*3.2.3 Synthesis of nanoparticles functionalized with guanidinium salt (**$S_G$**)*. **$S_N$** nanoparticles (1 g) were suspended in DMF (22 mL). Then, pyrazole carboxamidine (71.8 mg, 0.6 mmol) and DIEA (0.105 mL, 0.6 mmol) were added and the suspension stirred for 24 hours (room temperature).

*3.2.4 Synthesis of nanoparticles functionalized with sulforhodamine B and guanidinium salt (**S2**)*. Sulforhodamine derivative **1** (250 mg, 0.35 mmol) was added to an acetonitrile (50 mL) suspension of **$S_G$** nanoparticles (500 mg) and the final crude was refluxed for 24 hours. Afterwards, the final solid **S2** was isolated by filtration, washed with acetonitrile and dried at 70 ºC. The solid must be stored sheltered from light.

3.2.5 *Synthesis of nanoparticles functionalized with sulforhodamine B (**S3**).* **1** (0.2 g, 0.28 mmol) was placed in a round bottom flask and then dissolved with ethanol (100 mL), water (60 mL) and acetic acid (60 mL). Then a water suspension of silica nanoparticles (12 mL LUDOX AS-30 colloidal silica) was added. The reaction mixture was warmed at 80°C under stirring for 48 hours. After this time ethanol was evaporated under reduced pressure and solid $NaHCO_3$ was added to the suspension until a pH value between 5 and 6 was reached. The silica nanoparticles were isolated by centrifugation and washed with water and acetone. The solid

was dried at 70 ºC during 16 h. The solid obtained must be stored sheltered from light.

## 4. RESULTS AND DISCUSSION

### 4.1 Design, synthesis and characterization of functionalized nanoparticles S1 and S2.

In this work we have prepared two different sensing materials for anions based on silica nanoparticles; i.e. **S1**, containing sulforhodamine B as signalling subunit and imidazolium binding sites and **S2** containing sulforhodamine B and guanidinium binding moieties. **S1** nanoparticles were prepared by the simultaneous grafting of derivatives **1** and **2** (see Scheme 1). **1** was synthesized by reaction of sulforhodamine B and (3-aminopropyl)trimethoxysilane,[25a] whereas the binding site **2** was prepared through reaction of 1-methylimidazole and (3-chloropropyl)trimethoxysilane.[25b] $^{1}$H-NMR of compound **1** showed typical signals of the propyl chain at 0.56, 1.50 and 3.60 ppm, a singlet centred at 3.26 ppm assigned to the methoxy moieties and aromatic protons in the 6.50-8.50 range. The most important feature of the $^{1}$H-NMR spectrum of compound **2** was the presence of a triplet centred at 4.2 ppm indicative of the presence of a methylene group directly linked to the positively charged imidazolium ring and singlets at 7.2, 7.9 and 9.6 ppm for the protons located in the positively charged heterocycle.

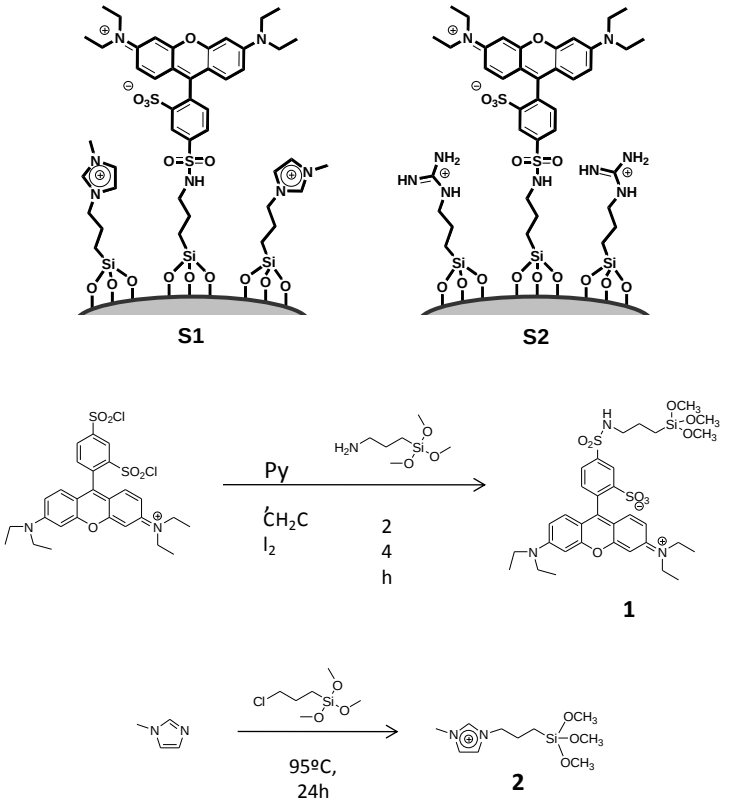


**Scheme 1.** Schematic representation of the hybrid nanoparticules **S1** and **S2** coated with imidazolium and sulforhodamine (left) and with guanidinium and sulforhodamine (right). The figure also shows the reactions involving the synthesis of **1** and **2**.

Coated silica nanoparticles **S1** were prepared using the trialcoxysilyl derivatives **1** and **2** following a previously reported procedure by Montalti and co-workers.[26] In this synthetic protocol, commercially available silica nanoparticles were heated at 70º C in a water:ethanol:acetic acid (1:2:1) solvent mixture in the presence of the coating subunits. Subsequent purification involved the evaporation of the ethanol, neutralization of the acetic acid with sodium hydrogencarbonate, centrifugation and washings of the nanoparticles with acetone. For the preparation of **S1** a 1:6 (**1:2**) ratio was selected.

The characterization of the functionalized **S1** nanoparticles was performed using thermogravimetric, elemental analysis and TEM. From the former

techniques it was observed that, despite the presence of a 1:6 relative amount of **1** and **2** in the reaction mixture, a 1:9 (**1:2**) ratio was found in the final solid, indicating that the velocity of the anchoring reaction of the trimethoxysilyl derivatives **1** and **2** on the nanoparticles was different (the derivative **2** was slightly more reactive than **1**). This difference is most likely due to the larger size of the sulforhodamine derivative **1** when compared with **2**. The distance between each molecule in the nanoparticle surface of the synthesized solid can be roughly estimated through the approximation of a single monolayer of subunits on a smooth sphere by taking into account several parameters such as: the total organic matter content (determined by thermogravimetric and elemental analysis) and the specific surface of the silica nanoparticles (200 $m^2/g$). Based on these parameters an average distance between two molecules in **S1** amounts to 9.4 Å that was indicative of the formation of a relatively dense monolayer of functionalized groups on the surface of the nanoparticle (see Table 1). TEM images of **S1** showed well dispersed and defined nanoparticles with a mean diameter of 18 nm (see Figure 1).

**Table 1**. Contents of signalling subunit and binding site in hybrid nanoparticles **S1** and **S2**.

| | ***Sulforhodamine Derivative*** *(mmol/g $SiO_2$)* | ***Imidazole Derivative*** *(mmol/g $SiO_2$)* | ***Guanidinium Derivative*** *(mmol/g$SiO_2$)* | ***Distance (Å)*** |
|---|---|---|---|---|
| **S1** | 0.039 | 0.33 | - | 9.4 |
| **S2** | 0.34 | - | 0.27 | 7.4 |

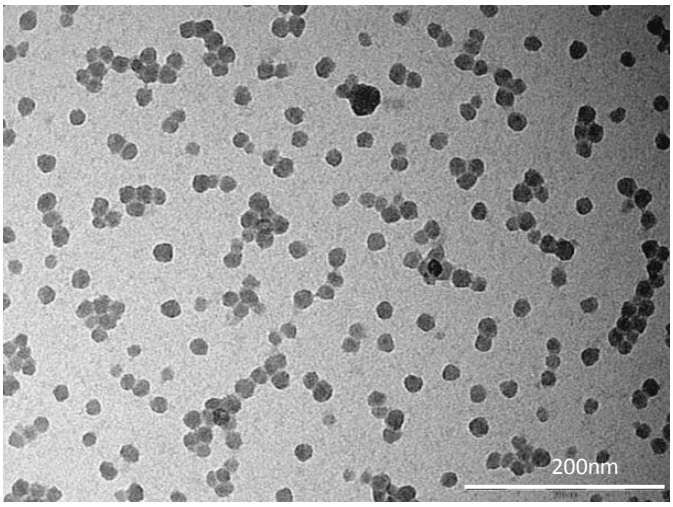


**Figure 1.** TEM image of hybrid **S1** nanoparticles.

In the preparation of **S2,** a two step grafting procedure was used. In the first step the external surface of LUDOX nanoparticles was functionalized with (3-aminopropyl)trimethoxysilane to give the intermediate solid $\mathbf{S_N}$. In a further step the amino groups in the surface of $\mathbf{S_N}$ nanoparticles were transformed to guanidinium moieties by the reaction of the anchored amines with pyrazole carboxamidine leading to solid $\mathbf{S_G}$.[27] A final reaction involved the grafting of the signalling derivative **1** in the surface of $\mathbf{S_G}$ yielding **S2**. This latter reaction was carried out at reflux in acetonitrile containing a mixture of $\mathbf{S_G}$ nanoparticles and **1** for 24 hours. Thermogravimetric and elemental analysis performed on **S2** showed a 1:1.3 sulforhodamine : guanidinium ratio in the final solid. TEM image of **S2** showed well defined nanoparticles with a mean diameter of 18 nm. The average distance between two subunits in **S2** was calculated to be 7.4 Å indicating the formation of dense monolayer of anchored groups on the nanoparticles surface.

**4.2 Sensing of anions**

Coated nanoparticles **S1** and **S2** bearing sulforhodamine as fluorescent signalling subunit and positively charged binding sites (imidazolium and guanidinium groups, respectively) are hybrid materials with the potential ability to recognize anions. The underlying idea was that coordination of anions with the anchored binding sites, via electrostatic and/or hydrogen bonding interactions, might induce modulation of the emission behaviour of sulforhodamine groups via energy or electron transfer process from the anion to the photo-excited fluorophore. It was also expected that the use of different binding sites may result in a different sensing behaviour. Imidazolium cations are known to form complexes with anions through $(C\text{-}H)^{+}\cdots X^{-}$-type ionic hydrogen bonding interactions.[28] Moreover, guanidinium binding sites can form complexes with anions via electrostatic forces and have also the ability of forming directional hydrogen bonds with Y-shaped anions.[29]

As we have stated above, few examples dealing with the use of hybrid materials based on silica nanoparticles for anion sensing have been described until now. The UV-visible and fluorescence behaviour of acetonitrile suspensions of **S1** and **S2** nanoparticles (3 mg in 20 mL) was studied. Both suspensions showed the typical absorption band of the sulforhodamine fluorophore at 552 and 549 nm, for **S1** and **S2**, respectively. Upon excitation ($\lambda_{ex}$ = 550 nm) the suspensions displayed a broad emission band at 577 and 573 nm for **S1** and **S2**, respectively of the sulforhodamine subunit. This value is similar to the absorption and emission bands of the sulforhodamine B dye in acetonitrile (559 nm and 575 nm, respectively) indicating that the grafting procedure used for the preparation of **S1** and **S2** did not basically affect the photo-physical properties of the fluorophore. The quantum yield of **S1** and **S2** suspensions were also determined using quinine sulphate as standard. The quantum yield of the sulforhodamine fluorophore in acetonitrile amounts to 0.474 whereas it is 0.038 and 0.115 for **S1** and **S2** respectively. The reduced quantum yield of **S1** and **S2**, when compared to sulforhodamine in solution, is most likely a consequence of the formation of a dense monolayer of binding sites and fluorophores in the nanoparticle surface, the spatial proximity between two fluorophores might enable $\pi$-stacking

interactions that induced emission quenching. Additionally the lower quantum yield of **S1** might be assigned to electron transfer or energy transfer process between the excited sulforhodamine fluorophore and the electron acceptor imidazolium cation.

In a further study, the fluorescence behaviour of acetonitrile suspensions of **S1** nanoparticles was tested in the presence of organic (acetate, benzoate) and inorganic (fluoride, chloride, bromide, iodide, cyanide, nitrate, dihydrogen phosphate and hydrogen sulphate) anions. In typical experiments, suspensions of **S1** (3 mg) in dry acetonitrile (20 mL) were prepared and fluorimetric titrations with anions were carried out. As a representative example, Figure 2 shows the relative emission changes, as difference between the emission intensity of **S1** in the presence of 12 equivalents of the corresponding anion (E) and **S1** alone ($E_0$). Three different behaviours were observed; i.e. (i) negligible emission change, (ii) fluorescence enhancement and (iii) fluorescence quenching. The addition of acetate, fluoride, chloride, bromide, cyanide, nitrate, dihydrogen phosphate and hydrogen sulphate induced poor changes in the emission of the anchored sulforhodamine in **S1**. Addition of iodide induced a moderate quenching (by about 7 % with 12 equivalents, quantum yield of 0.035) whereas addition of benzoate induced an enhancement of the emission intensity (by about 20 % with 12 equivalents, quantum yield of 0.045).

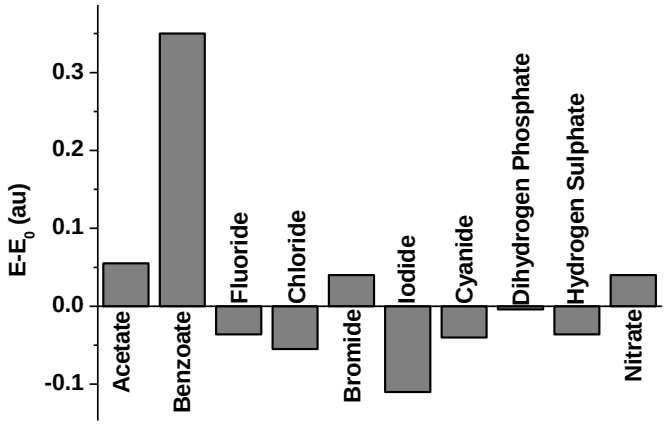


**Figure 2.** Relative emission changes, as difference between the emission intensity of **S1** nanoparticles (3 mg in 20 mL) in the presence of 12 equivalents of the corresponding anion (E) and the nanoparticles alone ($E_0$), in acetonitrile (molar equivalents with respect to binding sites).

The quenching of the sulforhodamine emission upon addition of iodide might be ascribed to a heavy atom effect.[30] On the other hand, the fluorescence enhancement in the presence of benzoate can tentatively be attributed to coordination of this anion with imidazolium binding sites on the surface of the nanoparticles, which resulted in restricting the mobility of the sulforhodamine fluorophore.[31] This disables the possibility of de-excitation of the excited fluorophores by non-emissive channels, thus leading to an increase in the emission intensity. In a further study, the emission behaviour in the presence of anions in acetonitrile-water 9:1 (v/v) mixtures was studied. The response was similar to that found in acetonitrile except for benzoate that only induced, in this case, a moderate quenching.

Similar titration experiments to those carried out with **S1** were performed using **S2** in the presence of the anions acetate, benzoate, fluoride, chloride, bromide, iodide, cyanide, nitrate, dihydrogen phosphate and hydrogen sulphate. As a representative example of the response observed, Figure 3 shows the relative emission changes, as difference between the emission intensity of acetonitrile suspensions of **S2** in the presence of 8 equivalents of the

corresponding anion (E) and **S2** alone ($E_0$). Fluoride, chloride, bromide, iodide, acetate, nitrate, benzoate and cyanide induced negligible changes in the emission profile whereas addition of hydrogen sulphate resulted in a significant quenching of the emission intensity. On the other hand, the addition of dihydrogen phosphate induced the precipitation of the **S2** hybrid nanoparticles.

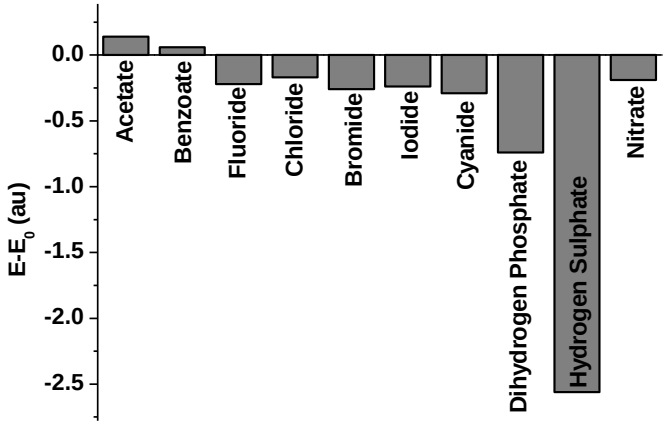


**Figure 3.** Relative emission changes, as difference between the emission intensity of **S2** nanoparticles (3 mg in 20 mL) in the presence of 8 equivalents of the corresponding anion (E) and the nanoparticles alone ($E_0$), in acetonitrile (molar equivalents with respect to binding sites). Quenching in the presence of dihydrogen phosphate was due to coordination-induced precipitation of **S2** nanoparticles

Moreover, a closer look to the sensing behaviour in the presence of sulphate showed a more complex behaviour. Addition of increasing quantities of hydrogen sulphate anion to **S2** induced a remarkable quenching (by about 95 %) with a significant reduction in the quantum yield (from 0.115 for **S2** nanoparticles alone to 0.011) until 8 equivalents of the anion were added, whereas addition of more equivalents resulted in an enhancement of emission intensity (see Figure 4) and of quantum yield (0.093 upon addition of 80 equivalents of hydrogen sulphate). The initial quenching must be related with non-emissive deactivation pathways of the

excited fluorophore, via electron or energy transfer processes, triggered upon coordination of the anion with guanidinium binding groups. Enhancement in the presence of increasing amounts of hydrogen sulphate may tentatively be attributed to rigidification of the fluorophore due to the presence of a large number of anions interacting with the coordination sites on the surface of **S2**.

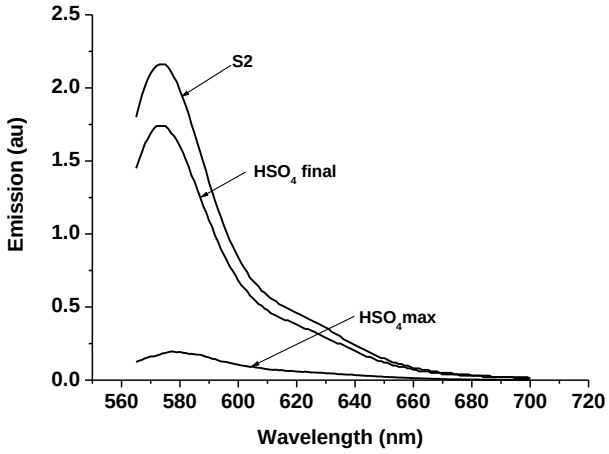


**Figure 4.** Emission spectra of acetonitrile suspensions of **S2** nanoparticles in the presence of hydrogen sulphate anion ($\lambda_{ex}$ = 550 nm). The maximum quenching is achieved in the presence of 8 equivalents of hydrogen sulphate whereas the addition of 80 equivalents results on the enhancement of the fluorescence.

As cited above, addition of dihydrogen phosphate anion induced the precipitation of the hybrid nanoparticles (see Figure 5). Most likely in this case the formation of strong hydrogen bonds and electrostatic interactions between guanidinium binding sites and dihydrogen phosphate anions induced the agglomeration of nanoparticles and precipitation.


**Figure 5.** Hybrid materials **S2** in acetonitrile in the absence (left) and in the presence of dihydrogen phosphate (right).

In a further experiment the emission behaviour of **S2** in the presence of anions in acetonitrile-water 9:1 (v/v) mixtures was studied. A selective response in the presence of hydrogen sulphate was found; i.e. a slight enhancement of the emission intensity (by about 5 % with 8 equivalents) was observed. The anions fluoride, chloride, bromide, iodide, acetate, nitrate, benzoate and cyanide in acetonitrile-water 9:1 (v/v) suspensions of **S2** induced no significant effects in terms of fluorescence changes. Dihydrogen phosphate in this medium did not induce precipitation of the hybrid **S2** nanoparticles and no changes in the fluorescence emission were observed.

Finally the material **S3** containing only sulforhodamine, but not binding sites, was prepared as model system. The addition of increasing quantities of anions to acetonitrile suspension of **S3** induced negligible changes in the intensity of the sulforhodamine emission bands (data not shown) revealing the importance of the presence of coordination sites in the observed sensing behaviour.

## 5. CONCLUSIONS

Fluorescent signalling materials based on silica nanoparticles functionalized with sulforhodamine B as signalling subunit and with imidazolium (**S1**) or guanidinium (**S2**) groups have been prepared. Typical sulforhodamine B

absorption and emission bands were observed in acetonitrile suspensions of **S1** and **S2**. The addition of target anions to suspensions of the hybrid nanoparticles in acetonitrile induced changes in the emission intensity with patterns of selectivity. Nanoparticles functionalized with imidazolium cations favoured the selective response to iodide and benzoate, whereas nanoparticles functionalized with guanidinium moieties gave selective response in the presence of hydrogen sulphate. Also **S2** nanoparticles precipitate upon addition of dihydrogen phosphate anion. The sensing behaviour of **S1** and **S2** was also tested in acetonitrile-water 9:1 (v/v) mixtures. The independent anchoring of signalling and binding units on silica nanoparticles is highly modular and follows routes that require a low synthetic effort. We are currently developing novel chromo-fluorogenic probes based on silica nanoparticles for the signalling of different target species.

**References.**

1. (a) R. Martínez-Máñez, F. Sancenón, Chem. Rev. 103 (2003) 4419. (b) R. A. Bissell, A. P. de Silva, H. Q. N. Gunaratne, P. L. M. Lynch, G. E. M. Maguire, K. R. A. S. Sandanayake, Chem. Soc. Rev. (1992) 187.

2. P. D. Beer, P. A. Gale, Angew. Chem. Int. Ed. 40 (2001) 486.

3. (a) B. Valeur, I. Leray, Coord. Chem. Rev. 205 (2000) 3. (b) A. W. Czarnik, Acc. Chem. Res. 27 (1994) 302. (c) K. Rurack, U. Resch-Genger, Chem. Soc. Rev. 31 (2002) 116.

4. A. P. de Silva, H. Q. M. Gunaratne, T. Gunnlaugsson, J. M. Huxley, C. P. McCoy, J. T. Rademacher, T. E. Rice, Chem. Rev. 97 (1997) 1515.

5. M. Moragues, R. Martínez-Máñez, F. Sancenón, Chem. Soc. Rev. 40 (2011) 2593.

6. (a) S. Royo, R. Martínez-Máñez, F. Sancenón, A. M. Costero, M. Parra, S. Gil, Chem. Commun. (2007) 4839. (b) S. W. Thomas III, G. D. Joly, T. W. Swager, Chem. Rev. 107 (2007) 1339. (c) M. E. Germain, M. J. Knapp, Chem. Soc. Rev. 38 (2009) 2543.

7. R. Martínez-Máñez, F. Sancenón, M. Hecht, M. Biyical, K. Rurack, Anal. Bioanal. Chem. 399 (2011) 55.

8. A. B. Descalzo, R. Martínez-Máñez, F. Sancenón, K. Hoffmann, K. Rurack, Angew. Chem. Int. Ed. 45 (2006) 5924.

9. (a) S. Bonacchi, D. Genovese, R. Juris, M. Montalti, L. Prodi, E. Rampazzo, M. Sgarzi, N. Zaccheroni, Top. Curr. Chem. 300 (2011) 93. (b) S. Bonacchi, D. Genovese, R. Juris, M. Montalti, L. Prodi, E. Rampazzo, N. Zaccheroni, Angew. Chem. Int. Ed. 50 (2011) 4056. (c) A. Burns, H. Ow, U. Wiesner, Chem. Soc. Rev. 35 (2006) 1028. (d) W. Zhong, Anal. Bioanal. Chem. 394 (2009) 47.

10. W. Stöber, A. Fink, E. Bohn, J. Colloid Interface Sci. 26 (1968) 62.

11. C. Beck, W. Härtl, R. Hempelmann, Angew. Chem. Int. Ed. 38 (1999) 1297.

12. (a) M. Crego-Calama, D. N. Reinhoudt, Adv. Mater. 13 (2001) 1171. (b) S. Flink, F. C. J. M. van Veggel, D. N. Reinhoudt, Adv. Mater. 12 (2000) 1315.
13. (a) A. Arduini, D. Demuru, A. Pochini, A. Secchi, Chem. Commun.(2005) 645. (b) R. Tshikhudo, D. Demuru, Z. Wang, M. Brust, A. Secchi, A. Anduini, A. Pochini, Angew. Chem. Int. Ed. 44 (2005) 2913.
14. E. Brasola, F. Mancin, E. Rampazzo, P. Tecilla, U. Tonellato, Chem. Commun. (2003) 3026.
15. E. Rampazzo, E. Brasola, S. Marcuz, F. Mancin, P. Tecilla, U. Tonellato, J. Mater. Chem. 15 (2005) 2687.
16. P. Teolato, E. Rampazzo, M. Arduini, F. Mancin, P. Tecilla, U. Tonellato, Chem. Eur. J. 13 (2007) 2238.
17. S. Seo, H. Y. Lee, M. Park, J. M. Lim, D. Kang, J. Yoon, J. H. Jung, Eur. J. Inorg. Chem. (2010) 843.
18. P. Calero, E. Aznar, J. M. Lloris, M. D. Marcos, R. Martínez-Máñez, J. V. Ros-Lis, J. Soto, F. Sancenón, Chem. Commun. (2008) 1668.
19. P. Calero, R. Martínez-Máñez, F. Sancenón, J. Soto, Eur. J. Inorg. Chem. (2008) 5649.
20. E. Climent, R. Casasús, M. D. Marcos, R. Martínez-Máñez, F. Sancenón, J. Soto, Chem. Commun. (2008) 6531.
21. E. Climent, P. Calero, M. D. Marcos, R. Martínez-Máñez, F. Sancenón, J. Soto, Chem. Eur. J. 15 (2009) 1816.
22. E. Climent, A. Martí, S. Royo, R. Martínez-Máñez, M. D. Marcos, F. Sancenón, J. Soto, A. M. Costero, S. Gil, M. Parra, Angew. Chem. Int. Ed. 49 (2010) 5945.
23. E. Climent, C. Giménez, M. D. Marcos, R. Martínez-Máñez, F. Sancenón, J. Soto, Chem. Commun. 47 (2011) 6873.
24. See for instance: (a) J.V. Ros-Lis, R. Casasús, M. Comes, C. Coll, M.D. Marcos, R. Martínez-Máñez, F. Sancenón, J. Soto, P. Amorós, J. El Haskouri, N. Garró, K. Rurack, Chem. Eur. J. 14 (2008) 8267. (b) E. Climent, M.D. Marcos, R. Martínez-Máñez, F. Sancenón, J. Soto, K. Rurack, P. Amorós, Angew. Chem. Int. Ed. 48 (2009) 8519. (c) E. Climent, A. Bernardos, R. Martínez-Máñez, A. Maquieira, M.D. Marcos, N. Pastor-Navarro, R. Puchades, F. Sancenón, J. Soto, P. Amorós, J. Am. Chem. Soc. 131 (2009) 14075. (d) E. Aznar, C. Coll, M.D. Marcos, R. Martínez-Máñez, F. Sancenón, J. Soto, P. Amorós, J. Cano, E. Ruiz, Chem. Eur. J. 15 (2009) 6877.
25. (a) M. Ganschow, M. Wark, D. Wöhrle, G. Schulz-Ekloff, Angew. Chem. Int. Ed. 39 (2000) 160. (b) M. H. Valkenberg, C. De Castro, W. F. Hölderich, Top. Catal. 14 (2001) 139.
26. M. Montalti, L. Prodi, N. Zacheroni, G. Falini, J. Am. Chem. Soc. 124 (2002) 13540.
27. I. Slowing, B. G. Trewyn, V. S. –Y. Lin, J. Am. Chem. Soc. 128 (2006) 14793.
28. J. Yoon, S. K. Kim, N. J. Singh, K. S. Kim, Chem. Soc. Rev. 35 (2006) 355.
29. P. Blondeau, M. Segura, R. Pérez-Fernández, J. de Mendoza, Chem. Soc. Rev. 36 (2007) 198.
30. (a) A. Chmyrov, T. Sanden, J. Widengren, J. Phys. Chem. B 114 (2010) 11282. (b) Z. S. Romanova, K. Deshayes, P. Piotrowiak, J. Am. Chem. Soc. 123 (2001) 2444. (c) M. Mac, J. Najbar, D. Phillips, T. A. Smith, J. Chem. Soc., Faraday Trans. 88 (1992) 3001.

31. (a) L. Zhang, R. J. Clark, L. Zhu, Chem. Eur. J. 14 (2008) 2894. (b) K. R. A. S. Sandanayake, K. Nakashima, S. Shinkai, J. Chem. Soc., Chem. Commun. (1994) 1621.

# 3. SENSING AND REMEDIATION OF NEUROTOXIC AGENTS

## 3.1 **Introduction.**

### *3.1.1 Neurotoxic Agents.*

According to the Organization for the Prohibition of Chemical Weapons, the term *chemical weapon* is applied to "any toxic chemical or its precursor that can cause death, injury, temporary incapacitation or sensory irritation through its chemical action".[1] Among all Chemical Weapons species, neurotoxic agents (also referred to as nerve agents) are classified by United Nations as weapons of mass destruction. They are particularly dangerous because of their high toxicity and ease of production. Development of nerve agents was a by-product of insecticide research and development and they were not used as chemical weapon until the Second World War.

Neurotoxic agents are able to enter the human body by inhalation or through the skin and they attack the nervous system by inhibiting the transmission of the nerve impulse.[2] The effects of neurotoxic agents are caused, mainly, by their ability to inhibit acetilcholinesterase enzyme function, by reacting with the serine active-site of the enzyme.[3] Given the normal role of this enzyme is to hydrolyze acetylcholine neurotransmitter, its inhibition results in the excessive increase of acetylcholine concentration, leading to the accumulation of this molecule in several sites of action.[4] Symptoms vary with the route of exposure and they comprise contraction of pupils, profuse salivation, convulsions, involuntary urination and defecation, and eventual death by asphyxiation as control is lost over respiratory muscles.

Most common neurotoxic agents are:

- *G-Agents*: Sarin (GB), Soman (GD), Tabun (GA), cyclosarin (GF).
- *V-Agents*: VG, VX, VM, VE.

[1] See http://www.opcw.org/about-chemical-weapons/what-is-a-chemical-weapon/
[2] S. M. Somani, *Chemical Warfare Agents*, Academic Press, San Diego, (1992).
[3] M. Ehrich, Encyclopedia of Toxicology, ed. P. Wexler, Academic Press, San Diego, CA, **1998**.
[4] (a) T. C. Marrs, *Pharmacol. Ther.,* **1993**, *58*, 51.(b) F. R. Sidell and J. Borak, *Ann. Emerg. Med.,* **1992**, *21*, 865.

The main difference between G-agents (tabun, sarin, soman and cyclosarin) and V-agents is related with the non persistence of the former whereas the later are persistent. The term persistent agent generally refers to neurotoxic compounds that are not rapidly hydrolysed and are not very volatile so that are able to persist in an area for a long period of time.[5]

Regarding its chemical structure, nerve agents are organophosphorous compounds having a good leaving group. Studies dealing with this kind of substances are normally performed with compounds having a similar chemical structure but showing less toxicity (DCP, DCNP, DFP). In the following, these compounds will be referred to as *nerve agent simulants*. Figure 1, shows the chemical structure of G- and V- agents and several nerve agent simulants.

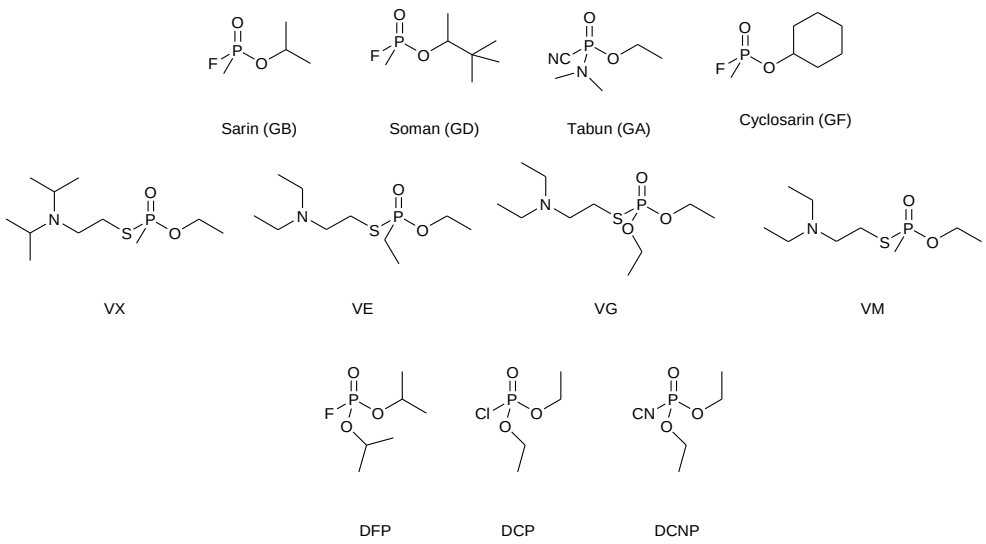


**Figure 1**. Chemical structure of G-agents, V-agents and neurotoxic agent simulants.

The lower toxicity of nerve agents simulants is due to their rapid hydrolysis. Both neurotoxic agents and their simulants are very reactive. Most significant reactions that

[5] S. Royo, R. Martínez-Máñez, F. Sancenón, A. M. Costero, M. Parra, S. Gil, *Chem. Commun.,* **2007**, 4839.

these compounds can undergo are related to the phosphorous atom. They can be involved in nucleofilic attacks where the P-X bond is broken. It is well known that all these agents hydrolyze very quickly in aqueous basic solutions whereas the hydrolysis is slow at neutral pH.

### *3.1.2 Chromogenic detection of nerve agents.*

Due to the above mentioned toxicity of the neurotoxic agents, and bearing in mind the attacks with these compounds are very silent (as they are colourless gases), there is great interest in developing selective, sensitive and fast methods to detect these chemical weapons. Several detection systems have been already reported, most of them based on physical and enzymatic methodologies.[6] To overcome the disadvantages these methods pose, such as complexity and lack of portability, chromogenic and fluorogenic chemosensors have been developed.[5,7] Several examples of chromogenic and fluorogenic detection of neurotoxic agents will be detailed below.

*Royo et al*. developed a chemosensor able to detect nerve agents mimics.[8] The authors designed colorimetric probes where 2-(2-(dimethylamino)-phenyl)ethanol derivatives play the role of binding site due to the ability of hydroxyl moiety to react with phosphonate compounds to yield quaternary ammonium salts. In the presence of DCP, the selected derivative (synthesized by reacting 2-(2-(dimethylamino)-phenyl)etanol with the diazonium salt of 4-nitroaniline) undergoes a cyclation reaction which results in a hypsochromic shift (see figure 2)

[6] (a) L. M. Eubanks, T. J. Dickerson, K. D. Janda, *Chem. Soc. Rev.*, **2007**, *36*, 458. (b) J. Zhang, X. Li, J. White, P. K. Dutta, *Sensors* **2012**, *12*, 13284. (c) I. Campos, L. Gil, R. Martínez-Máñez, J. Soto, J.L. Vivancos, *Electroanalysis*, **2010**, *22*, 164. (d) J. H. Lee, J. Y. Park, K. Min, H. J. Cha, S. S. Choi, Y. J. Yoo, *Biosensors and Bioelectronics* **2010**, *25*, 1566.

[7] (a) *J. Lee , S. Seo , J. Kim, Adv. Funct. Mater.* ***2012****, 22, 1632. (b) L. Ordronneau, A. Carella, M. Pohankab, J.P. Simonato, Chem. Commun.,* **2013**, *49*, 8946.

[8] A. M. Costero, S. Gil, M. Parra, P. M. E. Mancini, R. Martínez-Máñez, F. Sancenón, Santiago Royo, *Chem. Commun*., **2008**, 6002.

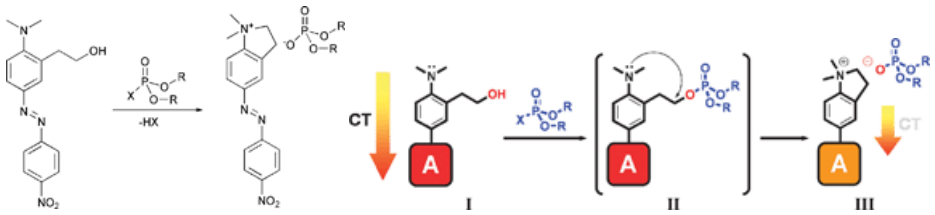


**Figure 2.** Phosphorilation of the chromogenic probe upon reaction with a nerve agent simulant (left) and schematic representantion of the sensing paradingm involving colour change (right). *Reprinted (adapted) with permission from Chem. Commun*., 2008, 6002 . *Copyright (2003) Royal Society of Chemistry*.

*Gotor et al*. have also designed a chromogenic probe for the detection of nerve agents simulants.[9] They developed a sensor system where 4-pyridine green cation and a 2-hydroxyethyl derivative compound of cristal violet dye are able to undergo batocromic shifts in the presence of neurotoxic agents mimics (DCP and DCNP). Upon reaction with certain organophosphorous compounds, pyridine transforms into the corresponding pyridinium salt which results in a modulation of the colour. Likewise, the phosphorilation of the additional hydroxy moiety of the cristal violet derivative and the subsequent intramolecular nucleofilic substitution reaction also results in a colour change (see figure 3).

[9] R. Gotor, S. Royo, A. M. Costero, M. Parra, S. Gil, R. Martínez-Máñez, F. Sancenón, *Tetrahedron* **2012**, *68*, 8612.

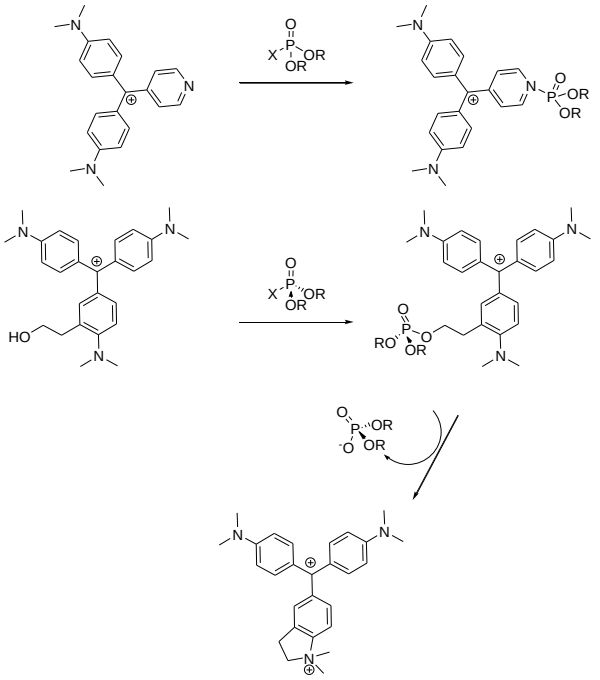

**Figure 3**. Reactivity of 4-pyridine green cation and the 2-hydroxyethyl derivative compound of cristal violet dye upon organophosphorous mimics of neurotoxic agents. Reprinted from Tetrahedron, 68, R. Gotor, S. Royo, A. M. Costero, M. Parra, S. Gil, R. Martínez-Máñez, F. Sancenón, Nerve agent simulant detection by using chromogenic triaryl methane cation probes, 8612, Copyright (2012), with permission from Elsevier.

### *3.1.3 Remediation and elimination of neurotoxic agents*

Many efforts have been done not only to detect nerve agents, but also to eliminate them. It is possible to find in the literature different decontamination methods such as: electrolytic systems,[10] oxidative degradation on active sorbents,[11] or catalytic degradation methods.[12] However, these methods show several disadvantages such as complexity and/or lack of portability.

[10] T-J Leea, B. C. Chunb, Y-C Chunga, *Reactive & Functional Polymers* **2003**, *56*, 37.
[11] D. M. Mizrahi, S. Saphier, I. Columbus, *Journal of Hazardous Materials* **2010***, 179,* 495.
[12] (a) M. F. Mohamed, A.A. Neverov, R. S. Brown**,** *Inorg. Chem.* **2009**, *48*, 1183. (b) G. R. M. Echavia, F.Matzusawa, N. Negishi, *Chemosphere* **2009**, *76*, 595.

It has been found that several organic or biologic compounds such as hydrolases enzymes are able to act as nerve agents scavengers. This is also the case of oximes. Based on the nucleofilic ability of oximes to react with organophosphorous compounds, *Saint-André et al*. developed a family of new α-nucleophiles for the hydrolysis of nerve agents.[13]

### *3.1.4 Gated materials as sensors*

Among all the previously stated applications of gated materials, these systems are able to act also as sensor materials when the system is designed in a way that the external stimulus that will open/close the gate is the target molecule to be sensed.

Many examples where gated materials have been used for sensing applications for anions, cations and neutral molecules have been reported.[14] Some examples of these kind of system are explained in detail below.

*He et al*. developed an ATP responsive gated system.[15] The authors designed a sensing material where an ATP aptamer is hybridized with DNA fragments and then anchored to the external surface of silica nanoparticles, thus, blocking the pores, which have been previously loaded with the fluorescent dye $Ru(bipy)_3^{2+}$. In the presence of ATP, a displacement reaction takes places since the ATP aptamer combines with ATP and leaves the pore. Therefore, the fluorescent dye can be released as DNA fragment chains are flexible. In this case, the presence of ATP is revealed by a fluorescence enhancement (see figure 4).

[13] G.Saint-André, M. Kliachyna, S. Kodepelly, L. Louise-Leriche, E. Gillon, P.-Y. Renard, F. Nachon, R. Baati, Alain Wagner *Tetrahedron* **2011**, *67*, 6352.
[14] (a) M. Chen, C. Huang, C. He, W. Zhu, Y. Xua, Y. Lu*, Chem. Commun*., **2012**, *48*, 9522. (b) H. Li, T-Y Ma, D-M Kong, Z-Y Yuan, *Analyst*, **2013**, *138*, 1084.
[15] X. He, Y. Zhao, D. He, K. Wang, F. Xu, J. Tang, *Langmuir* **2012**, *28*, 12909.

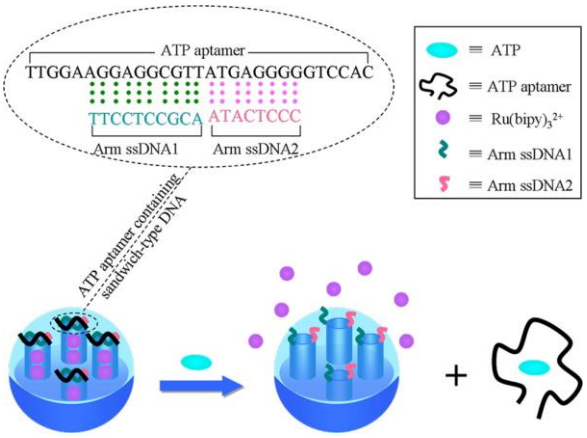


**Figure 4**. Schematic representation of the sensing paradigm. In the presence of ATP, the ATP aptamer is no longer attached to the DNA fragments on the silica surface and, thus, the dye in the pores can be released. *Reprinted (adapted) with permission from Langmuir 2012, 28, 12909. Copyright (2012) American Chemical Society*.

*Salinas et al*. have designed a gated system able to selectively recognize certain nitroaromatic explosives.[16] In this case, mesoporous silica nanoparticles were also selected as inorganic scaffolding and the mesopores were loaded with the ruthenium complex tris(2,2'-bipyridyl)ruthenium(II) chloride $Ru(bipy)_3^{2+}$. The pore outlets were functionalized with 3-(azidopropyl) triethoxysilane. The system was then capped with a pyrene derivative (which is bulky enough to block the pore entrances and avoid dye release). In the presence of suitable nitroaromatic compounds (Tetryl and TNT explosives), the formation of pyrene-nitroaromatic complexes pushes apart the pyrene from the pore outlets, thus, allowing the dye release (see figure 5). Therefore, the presence of tetryl and TNT is signaled by a fluorescence enhancement.

[16] Y. Salinas, A. Agostini, E. Pérez-Esteve, R. Martínez-Máñez, F. Sancenón, M.D. Marcos,J. Soto, A. M. Costero, S. Gil, M. Parra, Pedro Amorós, *J. Mater. Chem. A*, **2013**, *1*, 3561–3564.

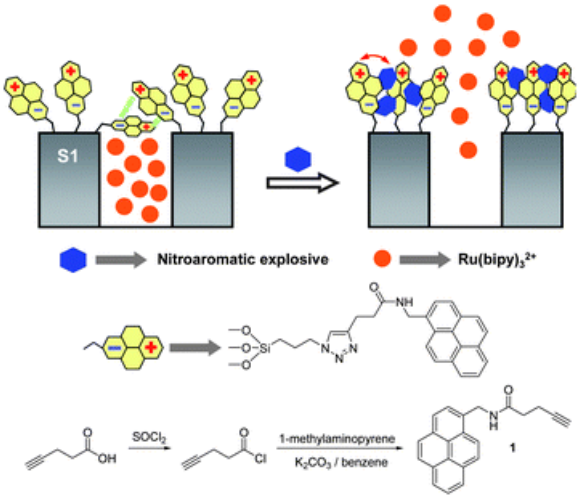


**Figure 5.** Schematic representation of the gated system and the sensing paradigm. The gates open in the presence of TNT and Tetryl due to the formation of pyrene-nitroaromatic complexes that push apart the pyrene moieties from the pore outlets. *Reproduced ("Adapted" or "in part") from J. Mater. Chem. A, 2013, 1, 3561–3564 with permission of The Royal Society of Chemistry*.

## 3.2 **Objectives**

Bearing in mind these examples we considered the possibility of designing different hybrid materials for the detection and elimination of neurotoxic agents. Specifically, our aim was:

- To design and to synthesize gated sensor systems being able to detect nerve agents mimics through a colorimetric response.
- To design hybrid materials able to eliminate nerve agents simulants.
- Characterization of new hybrid systems by the usual techniques used in material chemistry for hybrid organic-inorganic solids.
- Evaluate the sensing or hydrolizing abilities of the prepared materials in the presence of the corresponding organophosphorous compounds.

## 3.3 **Design of the systems**

### *3.3.1 Design of neurotoxic agents responsive gated material*

A mesoporous MCM-41 phase was first loaded with the dye tris(2,2'-bipyridyl)ruthenium(II) chloride ($[Ru(bipy)_3]Cl_2$) and was then capped with bis(2-hydroxyethyl)aminopropyltriethoxysilane (HET) groups. The HET moieties anchored on the external surface were expected to inhibit the release of the dye by forming a thick hydrogen-bonding network. The signalling paradigm relies on the nucleofilic substitution reaction of the nerve agents simulants with the hydroxyl groups. The subsequent rupture of the hydrogen bond network would allow the delivery of the dye (see figure 6).

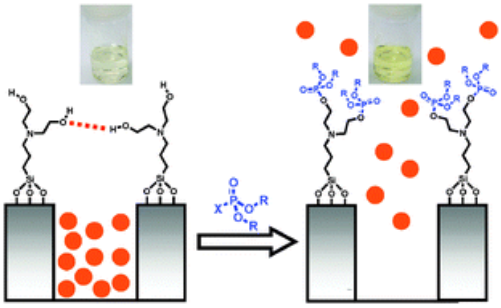

**Figure 6.** Schematic representantion of the sensing material and the sensing paradigm. In the presence of nerve agents mimics, these compounds react with the hydroxyl moieties on the gate molecule, avoiding the formation of the hydrogen bond layer and, thus, allowing the release of the cargo. *[Chem. Commun., 2011, 47, 8313–8315] - Reproduced by permission of The Royal Society of Chemistry*

### *3.3.2 Design of the hydrolyzing material*

Our aim was to prepare and use MCM-41 mesoporous silica nanoparticles (MSN) as catalysts for the hydrolysis of nerve agent simulants (DFP, DCP and DCNP). Our aim was accomplished by enhancing the nucleophilia of silanol moieties. Basic treatment induces the formation of silanolate moieties able to react with the organophosphorous compounds leading to the formation of non-toxic products (see figure 7).

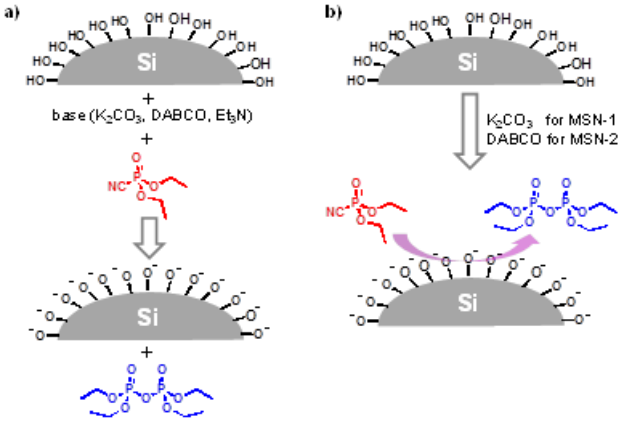


**Figure 7.** Schematic representation of the elaboration of the hydrolyzing materials and the hydrolysis process that takes place on the siliceous surface.

# *Selective opening of nanoscopic capped mesoporous inorganic materials with nerve agent simulants; an application to design chromo-fluorogenic probes*

*Inmaculada Candel,[a,b] Andrea Bernardos,[a,b] Estela Climent,[a,b] M. Dolores Marcos,[a,b,c] Ramón Martínez-Máñez,*[a,b,c] Félix Sancenón,*[a,b,c] Juan Soto,[a,b,c] Ana Costero,[a,d] Salvador Gil,[a,d] Margarita Parra[a,d]*

*[a] Centro de Reconocimiento Molecular y Desarrollo Tecnológico (IDM), Unidad Mixta Universidad Politécnica de Valencia-Universidad de Valencia, Spain.*

*[b] Departamento de Química, Universidad Politécnica de Valencia, Camino de Vera s/n, 46022, Valencia, Spain.*

*[c] CIBER de Bioingeniería, Biomateriales y Nanomedicina (CIBER-BBN).*

*[d] Departamento de Química Orgánica, Facultad de Ciencias Químicas, Universitat de Valencia, 46100 Burjassot, Valencia, Spain.*

***Received 9th May 2011, Accepted 31st May 2011***

***First published on the web 20 Jun 2011***

*Chem. Commun.*, *2011*, ***47***, *8313–8315*

*(Reproduced with permission of the Royal Society of Chemistry)*

**A hybrid nanoscopic capped mesoporous material that is selectively opened in the presence of nerve agent simulants has been prepared and used as a probe for the chromo-fluorogenic detection of these chemicals.**

Current international public awareness on criminal terrorism using chemical warfare agents (CWA) makes the development of quick and sensitive methods necessary to detect these lethal chemicals.[1] Among CWA, nerve agents are, perhaps, the most dangerous substances, and are highly toxic organophosphorous compounds developed as a by-product of insecticide research. Nerve agents can cause severe effects on human health as they can affect the central nervous system by inhibiting the nerve impulse.[2] Furthermore, the use of these lethal gases in terrorist attacks is quite silent; since they are colourless gases, their presence is not easily noticed until they have already been inhaled. For these reasons, certain detection systems have been developed, most of which are based on physical and enzymatic methodologies.[3] However, some of these procedures have their limitations, such as difficult portability and certain complexity in their use. An alternative to these methods is the development of fluorogenic and chromogenic chemosensors and reagents.[4] For instance, the chemosensors described in the literature make use of easily observable and measurable fluorescence and colour changes, and involve PET-based processes,[5] oximate-containing derivatives,[6] molecularly imprinted polymers,[7] nanoparticles,[8] carbon nanotubes,[9] cyclisation reactions in push-pull chromophores[10] and displacement assays.[11] In addition, the colorimetric and fluorimetric detection of nerve agents using organic-inorganic hybrid materials has recently been described.[12]

Given our concern to develop new bio-inspired strategies on inorganic supports for sensing applications,[13] we combined herein our experience in designing supramolecular hybrid materials, and we developed a new capped mesoporous support that is selectively opened in the presence of nerve agent mimics. Additionally, we used such a system for the selective detection of nerve agent simulants. Inspired by gated ion channels, the mechanism we propose is related with the selective opening of pores via the interaction of the target analyte with

the capping molecules at the pore outlets. As the pores are loaded with a dye, the opening results in a signalling event. To date, apart from some reports on pore blockage induced by the presence of certain analytes, very few examples of pore-opening protocols for sensing applications have been reported.[14]

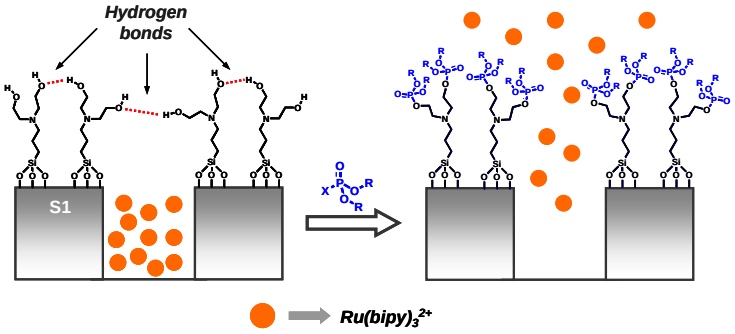


**Scheme 1.** Schematic representation of the sensing mechanism of **S1** in the presence of nerve agents.

An illustration of the sensing paradigm is shown in Scheme 1. A mesoporous MCM-41 phase was selected as the inorganic scaffolding. This solid provides suitable characteristics for this protocol, such as high loading capacity and easy surface functionalisation. The mesoporous support was first loaded with the dye tris(2,2'-bipyridyl)ruthenium(II) chloride ($[Ru(bipy)_3]Cl_2$) and was then capped with bis(2-hydroxyethyl)aminopropyltriethoxysilane (HET) groups. The HET moieties anchored on the external surface were expected to form a thick hydrogen-bonding network, especially in aprotic solvents inhibiting the delivery of the dye. The signalling paradigm relies on the reaction of the nerve simulants (the key) with the hydroxyl groups, the rupture of the hydrogen bond network (to unlock the gate) and the delivery of the dye.

The MCM-41 mesoporous support was prepared by using tetraethyl orthosilicate (TEOS) as the hydrolytic inorganic precursor, as well as surfactant hexadecyl-trimethylammonium bromide (CTABr) as the porogen species.[15] After removing the surfactant by calcination, the MCM-41 solid (2.8 nm of pore diameter) was obtained. The MCM-41 structure of the starting material was confirmed by X-Ray diffraction and transmission electron microscopy (TEM; see Supporting Information). The $N_2$ adsorption-desorption isotherms of the prepared phase show a typical type IV-curve with a specific surface area of 1140 $m^2g^{-1}$, a narrow pore size distribution and an average pore diameter of 2.8 nm. The inorganic support was first loaded with the $[Ru(bipy)_3]^{2+}$ complex as a suitable dye. Then the surface was functionalised with the HET groups. The dye $[Ru(bipy)_3]^{2+}$ was also confirmed to not react with nerve agent simulants. This synthetic procedure guarantees that the functional HET groups are preferentially attached to the outer surface rather than inside the pore walls, which are filled with the bulky $[Ru(bipy)_3]^{2+}$ dye. The final orange gated solid (**S1**) was filtered, intensively washed with acetonitrile and dried overnight at 36 ºC.

Figure 1 shows the powder X-ray pattern of the final **S1** material. **S1** displayed the expected MCM-41 phase features, indicating that the mesopore in the inorganic scaffolding was preserved throughout the filling process with the dye and the anchoring of the dialcohol HET derivative at the pore outlets. Figure 1b provides a TEM image of solid **S1** displaying the typical porosity of the MCM-41 phase. The $N_2$ adsorption-desorption isotherm of **S1** (see Supporting Information) was typical of gated mesoporous systems with filled mesopores and a significant decrease in the $N_2$ volume adsorbed was observed. Organic content was determined by thermogravimetric and elemental analyses. Solid **S1** contained 0.163 mmol of ruthenium complex / g $SiO_2$ and 0.653 mmol of HET moieties / g $SiO_2$. The ruthenium complex content was confirmed by a scanning electron microscopy (SEM) analysis (See Supporting Information).

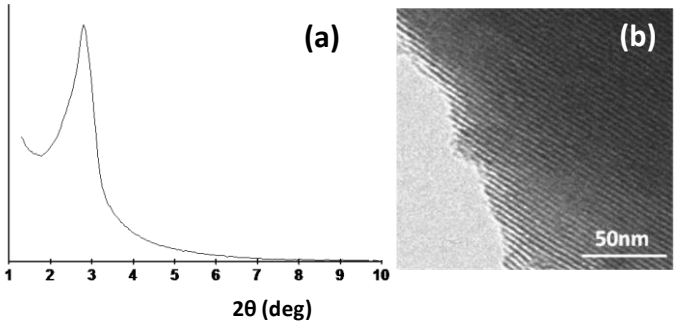


***Figure 1.*** *(a) Powder X-Ray pattern of solid* ***S1****. (b) TEM image of* ***S1****.*

Studies on the nerve agent simulants-induced uncapping paradigm were carried out in acetonitrile. This solvent was chosen because it is able to achieve a rather tight pore closure. Additionally, ruthenium dye presented suitable solubility in this medium. Nerve agent mimics are organophosphorous compounds with a very similar chemical structure and reactivity to the corresponding nerve agents, but with much lower toxicity. Some derivatives, such as diethyl chlorophosphate (DCP), diisopropyl fluorophosphate (DFP) and diethyl cyanophosphate (DCNP), have been traditionally used as simulants of nerve gases Sarin, Soman and Tabun. The reactivity of nerve agents and their simulants is related with the presence of an electrophilic phosphorus atom and good leaving groups (halogen atoms and cyanide). The reaction of the electron-deficient phosphorus atom in these systems with nucleophiles (alcohols in our case) induces the formation of phosphate derivatives. This reaction is the main force that governs the **S1** solid pore openings (see Scheme 1). Other organophosphorous derivatives were also tested (see Scheme 2).

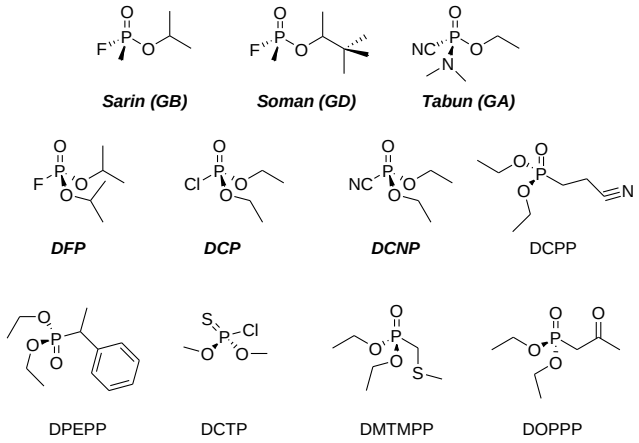


***Scheme 2.*** *Chemical structure of nerve agents Sarin, Soman and Tabun, nerve agent simulants and other organophosphorous derivatives.*

In a typical preliminary experiment, 5 mg of **S1** were suspended in 12.5 mL of acetonitrile in the presence of a target simulant (DCP). Delivery of the dye to the bulk solution was easily detected by monitoring the spin allowed d-π metal-to-ligand charge transfer (MLCT) transition band of the $[Ru(bipy)_3]^{2+}$ complex centred at 451 nm.[16] Figure 2 shows that the visible ruthenium dye band in the solution was largely enhanced in the presence of DCP due to the uncapping of the gated material as a result of the reaction of DCP with the HET groups. A very similar dye delivery was also observed in the presence of simulants DFP and DCNP. DCTP also induced a partial release of the ruthenium complex, but to a very low extent, whereas the other organophosphorous compounds tested (see Scheme 2) induced no response.

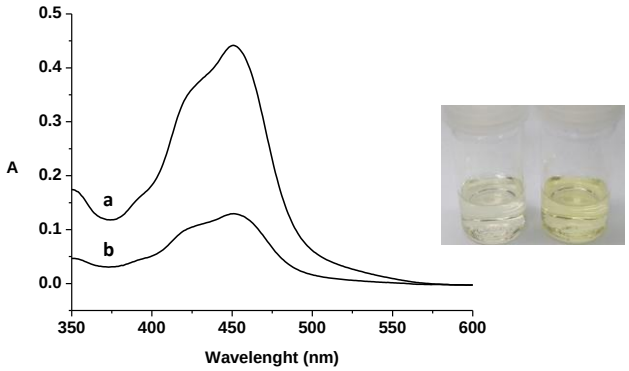


**Figure 2.** Absorption spectrum of the acetonitrile suspensions of **S1** in the presence of DCP (a) and in the absence of simulant (b). The photograph shows the colour modulation in both the absence (left) and presence of DCP (10 mM) at 5 minute post-addition.

In order to prove the proposed sensing mechanism, **S1** was reacted with an excess of DCP in acetonitrile to obtain the corresponding solid **S1-e**. In a second step, EDX and MAS $^{31}$P NMR studies were done on this solid to confirm that the phosphorylation reaction, responsible for the rupture of the hydrogen bonding network and dye delivery, occurred. The SEM analysis using Energy Dispersive X-ray spectroscopy (EDX, 20 kV) on solid **S1-e** revealed the presence of phosphorus (1.02 mmol P/g $SiO_2$), indicating efficient phosphorylation of the hydroxyl groups of the HET moiety. By considering the hydroxyl content in **S1** (1.30 mmol/g $SiO_2$), it was estimated that ca. 80% of the OH groups were phosphorylated. Furthermore, MAS $^{31}$P-NMR studies on **S1-e** showed a broad singlet in the 1-2 ppm interval, indicative of the presence of phosphate groups, which is also in agreement with the phosphorylation of the HET scaffolding (see Supporting Information).

Further studies were carried out with simulant DCP. For instance, Figure 3 shows the spectrophoto- and fluorimetric titration curves for **S1** in acetonitrile in the

presence of DCP. The increased intensity in the emission band of the $[Ru(bipy)_3]^{2+}$ dye was proportional to the DCP concentration, which is in agreement with the above-described assisted uncapping protocol. A simple chromogenic titration allowed the detection of DCP down to ca. 15 ppm, whereas the use of fluorometric standard procedures permitted the detection of DCP at concentrations lower than 0.1 ppm (see Figure 3). Similar studies were also carried out with DFP and DCNP, and similar detection limits were found for these simulants.

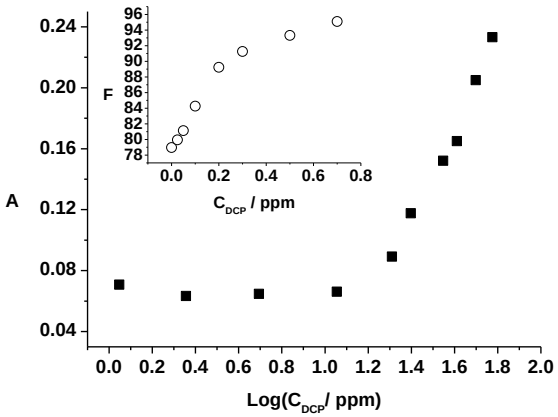


**Figure 3.** Spectrophotometric titration curves for $[Ru(bipy)_3]^{2+}$ delivery monitored at 451 nm in the acetonitrile suspensions of **S1** in the presence of increasing amounts of nerve agent simulant DCP. Inset: titration curve obtained from monitoring the emission intensities for the $[Ru(bipy)_3]^{2+}$ dye at 615 nm ($\lambda_{exc}$ = 451 nm).

Additionally based on this proof-of-principle, after studying the detection of nerve agents in solution, we extended our research by including the possibility of using the **S1** material for nerve agent detection in the vapour phase. To test this possibility, acetonitrile suspensions of gated mesoporous solid **S1** (5 mg/12.5 mL) were exposed to air containing 50 ppm of DCP for 30 minutes. In this scenario, DCP vapours partially dissolved in the **S1** acetonitrile suspension, inducing the release of the $Ru(bipy)_3^{2+}$ dye which indicated the presence of DCP (see Supporting Information).

In summary, a novel approach for the colorimetric and fluorimetric sensing of nerve agent mimics using hybrid materials functionalised with gate-like scaffoldings is reported. The presence of nerve agent simulants in acetonitrile suspensions of the hybrid material induces pore opening with the subsequent release of an entrapped dye. The use of mesoporous scaffoldings, which can be loaded with a variety of dyes and fluorophores, and functionalised on the outer surface with tailor-made organic moieties acting as molecular gates, makes this approach appealing and versatile for the design of supports that can be selectively opened in the presence of target substrates. We believe that the design of similar capped materials, which could be selectively opened by nerve agents, could be applied not only in sensing procedures, but also to develop advanced remediation supports or smart alarm systems.

Financial support from the Spanish Government (project MAT2009-14564-C04-01 and -02) and Generalitat Valenciana (project PROMETEO/2009/016) is gratefully acknowledged. I. C. thanks the UPV for her Fellowship. SCSIE (Universidad de Valencia) is gratefully acknowledged for all the equipment employed.

### *References*

1. H. H. Hill, Jr., S. J. Martin, *Pure Appl. Chem*., **2002**, *74*, 2281.
2. S. M. Somani, Chemical Warfare Agents, Acadenic Press, San Diego, **1992**.
3. L. M. Eubanks, T. J. Dickerson, K. D. Janda, *Chem. Soc. Rev.*, **2007**, *36*, 458.
4. S. Royo, R. Martínez-Máñez, F. Sancenón, A. M, Costero, M. Parra, S. Gil, *Chem. Commun.*, **2007**, 4839.
5. (a) K. A. Van Houten, D. C. Heath, R. S. Pilato, *J. Am. Chem. Soc.*, **1998**, *120*, 12359. (b) S. – W. Zhang, T. M. Swager, *J. Am. Chem. Soc.*, **2003**, *125*, 340. (c) T. J. Dale, J. Rebek Jr., *J. Am. Chem. Soc.*, **2006**, *128*, 4500. (d) S. Bencic-Nagale, T. Sternfeld, D. R. Walt, *J. Am. Chem. Soc.*, **2006**, *128*, 5041.
6. (a) K. J. Wallace, J. Morey, V. M. Lynch, E. V. Anslyn, *New. J. Chem.*, **2005**, *29*, 1469. (b) K. J. Wallace, R. I. Fagbemi, F. J. Folmer-Andersen, J. Morey, V. M. Lynch, E. V. Anslyn, *Chem.*

*Commun.*, **2006**, 3886. (c) S. Han, Z. Xue, Z. Wang, T. B. Wen, *Chem. Commun.*, **2010**, *46*, 8413.

7. (a) A. L. Jenkins, S. Y. Bae, *Anal. Chim. Acta*, **2005**, *542*, 32. (b) G. E. Southard, K. A. Van Houten, E. W. Ott Jr., G. M. Murray, *Anal. Chim. Acta*, **2007**, *581*, 202.
8. V. Pavlov, Y. Xiao, I. Willner, *Nano Lett.*, **2005**, *5*, 649.
9. L. Kong, J. Wang, T. Luo, F. Meng, X. Chen, M. Ll, J. Liu, *Analyst*, **2010**, *136*, 368.
10. (a) A. M. Costero, S. Gil, M. Parra, P. M. E. Mancini, R. Martínez-Máñez, F. Sancenón, S. Royo, *Chem. Commun.*, **2008**, 6002. (b) A. M. Costero, M. Parra, S. Gil, R. Gotor, P. M. E. Mancini, R. Martínez-Máñez, F. Sancenón, S. Royo, *Chem. Asian J.*, **2010,** *5*, 1573.
11. D. Knapton, M. Burnworth, S. J. Rowan, C. Weder, *Angew. Chem. Int. Ed.*, **2006**, *45*, 5825.
12. E. Climent, A. Martí, S. Royo, R. Martínez-Máñez, M. D. Marcos, F. Sancenón, J. Soto, A. M. Costero, S. Gil, M. Parra, *Angew. Chem. Int. Ed.*, **2010**, *49*, 5945.
13. (a) A. Bernardos, E. Aznar, M. D. Marcos, R. Martínez-Máñez, F. Sancenón, J. Soto, J. M: Barat, P. Amorós, *Angew. Chem. Int. Ed.*, **2009**, *48*, 5884. (b) A. Bernardos, L. Mondragón, E. Aznar, M. D. Marcos, R. Martínez-Máñez, F. Sancenón, J. Soto, J. M. Barat, E. Pérez-Payá, C. Guillem, P. Amorós, *ACS Nano*, **2010**, *11*, 6353. (c) E. Climent, R. Martínez-Máñez, F. Sancenón, M. D. Marcos, J. Soto, A. Maquieira, P. Amorós, *Angew. Chem. Int. Ed.*, **2010**, *49*, 7281.
14. (a) E. Climent, A. Bernardos, R. Martínez-Máñez, A. Maquieira, M. D. Marcos, N. Pastor-Navarro, R. Puchades, F. Sancenón, J. Soto, P. Amorós, *J. Am. Chem. Soc.*, **2009**, *131*, 14075. (b) E. Climent, M. D. Marcos, R. Martínez-Máñez, F. Sancenón, J. Soto, K. Rurack, P. Amorós, *Angew. Chem. Int. Ed.*, **2009**, *48*, 8519.
15. S. Cabrera, J. El Haskouri, C. Guillem, J. Latorre, A. Beltrán, D. Beltrán, M. D. Marcos, P. Amorós, *Solid State Sci.*, **2000**, *2*, 405.
16. (a) F. Felix, J. Ferguson, H. U. Guedel, A. Ludi, *J. Am. Chem. Soc.*, **1980**, *102*, 4096. (b) F. E. Lytle, D. M. Hercules, *J. Am. Chem. Soc.*, **1969**, *91*, 253.

*Chem. Commun.*, *2011*, ***47***, *8313–8315*

## *SUPPORTING INFORMATION*

# *Selective opening of nanoscopic capped mesoporous inorganic materials with nerve agent simulants; an application to design chromo-fluorogenic probes.*

Inmaculada Candel, Andrea Bernardos, Estela Climent, M. Dolores Marcos, Ramón Martínez-Máñez, Félix Sancenón, Juan Soto, Ana Costero, Salvador Gil, Margarita Parra

***Chemicals***

The chemicals tetraethylorthosilicate (TEOS) (98%), *n*-cetyltrimethylammonium bromide (CTABr) (≥99%), sodium hydroxide (≥98%), triethanolamine ($TEAH_3$) (≥99%), tris(2,2'-bipyridyl)dichlororuthenium(II) hexahydrate ($[Ru(bipy)_3]Cl_2{\cdot}6H_2O$) (100%), 3-[Bis(2-hidroxyethyl)amino]propyltriethoxysilane (HET) (65% in Ethanol), diethyl(2-cyanoethyl)phosphonate (**DCPP**) (95 %), diethyl 1-phenylethyl phosphonate (**DPEPP**) (98%), dimethyl chlorothiophosphate (**DCTP**) (97%), diethyl(methylthiomethyl)phosphate (**DMTMPP**) (96%), diethyl chlorophosphate (**DCP**) (97%), diethyl(2-oxopropyl)phosphonate (**DOPPP**) (96%), diisopropyl fluorophosphate (**DFP**) (99%) and diethyl cyanophosphate (**DCNP**) (≥90%) were provided by Aldrich and used as received. Analytical-grade solvents were acquired from Scharlab (Barcelona, Spain). All the reagents were used as received.

***General Techniques***

Powder XRD, TG analysis, elemental analysis, EDX microscopy and $N_2$ adsorption-desorption techniques were employed to characterise the prepared materials. UV-visible and fluorescence spectroscopy were used to study the controlled release behaviour of synthesised materials. Powder X-ray diffraction measurements were performed on a Philips D8 Advance diffractometer using Cu $K_\alpha$ radiation. The thermo-gravimetric analysis were carried out on a TGA/SDTA 851e Mettler Toledo balance, using an oxidant atmosphere (air, 80 mL/min) with a heating programme consisting in a heating ramp of 10$^o$C per minute from 393 K to 1273 K, and an isothermal heating step at this temperature for 30 minutes. The elemental analysis was performed in a CE Instrument EA-1110 CHN Elemental Analyser. The SEM analysis was performed with a JSM-6300 scanning microscope. TEM images were obtained with a 100 kV Philips CM10 microscope. $N_2$ adsorption-desorption isotherms were recorded on a Micromeritics ASAP2010 automated sorption analyser. Samples were degassed overnight at 120$^o$C in vacuum. The specific surface areas were calculated from the adsorption data in the low pressures range using the BET model. Pore size was determined following

the BJH method. UV-visible spectroscopy was carried out with a Lambda 35 UV/vis spectrometer (Perkin-Elmer Instruments). Fluorescence spectroscopy was carried out on a Felix 32 Analysis Version 1.2 (Build 56) PTI (Photon Technology International). MAS $^{31}$P-NMR spectra were measured in a Bruker AVIII, 400 MHz WB, equipped with a 4 mm DVT-CPMAS probe.

***Synthesis of the mesoporous silica support***

The molar ratio of the reagents in the mother liquor was fixed to 7 $TEAH_3$: 2 TEOS: 0.52 CTABr: 0.5 NaOH: 180 $H_2O$. In a typical synthesis leading to the MCM-41 pure silica, 4.67 g of CTABr (*n*-cetyltrimethylammonioum bromide) were added at 118$^o$C to a solution of $TEAH_3$ (25.76 g) containing 0.012 mol of NaOH and 0.049 mol of a silatrane derivative (e.g., 11 mL of TEOS were added at 70$^o$C to $TEAH_3$, e.g., in the form of Si(TEA)($TEAH_2$), where TEA is the fully deprotonated ligand). Then, 80 mL of deionised water were added with vigorous stirring at 70$^o$C. After a few minutes, a white suspension resulted. This mixture was aged at room temperature overnight. The resulting powder was collected by filtration and washed with water. Finally, the solid was dried at 70$^o$C (MCM-41 as synthesised). To prepare the final porous material (MCM-41), the as-synthesized solid was calcined at 550$^o$C for 5 h to remove the template.

***Synthesis of S1***

In a typical synthesis, 0.9 g of template-free MCM-41 and 0.8 mmol/g MCM-41 (0.54 g) of $[Ru(bipy)_3]Cl_2{\cdot}6H_2O$ were suspended in 50 mL of acetonitrile in a round-bottomed flask. To remove the adsorbed water, 10 mL of acetonitrile were distilled using a Dean-Stark set-up. After stirring 24 h at room temperature, 10 mmol/g MCM-41 of Bis(2-hidroxyethyl)aminopropyltriethoxysilane (1.27 ml) were added and the mixture was stirred for 5.5 h at room temperature. The obtained solid was filtered, washed with acetonitrile and dried overnight (38$^o$C).

***Material Characterisation***

MCM-41 as-synthesised, MCM-41 and **S1** materials were characterised by standard techniques. Figure SI-1 shows the powder X-ray patterns of the solid MCM-41 as-synthesised (without calcination), calcined MCM-41 and **S1**. Powder XRD of siliceous MCM-41 as-synthesised shows four low-angle reflections that are typical of the hexagonal ordered array, which can be indexed as (100), (110), (200), and (210) Bragg peaks. A significant shift of the (100) reflection and a broadening of the (110) and (200) peaks in the XRD powder of the MCM-41 calcined sample are clearly seen. This corresponds to an approximate cell contraction of ca. 6-8 Å during the calcination step. Despite this clear partial order loss, the observation of the overlapped (100) and (200) reflections indicates that certain relative mesopore symmetry is preserved after calcination. Figure SI-1 also depicts a curve that corresponds to **S1**. For this solid, reflections (110) and (200) are lost, most likely because of a reduction of contrast because of the pore voids becoming filled with the ruthenium complex. Nevertheless, the clear presence of the (100) peak in this pattern suggests that the loading process with the $[Ru(bipy)_3]^{2+}$ complex, and the additional functionalisation with dialcohol, have not substantially modified the mesoporous MCM-41 support. Preservation in the final functionalised solids of the mesoporous structure was also confirmed by the TEM analysis (see Figure 1b in the manuscript) in which the typical hexagonal porosity of the MCM-41 matrix can be clearly observed as alternate black and white stripes.

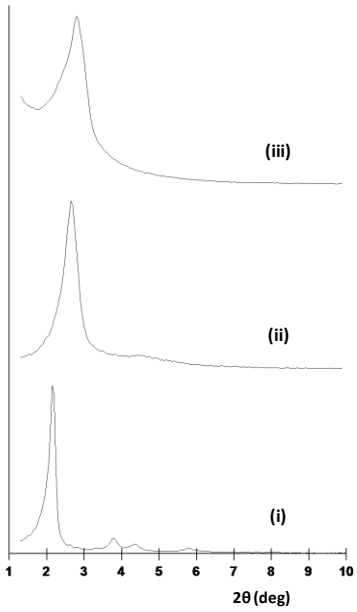


**Figure SI-1**. Powder X-Ray diffractograms showing X-Ray patterns of the MCM-41 scaffolding as synthesised (i), MCM-41 after the calcination process (ii) and of final solid **S1** (iii).

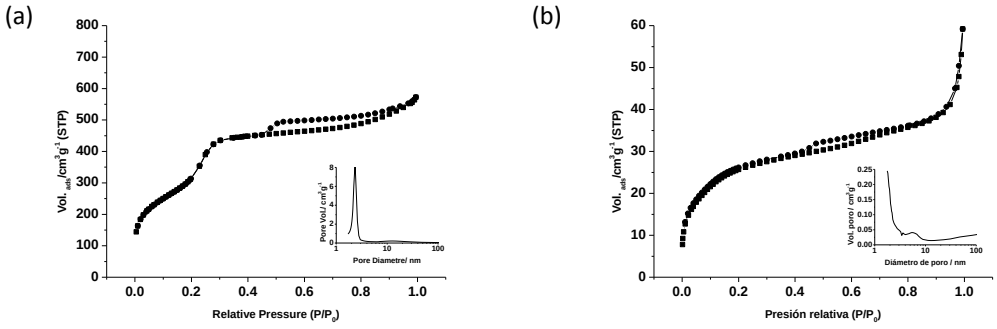


**Figure SI-2.** Nitrogen adsorption-desorption isotherms for (a) MCM-41 mesoporous material (b) **S1**.

The $N_2$ adsorption-desorption isotherms of the MCM-41 calcined material show a typical curve for these mesoporous solids; i.e., an adsorption step at the intermediate $P/P_0$ value (0.2-0.35). This curve corresponds to a type IV

isotherm in which the observed step can be related to the nitrogen condensation inside the mesopores through capillarity (see Figure SI-2). The mentioned isotherms present a slight hysteresis loop in a wide pressure range, which could probably be attributed to a textural-like porosity among particles. The application of the BET model resulted in a value for the total specific surface of 1140 $m^2/g$. From the XRD, porosimetry and TEM studies, the $a_0$ cell parameter (3.85 nm), the pore diameter (2.8 nm) and a value for wall thickness of 1.05 nm can be calculated. The $N_2$ adsorption-desorption isotherms of **S1** (see again Figure SI-2) are typical of mesoporous systems with filled mesopores, and the adsorbed $N_2$ volume significantly decreased. In fact, these solids present flat curves when compared (on the same scale) to those of the MCM-41 parent material, indicating significant pore blocking and the subsequent absence of appreciable porosity. This result was as expected considering that these solids have a high dye content filling the pores. The specific surface values, pore volumes and pore sizes for MCM-41 and **S1** are presented in Table SI-1.

**Table SI-1.** BET-specific surface values, pore volumes and pore sizes calculated from the $N_2$ adsorption-desorption isotherms for selected materials.

| | $S_{BET}$ ($m^2g^{-1}$) | Pore Volume ($cm^3g^{-1}$) | Pore Size (nm) |
|---|---|---|---|
| MCM-41 | 1139 | 0.98 | 2.8 |
| **S1** | 96 | 0.07 | - |

The content of $[Ru(bipy)_3]^{2+}$ complex and bis(2-hidroxyethyl)aminopropyltriethoxysilane in the prepared solid **S1** was determined by elemental and thermogravimetric measurements and amounts to 0.163 mmol/g $SiO_2$ and 0.653 mmol/g $SiO_2$, respectively. The heating ramp used to perform the thermogravimetric analysis consisted in a heating ramp of 10°C per minute from 120°C to 1000°C, and an isothermal step at this temperature for 30 minutes.

Examination of the thermogravimetric curve and its first derivative shows four weight loss steps (see Figure SI-3). One weight loss of 9.08% corresponding to solvents elimination (T < 200°C); another weight loss of 7.04% due to decomposition of the organic groups anchored on the siliceous surface (200 < T < 380 °C); a third weight loss of 7.77 % that can be assigned to the decomposition of the ruthenium complex (380 < T < 520 °C); finally, a loss of a 2.25 % owing to the condensation of silanols on the siliceous surface (T > 500°C).

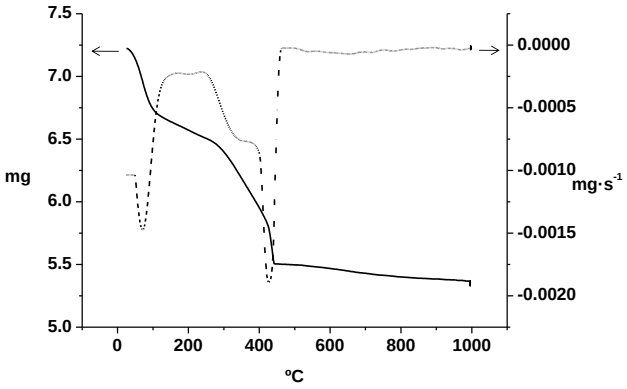


**Figure SI-3.** Thermogravimetric curve (straight line) and its derivative (dashed line) obtained from the thermogravimetric analysis of **S1**.

The amount of ruthenium complex in solid **S1**, measured by the SEM analysis using an energy dispersive X-ray spectroscopy (EDX, 5000x magnification, 20 kV), was 0.157 ± 0.018 mmol/g $SiO_2$. This value well matches the content obtained by the thermogravimetric measurements (0.163 mmol/g $SiO_2$).

***The Chromogenic Response Mechanism***

The sensing mechanism in the presence of nerve agent simulants relies on the breaking of the hydrogen bond network in solid **S1** upon the phosphorylation of the hydroxyl groups. In order to prove the proposed sensing mechanism, **S1** was reacted with an excess of DCP to obtain the corresponding solid **S1-e**.

This solid (**S1-e**) was studied by SEM analysis using energy dispersive X-ray spectroscopy (EDX, 20 kV). EDX measurements indicated the presence of a significant amount of phosphorus atoms on the surface of **S1-e** material, suggesting an efficient reaction between DCP and the hydroxyl moieties of the HET groups. As seen in Table SI-2, the OH content in **S1-e** determined by the thermogravimetric analysis is 1.30 mmol / g $SiO_2$, whereas the phosphorus content measured by SEM-EDX is 1.02 mmol / g $SiO_2$. By bearing in mind these contents, the reaction between DCP and HET offers an 80% yield. Furthermore, MAS $^{31}$P-NMR of solid **S1-e** shows a broad singlet centred in the 1-2 ppm range, which is a typical signal for phosphate groups (see Figure SI-4).

**Table SI-2.** Phosphorous content (from the SEM-EDX analysis) and OH groups content (from the thermogravimetric analysis) for solid **S1-e**.

| | mmol P/g $SiO_2$ | mmol OH/g $SiO_2$ |
|---|---|---|
| SEM-EDX | 1.02 ± 0.08 | - |
| TGA | - | 1.30 |

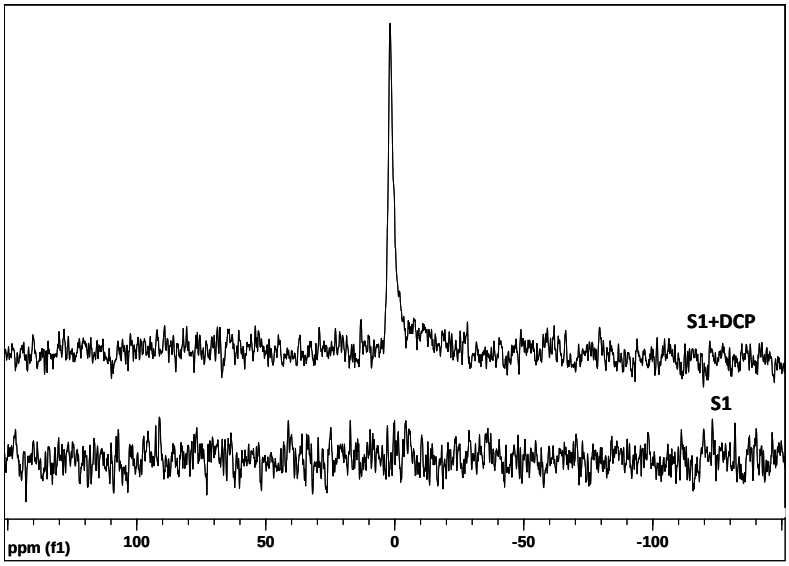


**Figure SI-4.** MAS $^{31}$P-NMR spectra of solid **S1** and solid **S1** in the presence of DCP.

As regards the sensing process steps' efficiency, EDX and MAS $^{31}$P-NMR spectra show an 80% yield for the reaction between the hydroxyl moieties in the HET groups and the DCP, whereas 50% of the ruthenium complex (measured by UV-visible) was released at 5 minutes after DCP addition.

***Dye release studies***

The release of the $[Ru(bipy)_3]^{2+}$ complex to the solution in the presence of several nerve agent simulants (see Scheme 2 in the paper) was studied. In a typical experiment, 5 mg of **S1** were suspended in 12.5 mL of the corresponding simulant solution in acetonitrile. This suspension was used to evaluate the gate-like effect by studying the dye release from the pore voids of the functionalised material. The delivery of the $[Ru(bipy)_3]^{2+}$ complex from the pore voids to the solution was easily monitored via the d-π metal-to-ligand charge transfer (MLCT) transition band of this complex centred at 451 nm (see Figure 2 in the paper).

***Detection limit studies***

In addition, the detection limit of **S1** solid in the presence of DFP, DCP and DCNP was measured. In order to carry out these measurements, 1.5 mg of solid **S1** were suspended in 11.25 mL of different solutions at increasing concentrations of the corresponding simulants (1, 2, 5, 11, 15, 20, 25, 35, 40, 50 and 60 ppm). Different aliquots (2 mL) were taken and filtered after 15 minutes. The delivery of the $[Ru(bipy)_3]^{2+}$ complex from the pore voids to the solution was easily monitored via the d-π metal-to-ligand charge transfer (MLCT) transition band of this complex centred at 451 nm (see Figure SI-5-a). To perform further fluorescence studies, 1.5 mg of **S1** were suspended in 11.25 mL of different solutions at increasing concentrations of DCP (0.025, 0.05, 0.1, 0.2, 0.3, 0.5 and 0.7 ppm). Different aliquots (2 mL) were taken and filtered after 15 minutes. The dye release was monitored via the emission band of the $[Ru(bipy)_3]^{2+}$ complex centred at 610 nm (excitation at 451 nm) (see Figure SI-5-b).

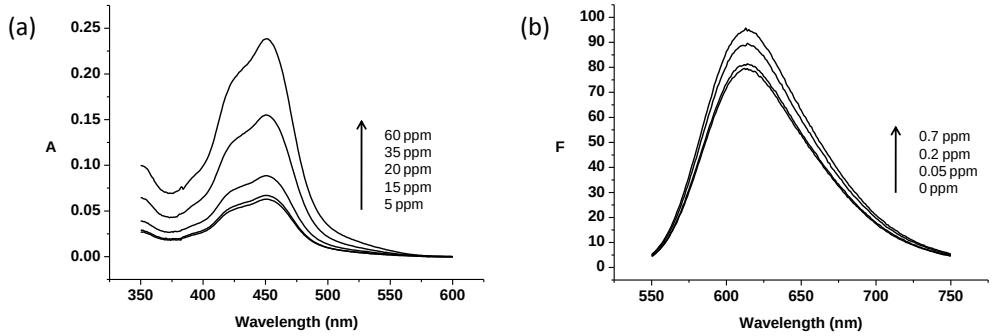


**Figure SI-5**. (a) Absorption spectrum of acetonitrile suspensions of **S1** in the presence of increasing concentrations of DCP. (b) Fluorescence emission spectrum (excitation at 451 nm) of acetonitrile suspensions of **S1** in the presence of increasing concentrations of DCP.

### *Dye release studies in the presence of other organophosphorous compounds*

The followed procedure is analogous to that described in the dye release studies. Briefly, 5 mg of **S1** were suspended in 12.5 mL of a solution ($10^{-3}$ mol $dm^{-3}$ in acetonitrile) of the following organophosphorous compounds (see Scheme 2 in the paper for their chemical structures): diethyl(2-cyanoethyl)phosphonate (**DCPP**), diethyl 1-phenylethyl phosphonate (**DPEPP**), dimethyl chlorothiophosphate (**DCTP**), diethyl(methylthiomethyl)phosphate (**DMTMPP**) and diethyl(2-oxopropyl)phosphonate (**DOPPP**). Different aliquots (2 mL) were separated and filtered after 15 minutes. The dye delivery from the pore voids to the solution was monitored via the d-π metal-to-ligand charge transfer (MLCT) transition band of the $[Ru(bipy)_3]^{2+}$ complex centred at 451 nm. Figure SI-6 shows the absorbance of the ruthenium band centred at 451 nm in the acetonitrile suspensions of **S1** upon addition of selected organophosphorous compounds. As seen, only DCP induced pore opening release the ruthenium complex, whereas the other organophosphorous compounds induced a negligible release.

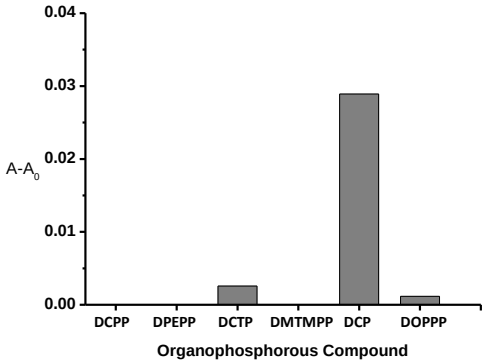


**Figure SI-6.** Absorbance at 451 nm (ruthenium complex band) of the acetonitrile suspensions of **S1** in the presence of organophosphorous compounds (1 mM).

### *Vapour phase studies*

Solid **S1** was also tested as a chromogenic material for the sensing of nerve agent simulants in the vapour phase. For this purpose, acetonitrile suspensions **S1** (5 mg / 12.5 mL) were exposed to air containing 50 ppm of DCP for 30 minutes. In this situation, the vapours of DCP partially dissolved in the acetonitrile suspension of **S1,** inducing the release of the $Ru(bipy)_3^{2+}$ dye, which indicates the presence of DCP in the gas phase.

# *Hydrolysis of DCNP (a Tabun mimic) catalysed by mesoporous silica nanoparticles.*

*Inmaculada Candel,[a,b,c] , María D. Marcos,[a,b,c] Ramón Martínez-Máñez,*[a,b,c] Félix Sancenón,[a,b,c] Ana M. Costero,*[a,d] Margartita Parra,[a,d] Salvador Gil,[a,d] Carmen Guillem,[e] Francisco Pérez-Pla[e] and Pedro Amorós[e]*

*a Centro de Reconocimiento Molecular y Desarrollo Tecnológico (IDM), Unidad Mixta Universidad de Valencia-Universidad Politécnica de Valencia.*

*bDepartamento de Química, Universidad Politécnica de Valencia. Camino de Vera s/n, 46022 Valencia, Spain.*

*c CIBER de Bioingeniería, Biomateriales y Nanomedicina (CIBER-BBN).*

*d Departamento de Química Orgánica, Universitat de València, Dr. Moliner 50, 46100, Burjassot, Valencia, Spain.*

*e Instituto de Ciencia de los Materiales (ICMUV), Universidad de Valencia, P.O. Box 22085, 46071 Valencia, Spain.*

**Submitted**

The hydrolysis of diethylcyanophosphonate, DCNP (a Tabun simulant) in the presence of mesoporous silica nanoparticles (MSN) has been studied in acetonitrile:water (99.5:0.5 v/v) mixtures using $^{31}$P-NMR as a suitable technique to follow the DCNP degradation. MSN alone was not capable to induce DCNP hydrolysis, yet MSN in combination with the presence of the bases potassium carbonate, triethylamine or DABCO enhanced DCNP degradation. When MSN was used combined with $K_2CO_3$, a hydrolysis of ca. 95% of the initial DCNP after 60 minutes was observed. In the presence of DABCO, MSN was able to induce the hydrolysis of ca. 90% of DCNP after the same time. However, the DCNP hydrolysis using MSN in the presence of $Et_3N$ was lower (ca. 30%). In the absence of nanoparticles, DCNP hydrolysis reached only ca. 30% for $K_2CO_3$ and DABCO and ca. 7% for $Et_3N$ after 60 min. Moreover, kinetic studies were also carried out with the use of solids MSN-1 and MSN-2 that were obtained by reaction of MSN with $K_2CO_3$ or DABCO. After the reaction the solids were isolated by centrifugation, washed with acetonitrile and dried. MSN-1 was able to hydrolyse DCNP in a similar way to that found with the MSN-$K_2CO_3$ mixture. However, MSN-2 nanoparticles induced a very low DCNP hydrolysis. From all these studies it was found that the main product of the DCNP hydrolysis is tetraethylpyrophosphate. The presence of diethyl phosphoric acid was also observed but at very low concentration. From kinetic data a catalytic mechanism is proposed.

**Introduction**

Chemical warfare agents (CWs) are classified in several groups; i.e. nerve agents, asphyxiant/blood agents, vesicant agents, choking/pulmonary agents, lachrymatory agents, incapacitating agents and cytotoxic proteins.[1] Among CWs, nerve gases are perhaps the most dangerous.[2] The development of nerve agents was a by-product of insecticide research and development. It was in early 1930s that German chemists first produced G-agents (Tabun (GA), Sarin (GB), Soman (GD) and Cyclosarin (GF)). Some years later further research resulted in discovery of new types of nerve agents; i.e. V-agents (VG, VM, VX, VE).

Due to its toxicity, nerve gases agents have been employed since their discovery as chemical weapons and even in the last years these poisonous compounds have been used in several terrorist acts as for instance in the subway attack in Tokyo in 1995, in the Iraq repression against Kurdish communities in 1988 and, very recently, in Syrian civil war. These compounds are strong inhibitors of the enzyme acetylcholinesterase inducing the accumulation of the neurotransmitter acetylcholine, thus, inhibiting nerve impulse.[3] The accumulation of acetylcholine produces a crisis of the nerve system characterized by convulsions, bradycardia, behavioral incapacitation, muscle weakness and respiratory failure that may lead to death.[4] Furthermore, the threat of these compounds as chemical weapons is enhanced by the fact they are colourless gases and their presence is not easily noticed until they have been already inhaled.

The easy fabrication of nerve gases (with severe environmental problems associated with spills and production) and their indiscriminate use by ambitious nations or by terrorist groups have boosted the efforts of the scientific community toward the detection and remediation of these deadly chemicals.[5]

Dealing with their detection, a variety of instrumental methods such as surface acoustic wave (SAW) devices,[6] enzymatic assays,[7] electrochemical,[8] interferometry[9] and gas chromatography coupled with mass spectrometry[10] have been extensively developed to detect nerve gases. More recently the design of chromo-fluorogenic chemical probes based on supramolecular concepts or in the use of hybrid silica-based organic-inorganic materials has freshly emerged in the last years.[11]

However, remediation of nerve gases is still a matter of concern and active research to find safe and effective methods to detoxify without endangering human life or the environment is currently underway.[12] Certain examples of compounds able to react with nerve gases to avoid their interaction with acetylcholinesterase and several methods to reactivate the poisoned enzyme have been reported.[13] Dealing with environmental decontamination,

experimental procedures such as electrolytic methods,[14] oxidative degradation on active sorbents,[15] catalytic[16] and biocatalytic[17] degradation methods,[18] atmospheric pressure plasma[19] and photolytic procedures[20] have been explored. Moreover, very recently, highly porous multifunctional metal oxide/hydroxide micro and nanoparticles,[21] clays,[22] metal-organic frameworks (MOFs)[23] and porous organic polymers (POPs)[24] have been also used as destructive adsorbents against nerve gases. Among these materials, microporous and mesoporous silicas are particularly attractive for nerve gases remediation.[25] These materials could be easily synthesized in different morphologies and pore sizes and show large surface areas (up to 1200 $m^2$ $g^{-1}$), are chemically inert and are easily functionalized through the use of the well-known alkoxysilane chemistries.[26] In this context, very recently, mesoporous silica materials have been used as scaffolds for the adsorption or encapsulation of decontaminant compounds or enzymes in order to prepare materials for environmental nerve gases degradation.[27] Besides, thermal decomposition of organophosphorous derivatives, previously adsorbed into zeolites, has also been reported.[28] Silica nanoparticles impregnated with reactive chemicals have been also prepared and used for the removal of sulfur mustard and the nerve gas simulant diethylchlorophosphate.[29]

From a chemical point of view, nerve gases are characterized by the presence of an electrophilic central phosphorus atom that is prone to suffer nucleophilic addition reactions with nucleophiles. In fact it is the reaction of the P atom with hydroxyl anions one of the paths of the degradation of nerve gases in the environment.[30]

Based in these concepts we were interested in testing the potential use of silica-based nanoparticles for the degradation of nerve gases. We envisioned that by using certain bases it would be possible to transform the silanol groups at the surface of silica on silanolate nucleophiles[31] that could react with these chemicals yielding non-toxic degradation products. With this idea in our aim, we report herein use of mesoporous silica nanoparticles (MSN) treated with different bases (i.e. potassium carbonate, triethylamine and DABCO) as potential new easy to prepare materials for the degradation of nerve gases. For our study we have

selected diethylcyanophosphonate (DCNP) as a suitable nerve agent simulant. DCNP has been typically used as model compound as it has similar reactivity but reduced toxicity when compared with the corresponding chemical warfare agent Tabun. The aim of the present study is to contribute to the design of simple remediation materials that could be of potential use in decontamination devices and filtration systems to remove toxic nerve gases from contaminated environments.

**Results and discussion**

**Design of the materials.** Nerve agent simulants are, from a chemically point of view, organic phosphates and phosphonates bearing good leaving groups. One of most remarkable chemical feature of these compounds is related with the presence of an electrophilic phosphorus atom that is prone to suffer nucleophilic attacks. In this work we have used MCM-41 mesoporous (MSN) silica nanoparticles as catalysts for the hydrolysis of the nerve agent Tabun simulant DCNP. The reactivity of the solids was enhanced via deprotonation of the silanol groups by using the bases $K_2CO_3$, DABCO and $Et_3N$.

MCM-41 mesoporous nanoparticles were prepared, via well-known procedures, from tetraethyl orthosilicate (TEOS) as inorganic precursor and *n*-cetyltrimethylammonium bromide (CTABr) as a porogen species.[32] The removing of the surfactant by calcination yielded the final MCM-41 mesoporous nanoparticles (MSN).

In a first step the hydrolysis of DCNP was carried out in acetonitrile:water (99.5:0.5 v/v) mixtures containing the silica nanoparticles (MSN), the base ($K_2CO_3$, DABCO and $Et_3N$) and the simulant. An illustrative picture of the hydrolysis procedure is shown in Scheme 1.

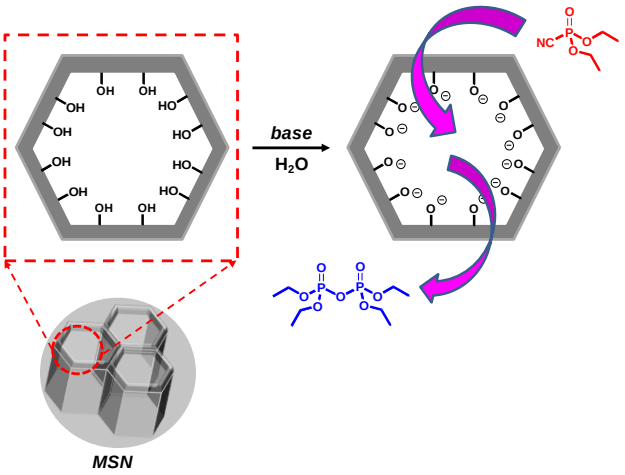


**Scheme 1.** Representation of the approach used for the hydrolysis of nerve agent simulants with mesoporous silica nanoparticles. MSN are previously deprotonated with certain bases and the materials used for the hydrolysis of the nerve agent simulant DCNP to give tetraethylpyrophosphate.

The above mentioned hydrolysis procedure required the suspension of the silica nanoparticles and the corresponding base in an organic solvent. Moreover, in order to simplify the procedure and, taking into account a possible application of the approach in remediation processes, we also prepared the materials MSN-1 and MSN-2 by treatment of MSN with $K_2CO_3$ and DABCO. For the preparation of these materials the MSN nanoparticles were treated with an aqueous solution of $K_2CO_3$ (for MSN-1) or with an acetonitrile solution of DABCO (for MSN-2). The suspensions were stirred at room temperature for 1 hour and then the solids were then centrifuged, washed with acetonitrile and dried at 60 ºC.

**Characterization of the materials.**

The prepared nanoparticles (MSN and MSN-1, and MSN-2) were characterized by standard solid state techniques. Figure 1 shows the PXRD patterns of the MCM-41 as synthesized, calcined MCM-41 nanoparticles (MSN), MSN-1 and MSN-2.

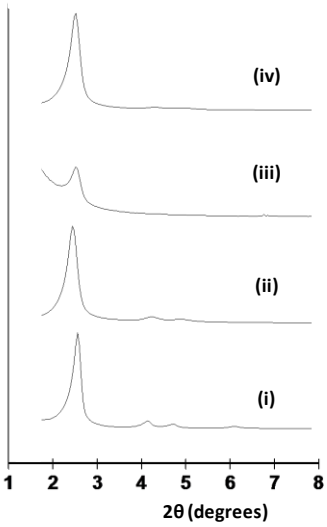


**Figure 1. P**XRD patterns for the nanoparticulated MCM-41 as-synthesized (i), calcined MCM-41 nanoparticles (MSN) (ii), MSN-1 (iii) and MSN-2 (iv).

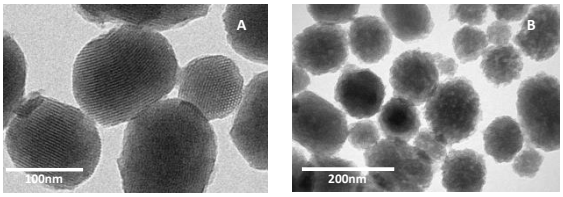


**Figure 2.** Representative Transmission Electron Microscopy (TEM) of MSN (A) and MSN-1 (B).

The PXRD of the mesoporous MCM-41 material as-synthesized (Figure 1, curve i) displayed the expected four peaks of a hexagonal ordered array indexed as (100), (110), (200), and (210) Bragg reflections. From the PXRD data, an $a_0$ cell parameter of 47 Å ($d_{100}$ spacing of 40.78 Å) was calculated. In curve ii, corresponding to the MCM-41 calcined sample (MSN), a significant shift of the (100) reflection in the PXRD is clearly observed. This displacement, together with the broadening of the (110) and (200) reflections, corresponds to an approximate cell contraction of 6–8 Å due to the condensation of silanol groups in the calcination step. Figure 1 also

depicts the PXRD patterns for solids MSN-1 and MSN-2. For these materials, reflections (110) and (200) were lost, most likely due to partially order loss induced by the basic treatment. In case of MSN-1 the treatment with $K_2CO_3$ induced the formation of amorphous inorganic silica and/or potassium silicate that is deposited on the mesoporous surface, thus, blocking the pores (*vide infra*) and reducing contrast which was not observed in case of MSN-2, presumably due to the fact that DABCO is not as strong base as $K_2CO_3$ and also to the presence of $K^+$ cations; nevertheless, the characteristic structure of MCM-41 materials is preserved as it is shown by the presence of the $d_{100}$ peak in the PXRD patterns of both MSN-1 and MSN-2.

The prepared materials were also studied by Transmission Electron Microscopy (TEM) images (see Figure 2). As expected, MSN was obtained as spherical particles showing a mean diameter of 100-150 nm. As it can be seen in the image, MSN shows the typical mesoporous structure of MCM-41 materials. From the images of MSN-1, it is apparent that the basic treatment induces amorphous silica particles to adsorb onto the external surface of MSN-1, which was not observed for MSN-2 (data not shown). DLS (Dynamic Light Scattering) studies with MSN and MSM-1 were also carried out. As seen in Figure 3, a Gaussian distribution of sizes is observed. It was also confirmed that the particle size was not significantly modified after the basic treatment.

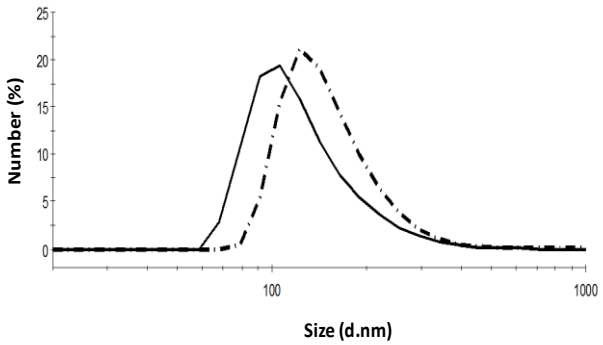


**Figure 3.** Statistical representation of particle size obtained by DLS (Dynamic Light Scattering) studies. The average size of nanoparticles of MSN (straight) was found to be ca. 130 nm whereas MSN-1 (dash) showed a mean diameter of 150 nm.

The $N_2$ adsorption–desorption isotherm of the nanoparticulated MCM-41 calcined material (MSN) is shown in Figure 4. A typical curve for this mesoporous support, consisting of an adsorption step at an intermediate $P/P_0$ value (0.1–0.3), is observed. This curve matches a type IV isotherm in which the observed step deals with nitrogen condensation inside the mesopores. The narrow pore distribution and the absence of a hysteresis loop in this interval suggest the existence of uniform cylindrical mesopores (pore diameter of 2.51 nm and pore volume of 0.59 $cm^3g^{-1}$ calculated by using the BJH model on the adsorption branch of the isotherm). Application of the BET model resulted in a value of 793.9 $m^2g^{-1}$ for the total specific surface. From the PXRD and porosimetry, the $a_0$ cell parameter (4.7 nm), the pore diameter (2.51 nm), and the wall thickness value of 2.19 nm were calculated. In addition to this adsorption step, a second feature is observed in the isotherm at a high relative pressure ($P/P_0$ 0.8), which corresponds to the filling of the large voids among the particles (0.35 $cm^3g^{-1}$ calculated by the BJH model) and must be considered a textural-like porosity. In this case, the curves show a characteristic H1 hysteresis loop and a wide pore size distribution. The $N_2$ adsorption–desorption isotherm of MSN-1 is typical of mesoporous systems with practically filled mesopores (see also Figure 4), since mesopores are filled with inorganic amorphous silica-based derivatives. Consequently, relatively low $N_2$ adsorbed volume (BJH mesopore volume 0.05 $cm^3g^{-1}$) and surface area (30 $m^2g^{-1}$) values were calculated, thus indicating effective pore blocking and the subsequent absence of appreciable mesoporosity. On the contrary, the structure of mesoporous particles treated with DABCO (MSN-2) showed a pore volume of 0.38 $cm^3g^{-1}$ and a specific surface area of 895.4 $m^2g^{-1}$. BET-specific surface values, mesopore volumes and mesopore sizes were calculated from the $N_2$ adsorption–desorption isotherms for MSN, MSN-1 and MSN-2 and are listed in Table 1.

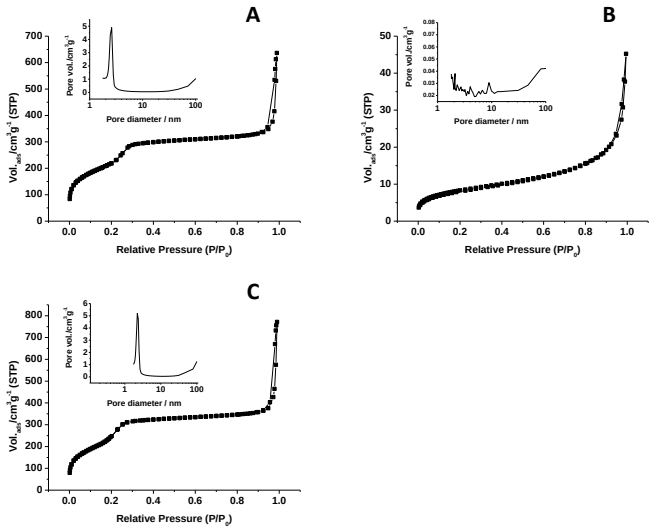


**Figure 4.** Nitrogen adsorption–desorption isotherms for (A) the MCM-41 mesoporous nanoparticles and (B) MSN-1 and (C) MSN-2.

**Table 1.** BET specific surface areas, pore volumes and pore sizes calculated from the $N_2$ adsorption-desorption isotherms.

| | **Mesopore Size (nm)** | **Mesopore volume ($cm^3g^{-1}$)** | **Large pore volume ($cm^3g^{-1}$)** | **BET surface area ($m^2g^{-1}$)** |
|---|---|---|---|---|
| **MSN** | 2.51 | 0.59 | 0.35 | 793.9 |
| **MSN-1** | - | - | 0.057 | 30 |
| **MSN-2** | 2.32 | 0.61 | 0.38 | 895.4 |

Figure 5 shows the $^{29}$Si-RMN spectra for MSN, MSN-1 and MSN-2. RMN data are in line with TEM and RX studies, confirming that the mesostructure remains in all solids. In fact as it can be seen the distribution of $Q^4$, $Q^3$, and $Q^2$ centers is maintained throughout in all materials.

Finally, the organic content in MSN-2 material (protonated DABCO acting as counterion of the deprotonated silanols) was calculated by thermogravimetric

analysis and it was found to be 0.85 mmol/g $SiO_2$. We also calculated the proportion Si/K on MSN-1 that was found to be Si/K=6.

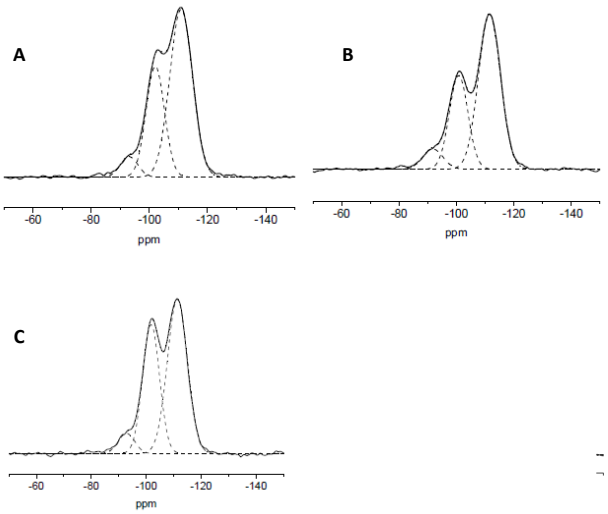


**Figure 5**. $^{29}$Si-RMN spectra of MSN shows the evolution of the $Q^2$ + $Q^3$ and T sites has not been significantly modified through the basic treatment MSN-1 (A, $Q^4$ 61.5%, $Q^3$ 32.7%, $Q^2$ 5.8%), MSN-1 (B, $Q^4$ 55.3%, $Q^3$ 31.3%, $Q^2$ 7.3%), MSN-2 (C, $Q^4$ 55. 3%, $Q^3$ 38.7%, $Q^2$ 6.0%).

**Hydrolysis studies**. As stated above, DCNP was selected as model nerve agent simulant. Hydrolysis studies were carried out in acetonitrile:water (99.5:0.5 v/v) solutions and the $^{31}$P-NMR technique was used to follow the reaction products and the kinetics of the reaction.

In a first step, the catalytic behaviour of the MSN nanoparticles in the absence of base was tested. In a typical experiment, MSN was suspended in acetonitrile:water (99.5:0.5 v/v) and then DCNP was added. $^{31}$P-NMR data showed the characteristic signal of the phosphorus atom of DCNP centred at -21.4 ppm that remained unchanged with time (data not shown) indicating that under these experimental conditions untreated MSN nanoparticles are unable to hydrolyse DCNP.

In the next step the catalytic behaviour of MSN nanoparticles in the presence of selected bases ($K_2CO_3$, DABCO and $Et_3N$) was studied. In a typical experiment 5 mg of MSN were introduced into an NMR tube containing acetonitrile:water (99.5:0.5 v/v) and 0.02 M of the corresponding base. Then DCNP was added and the kinetics was followed recording $^{31}$P-NMR spectra at different times for 1 h at room temperature.

The kinetic curves obtained are shown in Figure 6. As it can be seen, when $K_2CO_3$ was used as base combined with MSN, a hydrolysis of ca. 95% of the initial DCNP after 60 minutes was observed. The hydrolysis gives as main product organic pyrophosphate. This can be seen in Figure 7 that shows the $^{31}$P-NMR spectrum obtained with MSN and $K_2CO_3$. The initial signal centred at -21.4 ppm ascribed to the phosphorus atom on DCNP vanished progressively with the subsequent appearance of a resonance centred at -13.4 ppm that was assigned to the formation of an organic pyrophosphate.

In the presence of DABCO, MSN was able to induce the hydrolysis of ca. 90% of the added DCNP at 60 min. Finally, and as a clear contrast, the hydrolysis of DCNP observed for MSN in the presence of $Et_3N$ is lower (ca. 30%). In both cases the hydrolysis of DCNP also gives as main product organic pyrophosphate. The different DCNP hydrolysis degree obtained when using organic aliphatic amines (90% for MSN-DABCO and 30% for MSN-$Et_3N$) could not be ascribed to the different basicity of the bases because both have similar $pK_a$ values (8.82 and 9.00 for DABCO and $Et_3N$ in DMSO respectively). Probably, the different DCNP hydrolysis is related with the bigger size of $Et_3N$ when compared with that of DABCO. Molecular modelization studies using Hyperchem indicated that, considering both bases as spheres, the diameter of $Et_3N$ is about 6.6 Å, whereas that for DABCO was only 4.6 Å. Bearing in mind that the corresponding conjugated acid of the bases (i.e. DABCO-$H^+$ and $Et_3N$-$H^+$) would be located in the vicinity of the silanolate groups, it is expected that the lager is the counterion ($Et_3N$-$H^+$ larger than DABCO-$H^+$) the more inhibited would be the reaction of DCNP with to the nucleophilic silanolates, making hydrolysis slower.

Moreover, the crucial role played by MSN was demonstrated by the fact that, in the absence of nanoparticles, DCNP hydrolysis reached only ca. 30% for $K_2CO_3$ and DABCO and ca. 7% for $Et_3N$ after 60 min (see Figure 6).

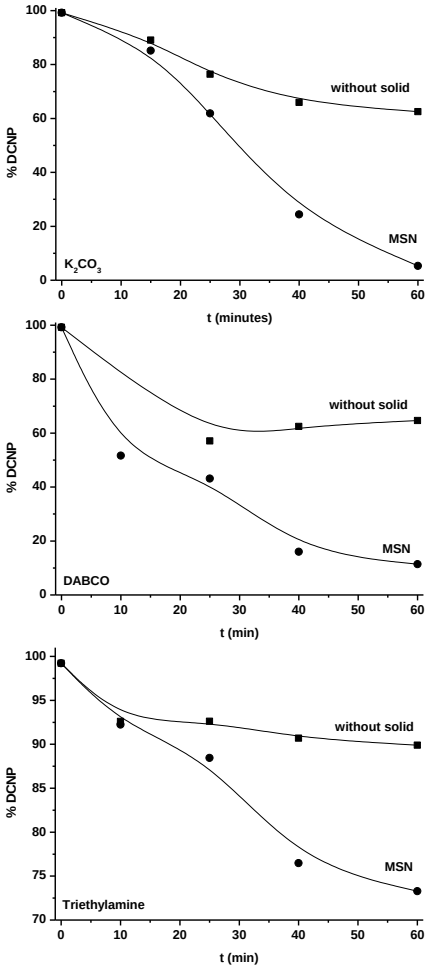


**Figure 6.** Hydrolysis of DNCP neurotoxic agent in the presence of different bases: $K_2CO_3$, DABCO and $Et_3N$. The graphic shows the different hydrolysis rate in the absence of silica material ( ■ ) and in the presence of MSN (●) for every selected base.

The hydrolysis of DCNP observed upon addition of a base to the nanoparticles suspensions is tentatively related to a silanol deprotonation process.[33] This deprotonation generated nucleophilic sites in the nanoparticle surface that are

able to react with the electrophilic phosphorus atom presented in the structure of DCNP.

The hydrolysis results obtained in Figure 6 above require the suspension of a mixture of the corresponding base and the mesoporous nanoparticles. Moreover, kinetic studies were also carried out with the use of solids MSN-1 and MSN-2 that were obtained by reaction of MSN with $K_2CO_3$ or DABCO. After the reaction the solids were isolated by centrifugation, washed with acetonitrile and dried.

The hydrolytic behaviour of MSN-1 and MSN-2 was also studied using $^{31}$P-NMR. In a typical experiment a suspension of MSN-1 or MSN-2 in acetonitrile:water (99.5:0.5 v/v) were mixed with DCNP and the changes in the $^{31}$P-NMR spectra measured with time. MSN-1 was able to hydrolyse DCNP in a similar way (80% of DCNP was hydrolysed after 60 minutes) to that found for the MSN-$K_2CO_3$ mixture (see Figure 8). However, MSN-2 nanoparticles induced a very low DCNP hydrolysis (see Figure 8).

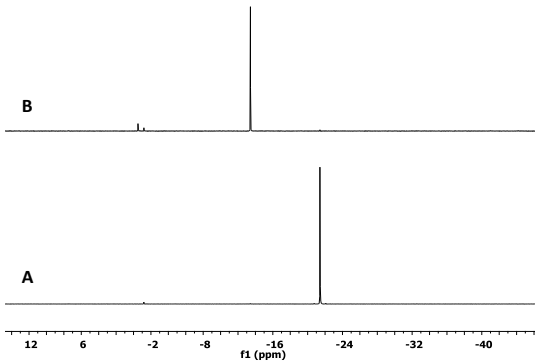


**Figure 7.** $^{31}$P-RMN spectra for a suspension of MSN material in $K_2CO_3$ in the presence of DCNP at initial time (0min) (A) and 60 min (B). The disappearance of the signal corresponding to DCNP (-21 ppm) and the appearance of the resonance due to pyrophosphate (-13 ppm) can be noticed

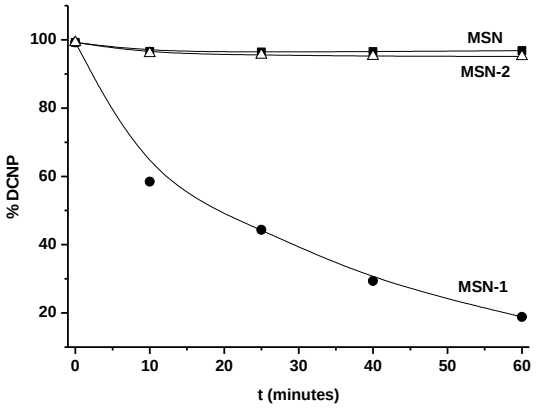


**Figure 8.** Hydrolysis of DCNP in acetonitrile:water (99.5:0.5 v/v) suspension of MSN (■), MSN-1 (●) and MSN-2 (△).

**Mechanism of DCNP hydrolysis.** In order to characterize more in detail the hydrolytic properties of the solids against the Tabun simulant DCNP, additional kinetic studies were carried out. From the $^{31}$P-NMR data obtained in the presence of MSN-11 and MSN-2 it was found that only DCNP, tetraethylpyrophosphate and diethyl phosphoric acid (the later in a very low proportion) signals were observed. From these studies it was also confirmed that DCNP and its derivatives were not adsorbed appreciably on the silica surface as the ratio of the sum of the peak areas of the phosphorous compounds and the area of the internal standard resulted nearly a constant through all the experiment.

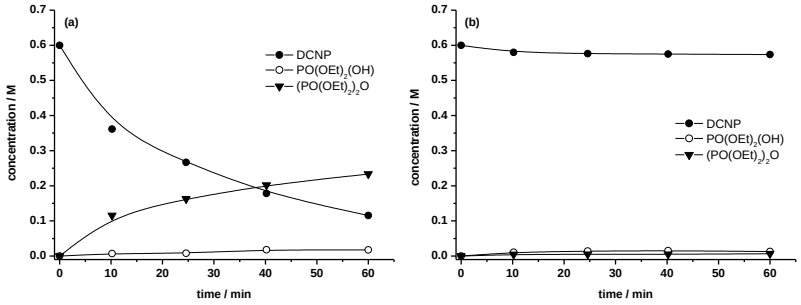


**Figure 9.** Kinetics of hydrolysis of DCNP using MSN-1 (a) or MSN-2 (b). Solid lines were calculated by least-squares fitting to the kinetic model described by equations (8) and (10).

Figure 9 shows the concentration of DCNP, diethyl phosphoric acid and tetraethylpyrophosphate versus time when using MSN-1 or MSN-2. As it can be observed the main product of the DCNP hydrolysis is tetraethylpyrophosphate. This contrast with results obtained in homogenous phase where the hydrolysis of DCNP was studied in the presence of certain amines.[34] In this later case diethyl phosphoric acid predominates over tetraethylpyrophosphate as the reaction product. It is therefore apparent from Figure 9, that the presence of silica inverts the distribution of products. Moreover, Figure 9 clearly shows that MSN becomes active as hydrolysis catalyst only after treatment with $K_2CO_3$ (MSN-1 material). The material obtained by deprotonation with DABCO (MSN-2) does not accelerate the hydrolysis reaction, behaving as untreated MSN.

From the data obtained the proposed mechanism for the hydrolysis of DCNP induced by MSN-1 material is shown in Scheme 2. The idea undelaying the mechanism is the ion-pair formation between $K^+$ cation and silanolate groups formed during the treatment of MSN with $K_2CO_3$. These $K^+$ cations would remain on the silica surface protecting silanolate groups from protonation when suspending the solid. For MSN-2 (material obtained upon treatment with DABCO) suspension should result in silanol regeneration due to dissociation of the ion pairs ($SiO^-HNR_3^+ \leftrightarrows SiOH + NR_3$) as amines are largely soluble in organic solvents. This would explain the low activity of solid MSN-2 in the hydrolysis of DCNP.

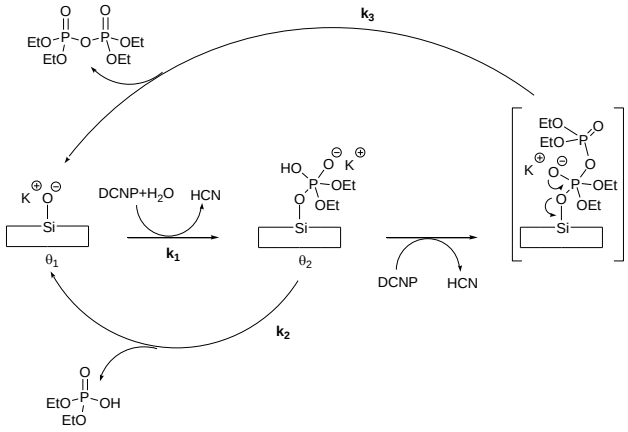


**Scheme 2.** Proposed mechanism for the hydrolysis of DCNP induced by MSN-1 material.

The proposed mechanism consists of three steps: (1) addition of DCNP to silanolate groups assisted by water forming an active intermediate phosphate species anchored to the silica surface; (2) rupture of the P-O bond from the intermediate species releasing diethyl phosphoric acid that regenerated a silanolate moiety; (3) reaction of the occupied site with DCNP forming tetraethylpyrophosphate regenerating the active site on the silica. The kinetic aspects of mechanism are summarized in Table 2.

**Table 2.** Reaction steps of the hydrolysis mechanism.

| | | |
|---|---|---|
| $R_1$: | $\theta_1 + DCNP + H_2O \rightarrow \theta_2 + HCN$ | $r_1 = k_1\theta_1[DCNP]$ |
| $R_2$: | $\theta_2 \rightarrow PO(OEt)_2(OH) + \theta_1$ | $r_2 = k_2\theta_2$ |
| $R_3$: | $\theta_2 + DCNP \rightarrow (PO(OEt)_2)_2O + HCN + \theta_1$ | $r_3 = k_3\theta_2[DCNP]$ |

As we have stated above phosphorous species remain largely into solution. Consequently, steady-state can be applied to the active sites on the silica surface, $\theta_1$ (free sites) and $\theta_2$ (occupied sites), in order to get the differential equation governing the concentration of DCNP, diethyl phosphoric acid ($PO(OEt)_2(OH)$) and tetraehylpyrophosphate ($(PO(OEt)_2)_2O$) in solution. The resulting stationary equations were:

$$\begin{pmatrix} 0 \\ \theta_T \end{pmatrix} = \begin{pmatrix} -k_1[DCNP] & k_2 + k_3[DCNP] \\ 1 & 1 \end{pmatrix} x \begin{pmatrix} \theta_1 \\ \theta_2 \end{pmatrix} \quad (1)$$

from which the following solutions were worked out

$$\Delta = 1 + \frac{k_1+k_3}{k_2}[DCNP] \quad (2)$$

$$\theta_1 = \frac{\theta_T}{\Delta}\left(1 + \frac{k_3}{k_2}[DCNP]\right) \quad (3)$$

$$\theta_2 = \frac{\theta_T}{\Delta}\frac{k_1}{k_2}[DCNP] \quad (4)$$

where $\theta_1$ is the number of active free sites, $\theta_2$ is the number of occupied active sites, and $\theta_T = \theta_1 + \theta_2$. On the other hand, the differential equations governing concentration of phosphorous species were:

$$\frac{d[DCNP]}{dt} = -k_1\theta_T[DCNP] + k_3\theta_2[DCNP] \quad (5)$$

$$\frac{d[\mathrm{PO(OEt)2(OH)}]}{dt} = k_2\theta_2 \quad (6)$$

$$\frac{d[(\mathrm{PO(OEt)2})2\mathrm{O}]}{dt} = k_3\theta_2[DCNP] \quad (7)$$

the rate law was obtained after removing steady-concentration of active sites from the differential equation set,

$$\frac{d[DCNP]}{dt} = \frac{\kappa_1[DCNP] + 2\kappa_2[DCNP]^2}{1 + \kappa_3[DCNP]} \quad (8)$$

$$\frac{d[\mathrm{PO(OEt)2(OH)}]}{dt} = \frac{\kappa_1[DCNP]}{1 + \kappa_3[DCNP]} \quad (9)$$

$$\frac{d[(\mathrm{PO(OEt)2})2\mathrm{O}]}{dt} = \frac{\kappa_2[DCNP]^2}{1 + \kappa_3[DCNP]} \quad (10)$$

where the meaning of kinetic coefficients $\kappa_i$ are,

$$\kappa_1 = k_1\theta_T \quad (11)$$

$$\kappa_2 = \frac{k_1k_3}{k_2}\theta_T \quad (12)$$

$$\kappa_3 = \frac{k_1 + k_3}{k_2} \quad (13)$$

It must be underlined that there are values of $\kappa_i$ accessible to measurement relating four parameters ($k_1$, $k_2$, $k_3$, $\theta_T$), therefore the values of rate constants, i.e. $k_1$, $k_2$ and $k_3$, will remain unknown unless the numbers of active sites were known.

$\kappa_i$ values were worked out by least-squares fitting of the phosphorous containing species concentration to the model given by equations (8) and (10). An excellent fit of experimental data to the model was found ($R$ = 0.996, $AIC$ = -96). Results are collected in Table 3.

Results indicated that $\kappa_3 \approx 0$ what actually means that $1 >> \kappa_3$, see denominators of equations (8) and (10). Therefore, calculations were not sensitive to this parameter. On the other hand $\kappa_1 << \kappa_2$[DCNP], so that kinetics was mainly governed by the term $\kappa_2$ [DCNP]$^2$, disappearing DCNP formally through a second-order rate law.

**Table 3.** Rate constants for the DCNP hydrolysis

| | $\kappa_1/min^{-1}$ | $\kappa_2/min^{-1}M^{-1}$ | $\kappa_3/M^{-1}$ | R | AIC |
|---|---|---|---|---|---|
| **MSN-1** | $1.2 \times 10^{-3}$ | $4.8 \times 10^{-2}$ | $\approx 0$ | 0.9958 | -95.9 |
| **MSN-2** | $5.3 \times 10^{-4}$ | $3.8 \times 10^{-4}$ | $\approx 0$ | 0.9998 | -107.6 |

$\kappa_i$ parameters have a difficult chemical reading, but not some of the relationships among them. Thus, the ratio $\kappa_2 / \kappa_1 = k_3 / k_2$ measures the relative importance of the hydrolysis routes leading to diethyl phosphoric acid or tetraehtylpyrophosphate. In the case of MSN-1, $\kappa_2 / \kappa_1 \approx 40$, indicating that tetraehylpyrophosphate hydrolysis path is 40-times faster than phosphate formation. Moreover, the ratio of the dominant kinetic $\kappa_2^{K_2CO_3} / \kappa_2^{DABCO}$ for $K_2CO_3$ and DABCO allows estimate the ratio of active sites provided that silanolate activity remains the same in both materials.

$$\frac{\kappa_2^{K_2CO_3}}{\kappa_2^{DABCO}} = \frac{(k_1 k_3/k_2)\theta_T^{K_2CO_3}}{(k_1 k_3/k_2)\theta_T^{DABCO}} = \frac{\theta_T^{K_2CO_3}}{\theta_T^{DABCO}}$$

$\kappa_2^{K_2CO_3} / \kappa_2^{DABCO} \approx 130$ that means that there are ca 130 active silanolate centres in MSN-1 per each silanolate centre in MSN-2, explaining the large reactivity of the former material.

## Conclusions

The hydrolysis of the Tabun simulant DCNP in the presence of mesoporous nanoparticles (MSN) has been studied. MSN alone was unable to enhance DCNP hydrolysis, however, MSN in the presence of certain bases enhanced DCNP degradation. In particular mixtures of MSN and potassium carbonate, triethylamine and DABCO have been studied. When $K_2CO_3$ was used as base combined with MSN, a hydrolysis of ca. 95% of the initial DCNP after 60 minutes was observed. In the presence of DABCO, MSN was able to induce the hydrolysis of ca. 90% after the same time. Finally, and as a clear contrast, the hydrolysis of DCNP observed for MSN in the presence of $Et_3N$ is lower (ca. 30%). In the absence of nanoparticles, DCNP hydrolysis reached only ca. 30% for $K_2CO_3$ and DABCO and ca. 7% for $Et_3N$ after 60 min. The hydrolytic behaviour of MSN-1 and MSN-2 was also studied. MSN-1 was able to hydrolyse DCNP in a similar way to that found with the MSN-$K_2CO_3$ mixture. However, MSN-2 nanoparticles induced a very low DCNP hydrolysis. From $^{31}$P-NMR data obtained in the presence of MSN-1 it was found the main product of the DCNP hydrolysis was tetraethylpyrophosphate. From kinetic data a proposed catalytic mechanism consisting of three steps is proposed that involve the addition of DCNP to silanolate groups assisted by water forming an active intermediate phosphate species anchored to the silica surface that forms diethyl phosphoric acid or is able to react with another DCNP molecule to give tetraethylpyrophosphate. We believe that these studies may contribute to the design of new remediation materials that could find application in devices and filtration systems to remove toxic nerve gases from contaminated environments.

## Experimental section

**General methods.** PXRD, TGA, elemental analysis, DLS, TEM and $N_2$ adsorption–desorption techniques were employed to characterize the prepared hydrolytic materials. Powder X-ray measurements were taken in a Philips D8 Advance diffractometer using Cu Kα radiation. Thermogravimetric analyses were carried out on a TGA/SDTA 851e Mettler Toledo balance using an oxidant atmosphere

(air, 80 mL $min^{-1}$) with a heating program consisting of a heating ramp of 10 $^{o}C$ per minute from 393 to 1273 K and an isothermal heating step at this temperature for 30 min. TEM images were obtained with a 100 kV Philips CM10 microscope. Dynamic Light Scattering (DLS) studies were conducted at 25 ºC using a in a Zetasizer Nano ZS equipment (Malvern Instruments, UK). The mean particle diameter was calculated from the quadratic fitting of the correlation function over 12 runs of 10 s duration. All measurements were performed in triplicate on previously sonicated highly dilute dispersions. $N_2$ adsorption–desorption isotherms were recorded with a Micromeritics ASAP2010 automated sorption analyzer. Samples were degassed at 70 $^{o}C$ in vacuum overnight. Specific surface areas were calculated from the adsorption data in the low pressure range using the BET model. Pore size was determined following the BJH method. $^{1}H$ and $^{31}P$ NMR spectra were recorded using two spectrometers: a Bruker Avance instrument operating at 400 MHz and a DPX Bruker instrument operating at 500 MHz.

**Chemicals.** *n*-cetyltrimethylammonium bromide (CTABr), tetraethylorthosilicate (TEOS), sodium hydroxide (NaOH), 1,4-Diazabicyclo[2.2.2]octane (DABCO), potassium carbonate, triethylamine ($Et_3N$), deuterated acetonitrile ($CD_3CN$), deuterium oxide ($D_2O$), diethylcyanophosphonate (DCNP) were purchased from Sigma–Aldrich and were used without any further purification.

**Synthesis of MCM-41 mesoporous silica nanoparticles (MSN).** NaOH (2.00 M, 3.5 mL) was added to a solution of *n*-cetyltrimethylammoniumbromide (CTABr, 1.00 g, 2.74 mmol) in 480 mL of deionized water. After adjusting the solution temperature to 80 $^{o}C$, TEOS (5 mL, 2.57 x $10^{-2}$ mol) was added dropwise to the surfactant solution. The mixture was stirred for 2 hours to lead to the formation of a white precipitate. The solid product was centrifuged and washed with deionized water and ethanol. Finally, the solid was dried at 60 $^{o}C$ (MCM-41 as-synthesized). To prepare the final porous material (MSN), the as-synthesized solid was calcined at 550 $^{o}C$ using an oxidant atmosphere for 5 hours to remove the template phase.

**Synthesis of MSN-1.** 250 mg of MSN were treated with 50 mL of an aqueous solution of $K_2CO_3$ (0.02 M). The suspension was stirred at room temperature for 1 hour. The solid was then centrifuged and washed with the minimum volume of dry acetonitrile. Finally, the solid was dried at 60 ºC to eliminate moisture.
**Synthesis of MSN-2.** 250 mg of MSN were treated with 50 mL of a solution of DABCO (0.02 M in acetonitrile). The suspension was stirred at room temperature for 1 h. The solid was then centrifuged and dried at 60 ºC to eliminate moisture.

**Hydrolysis using MSN.** Suspensions of 5 mg of the nanoparticulated material MSN in $CD_3CN$:$H_2O$ (99.5:0.5 v/v) (0.7 mL) in the presence of 0.02 M of the corresponding base ($K_2CO_3$, DABCO or TEA respectively) were prepared. Then, 10 µL of DCNP (9.4 x $10^{-2}$ mol $L^{-1}$) were added. The suspensions were stirred at 37 ºC for different periods of time and then centrifuged. The hydrolysis reaction was followed by performing $^{1}$H-NMR and $^{31}$P-NMR spectra on the aliquots of the supernatant.

**Hydrolysis using MSN-1 and MSN-2.** Suspensions of 5 mg of the corresponding materials (MSN-1 or MSN-2) in $CD_3CN$:$H_2O$ (99.5:0.5 v/v) (0.7 mL) were prepared. Then, 10 µL of DCNP were added (final concentration 9.4 x $10^{-2}$ mol $L^{-1}$). These suspensions were stirred at 37 ºC for different periods of time and then centrifuged. The hydrolysis reaction was followed by performing $^{1}$H-NMR and $^{31}$P-NMR spectra on the aliquots of the supernatant.

## Acknowledgments

This research was supported by the Ministerio de Educación y Ciencia (MAT2012-38429-C04). SCSIE (Universidad de Valencia) is gratefully acknowledged for all the equipment employed.

## References

1 (a) W. S. Angerson, *Chemical and Biological Warfare Agents*, RAND Reports, 2000, vol. 5; (b) D. R. Walt, D. R. Franz, *Anal. Chem.*, 2000, **72**, 738A.

2 O. A. Sadik, W. H. Land Jr., J. Wang, *Electroanalysis*, 2003, **15**, 1149.

3 S. M. Somani, *Chemical Warfare Agents,* Academic Press, San Diego, 1992.

4 K. E. Lejeune, B. C. Dravis, F. Yang, A. D. Hetro, B. P. Doctor, A. J. Russell, *Ann. N. Y. Acad. Sci.*, 1998, **864**, 153.

5 (a) L. M. Eubanks, T. J. Dickerson, K. D. Janda*, Chem. Soc. Rev.*, 2007, **36**, 458; (b) Y. C. Yang, J. A. Baker, J. R. Ward, *Chem. Rev.*, 1992, **92**, 1729.

6 (a) M. S. Nieuwenhuizen, J. L. N. Harteveld, *Sens. Actuators, B*, 1997, **40**, 167; (b) J. Negeh-Ngwainbi, P. H. Foley, S. S. Kuan, G. G. Guilbault, *J. Am. Chem. Soc.*, 1986, **108**, 5444; (c) Y. Yang, H. -F. Hi, T. Thundat, *J. Am. Chem. Soc.*, 2003, **125**, 1124; (d) C. Hartmann-Thompson, J. Hu, S. N. Kaganove, S. E. Keinath, D. L. Keeley, P. R. Dvornic, *Chem. Mater.*, 2004, **16**, 5357.

7 (a) A. J. Russel, J. A. Berberich, G. F. Drevon, R. R. Koepsel, *Annu. Rev. Biomed. Eng.*, 2003, **5**, 1; (b) M. Wheelis, *Pure Appl. Chem.*, 2002, **74**, 2247.

8 (a) Y. Lin, F. Lu, J. Wang, *Electroanalysis*, 2004, **16**, 145; (b) Y. Zhou, B. Yu, E. Shiu, K. Levon, *Anal. Chem.*, 2004, **76**, 2689; (c) D. Yu, J. Volponi, S. Chhabra, C. J. Brinker, A. Mulchandani, A. K. Singh, *Biosens. Bioelectron.*, 2005, **20**, 1433; (d) K. Anitha, S. V. Mohan, S. J. Reddy, *Biosens. Bioelectron.*, 2004, **19**, 848; (e) A. L. Simonian, J. K. Grimsley, A. W. Flounders, J. S. Schoeniger, C. T. Cheng, J. J. DeFrank, J. R. Wild, *Anal. Chim. Acta*, 2001, **442**, 15; (f) M. H. Hammond, K. J. Johnson, S. L. Rose-Pehrsson, J. Ziegler, H. Walker, K. Coudy, D. Gary, D. Tillett, *Sens. Actuators, B*, 2006, **116**, 135; (g) J. Wang, *Anal. Chim. Acta*, 2004, **507**, 3.

9 H. Sohn, S. Letant, M. J. Sailor, W. C. Trogler, *J. Am. Chem. Soc.*, 2000, **122**, 5399.

10 W. E. Steiner, S. J. Klopsch, W. A. English, B. H. Clowers, H. H. Hill, *Anal. Chem.*, 2005, **77**, 4792.

11 (a) S. Royo, R. Martínez-Máñez, F. Sancenón, A. M. Costero, S. Gil, M. Parra, *Chem. Commun.*, 2007, 4839; (b) I. Candel, A. Bernardos, E. Climent, M. D. Marcos, R. Martínez-Máñez, F. Sancenón, J. Soto, A. Costero, S.Gil, M. Parra, *Chem. Commun.*, 2011, **41**, 8313; (c) H. J. Kim, J. H. Lee, H. Lee, J. H. Lee, J. H. Lee, J. H. Jung, J. S. Kim, *Adv. Funct. Mater.*, 2011, **21**, 4035. (d) S. Royo, A. M. Costero, M. Parra, S. Gil, R. Martínez-Máñez, F. Sancenón, *Chem. Eur. J.*, 2011, **17**, 6931; (e) R. Gotor, A. M. Costero, S. Gil, M. Parra, R. Martínez-Máñez, F. Sancenón, *Chem. Eur. J.*, 2011, **17**, 11994; (f) E. Climent, A. Martí, S. Royo, R. Martínez-Máñez, M. D. Marcos, F. Sancenón, J. Soto, A. M. Costero, S. Gil, M. Parra, *Angew. Chem. Int. Ed*., 2010, **49**, 5945.

12 A. Watson, L. Hall, E. Raber, V. D. Hauschild, F. Dolislager, A. H. Love, M. L. Hanna, *Hum. Ecol. Risk Assess.*, 2011, **17**, 2.

13 (a) G. Saint-André, M. Kliachyna, S. Kodepelly, L. Louise-Leriche, E. Gillon, P. –Y. Renard, F. Nachon, R. Baati. A. Wagner, *Tetrahedron*, 2011, **67**, 6352; (b) T. -H. Kim, K. Kuca, D. Junb, Y. -S. Junga, *Bioorg. Med. Chem. Lett.*, 2005, **15**, 2914; (c) A. Chen, D. Du, Y. Lin, *Environ. Sci. Technol*., 2012, **46**, 1828.

14 T. –J. Leea, B. C. Chunb, Y. –C. Chunga, *React. Func. Polym.*, 2003, **56**, 37.

15 D. M. Mizrahi, S. Saphier, I. Columbus, *J. Hazard. Mater.*, 2010*,* **179***,* 495.

16 (a) M. F. Mohamed, A. A. Neverov, R. S. Brown**,** *Inorg. Chem.*, 2009, **48**, 1183; (b) G. R. M. Echavia, F. Matzusawa, N. Negishi, *Chemosphere*, 2009, **76**, 595; (c) B. M. Smith, *Chem. Soc. Rev.*, 2008, **37**, 470.

17 (a) M. Shimazu, A. Mulchandani, W. Chen, *Biotechnol. Bioeng.*, 2001, **76**, 318; (b) E. N. Efremenko, I. V. Lyagin, F. M. Plieva, I. Y. Galaev, B. Mattiasson, *Appl Biochem Biotechnol*, 2009, **159**, 251.

18 (a) M. Harper, *J. Environ. Monitor.*, 2012, **4**, 688; (b) S. Elias, S. Saphier, I. Columbus, Y. Zafrani, *Environ. Sci. Technol.*, 2014, **48**, 2893.

19 D. B. Kim, B. Gweon, S. Y. Moon, W. Choe, *Curr. Appl. Phys.*, 2009, **9**, 1093.

20 G. M. Zuo, Z. X. Cheng, G. W. Li, W. P. Shi, T. Miao, *Chem. Eng. J.*, 2007, **128**, 135.

21 (a) K. Dai, T. Y. Peng, H. Chen, J. Liu, L. Zan, *Environ. Sci. Technol.*, 2009, **43**, 1540; (b) G. W. Wagner, P. W. Bartram, O. Koper, K. J. Klabunde, *J. Phys. Chem. B*, 1999, **103**, 3225; (c) G. W. Wagner, L. R. Procell, R. J. O'Connor, S. Munavalli, C. L. Carnes, P. N. Kapoor, K. J. Klabunde, *J. Am. Chem. Soc.*, 2001, **125**, 1636; (d) G. W. Wagner, L. R. Procell, S. Munavalli, *J. Phys. Chem. C*, 2007, **111**, 17564; (e) T. H. Mahato, G. K. Prasad, B. Singh, J. Acharya, A. R. Srivastava, R. Vijayaraghavan *J. Hazard. Mater.*, 2009, **165**, 928; (f) D. A. Panayotov, J. R. Morris, *J. Phys. Chem. C*, 2008, **112**, 7496; (g) G. W. wagner, O. B. Koper, E. Lucas, S. Decker, K. J. Klabunde, *J. Phys. Chem. B*, 2000, **104**, 5116; (h) R. M. Narske, K. J. Klabunde, S. Fultz, *Langmuir*, 2002, **18**, 4819; (i) G. K. Prasad, T. H. Mahato, P. Pandey, B. Singh, M. V. S. Suryanarayana, A. Saxena, K. Sekhar, *Micropor. Mesopor. Mater.*, 2007, **106**, 256.

22 M. R. Seger, G. E. Maciel, *Eviron. Sci. Technol.*, 2006, **40**, 797.

23 (a) A. M. Schultz, O. K. Farha, J. T. Hupp, S. T. Nguyen, *J. Am. Chem. Soc.*, 2009, **131**, 4204; (b) L. Ma, C. Abney, W. Lin, *Chem. Soc. Rev.*, 2009, **38**, 1248.

24 R. K. Totten, Y. –S. Kim, M. H. Weston, O. K. Farha, J. T. Hupp, S. T. Nguyen, *J. Am. Chem. Soc.*, 2013, **135**, 11720.

25 K. El-Boubbou, D. A. Schofield, C. C. Landry, *J. Phys. Chem. C*, 2012, **116**, 17501.

26 (a) C. T. Kesge, M. E. Leonowicz, W. J. Roth, J. C. Vartuli, J. S. Beck, *Nature*, 1992, **359**, 710; (b) F. Hoffmann, M. Cornelius, J. Morell, M. Fröba, *Angew. Chem. Int. Ed.*, 2006, **45**, 3216.

27 (a) J. S. Edwards, A. Kumbhar, A. Roberts, A. C. Hemmert, C. C. Edwards, P. M. Potter, M. R. Redinbo, *Biotechnol. Prog.,* 2011, **27**, 863; (b) D. E. B. Gomes, R.D. Lins, P. G. Pascutti, C. Lei, *J. Phys. Chem. B*, 2010**, 114***,* 531.

28 (a) K. Knagge, M. Johnson, V. H. Grassian, S. C. Larsen, *Langmuir*, 2006**, 22***,* 11077; (b) Q. Meng, D. C. Doetschman, A. K. Rizos, M-H. Lee, J. T. Schulte, A.Spyros, C. W. Kanyi, *Environ. Sci. Technol.*, 2011, **45**, 3000.

29 A. Saxena, A. K. Srivastava, B. Singh, A. Goyal, *J. Hazard. Mater.*, 2012, **211-212**, 226.

30 *Nerve Agents*, A FOA Briefing Book on Chemical Weapons, 1992, (from www.fas.org/cw/cwagents).

31 B. C. K. Ip, D. V. Andreeva, G. Buntkowsky, D. Akcakayiran, G. H. Findenegg, I. G. Shenderovich, *Micropor. Mesopor. Mater.*, 2010, **134**, 22.

32 S. Cabrera, J. El Haskouri, C. Guillem, J. Latorre, A. Beltrán, D. Beltrán, M. D. Marcos, P. Amorós, *Solid State Sci.*, 2000, **2**, 405.

33 J. M. Rosenholm, T. Czuryszkiewicz, F. Kleitz, J. B. Rosenholm, M. Linden, *Langmuir*, 2007, **23**, 4315.

34 Unpublished results.

# 4. HYBRID MATERIALS FOR DRUG RELEASE

## 4.1 **Introduction.**

Many examples of molecular gated systems have already been described in the general introduction. In the latest years, research has been focused on the design of gated systems where biomolecules act either as cargo or external stimulus. In this kind of systems, pores are loaded with biologically active molecules[1] or silica surface is modified with silane derivatives of biomolecules such as polysaccharides, antibodies, peptides or oligonucleotides.[2] The cargo inside the mesopores is released when the molecule blocking the pores (peptides, DNA fragments, anti-bodies etc.) is modified by enzymatic hydrolysis mechanisms[3], hybridization with the complementary oligonucleotide[4], coupling with the specific antigen[5] etc.

### *4.1.1 Biomolecules as capping/uncapping agents.*

Stoddart's research group developed one of the first biologically responsive gate systems.[6] The authors reported an enzyme responsive snap-top system. As the authors stated "in general, an snap-top system consists of a [2]rotaxane tethered to the surface of a nanoparticle in which an α-cyclodextrin (α-CD) torus encircles a polyethylene glycol thread and is held in place by a cleavable stopper". In this case, a snap-top system entraps luminescent cargo molecules (rhodamine B) and, in order to make the device be responsive to the porcine liver esterase (PLE), the system was blocked by an ester linked adamantyl stopper. In the presence of the

---

[1] (a) N. Singh, A. Karambelkar, L. Gu, K. Lin, J.S. Miller, C.S. Chen, M.J. Sailor, S.N. Bhatia, *J. Am. Chem. Soc.*, **2011**, *133*, 19582 (b) Q. He, J. Shi, *J. Mater. Chem.*, **2011**, *21*, 5845.

[2] (a) C. Coll, A. Bernardos, R. Martínez-Máñez, F. Sancenón, *Accounts Chem Res*, **2013**, *46*, 339. (b) A. Schlossbauer, S. Warncke, F.M.E. Gramlich, J. Kecht, A. Manetto, T, Carell, T. Bein*, Angew. Chem. Int. Ed*. **2010**, *49*, 4734.

[3] C.Park, H. Kim, S. Kim, C. Kim, *J. Am. Chem. Soc*. **2009**, *131*, 16614.

[4] E.Climent, R. Martínez-Máñez, F. Sancenón, M.D. Marcos, J.Soto, A. Maquieira, P. Amorós, *Angew. Chem. Int. Ed*. **2010**, *49*, 7281

[5] E. Climent, A. Bernardos, R. Martínez-Máñez, A. Maquieira, M. D. Marcos, N. Pastor-Navarro, R. Puchades, F. Sancenón, J. Soto, P. Amorós, *J. Am. Chem. Soc***. 2009**, *131*, 14075.

[6] K. Patel, S. Angelos, W. R. Dichtel, A. Coskun, Y-W. Yang, J. I. Zink, J. F. Stoddart, *J. Am. Chem. Soc*. **2008**, *130*, 2382.

enzyme, the adamantyl ester stopper is hydrolyzed, thus, the α-CD is dethreated resulting in cargo release. (See figure 1)

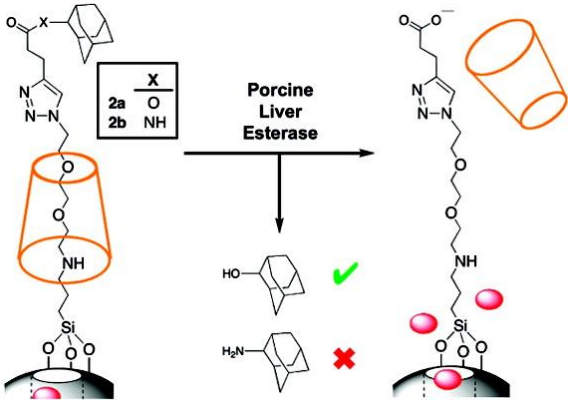


**Figure 1**. Schematic representation of the activation of the snap-top system in the presence of Porcine liver esterase. The enzyme is able to hydrolyze the esteric stopper, thus the cyclodextrine is no longer attached to the system and the cargo is released. *Reprinted (adapted) with permission from J. Am. Chem. Soc. 2008, 130, 2382. Copyright (2008) American Chemical Society.*

Another example of enzyme responsive system was reported by *Coll et al*. [7] In this case, the authors designed a gated system using mesoporous silica nanoparticles (MSN) as scaffolding. The pores were loaded with a fluorescent dye $[Ru(bipy)_3]Cl_2$ and the external surface was functionalized with a silane derivative having an azide group which acts as anchor point for a subsequent reaction with an specific peptide sequence. Thus, the peptidic chains attached to the siliceous surface block the pore outlets avoiding the release of the cargo. In the presence of proteolytic enzymes obtained from *Streptomyces griseus* (PESG), the hydrolysis of the peptide occurs and the fluorescent dye is released into the solution. (See figure 2).

[7] C. Coll, L. Mondragón, R.Martínez-Máñez, F. Sancenón, M. D. Marcos, J. Soto, P. Amorós, E. Pérez-Payá, *Angew. Chem. Int. Ed*. **2011**, *50*, 2138.

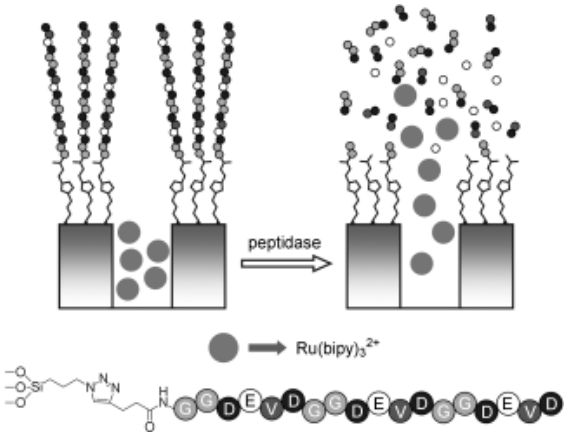


**Figure 2**. Representation of the gated material capped with a peptide silane derivative. Scheme of the dye release process in the presence of peptidase enzymes as a consequence of the hydrolysis of the capping peptidic sequence. *Adapted from Angew. Chem. Int. Ed. 2011, 50, 2138. Copyright © 2011 Wiley.*

*Climent et al.* reported a biologically responsive system where the external stimulus is a biomolecule different from an enzyme.[5] In this case, based on antibody-antigen specific interaction, the authors designed a highly specific gated system. The pores of a MCM-41 material were loaded with the dye $[Ru(bipy)_3]Cl_2$ and the external surface was first functionalized with an hapten, (4-(4-aminobenzenesulfonylamino)benzoic acid) and finally, an antibody showing good affinity toward said hapten is added in order to block the pores. In the presence of the antigen (sulfatiazole, STZ) which is complementary to the antibody, a displacement reaction takes place and thus, the system is uncapped and the dye is released to the solution (see figure 3).

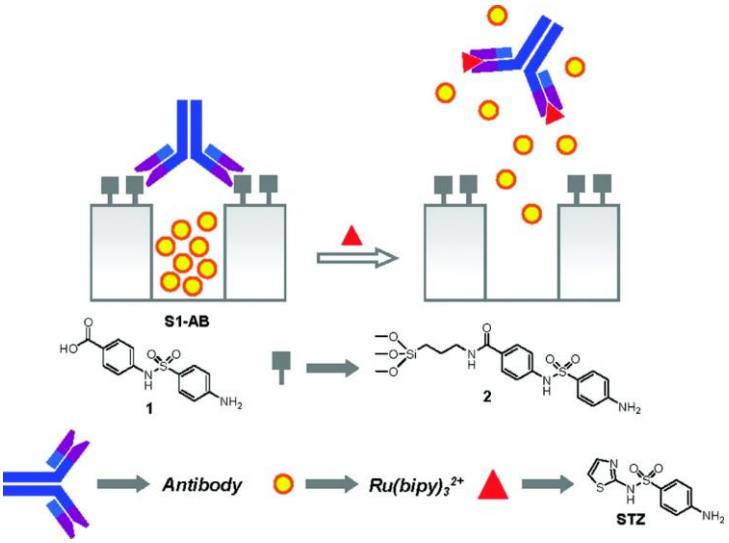


**Figure 3**. Schematic representation of the gated material and the opening paradigm. An MCM-41 material is loaded with a Ruthenium dye, the external surface being functionalized with a hapten and then blocked with an antibody. In the presence of the corresponding antigen, a displacement reaction is triggered and the system is uncapped, thus releasing the dye. *Reprinted (adapted) with permission from J. Am. Chem. Soc. 9 VOL. 131, NO. 39, 2009. Copyright (2009) American Chemical Society.*

### *4.1.2 Drug release.*

Biologically responsive materials have been used in medicine in the last years to deliver specific drugs on targeted intracellular regions. In particular, there are many examples on literature where gated materials have been used for anticancer drug delivery applications.

*Bernardos et al*. designed a device for the controlled release of a cytotoxic drug specifically in intracellular media.[8] This device was based on mesoporous silica nanoparticles whose pores were loaded with the cytotoxic chemotherapeutic agent doxorubicin (DOX) as guest molecules whereas the outlets of the pores were capped with the corresponding alkoxysilane derivative of different starch

[8] A. Bernardos, L. Mondragón, E. Aznar, M. D. Marcos, R. Martínez-Máñez, F. Sancenón, J. Soto, J. M. Barat, E. Pérez-Payá, C. Guillem, P. Amorós, *ACSNano* 2010, **4**, 6353.

hydrolizates. While it was found to be a zero release system in the absence of appropriate enzymes, in the presence of amylases the material is uncapped by the enzyme-induced hydrolysis of the glycosidic bonds in the anchored saccharides and the cargo is released. These nanoparticles are found to be easily internalized by cells (via endocytosis) where the lisosome enzymes hydrolyze the molecular gate, thus, releasing the cargo which causes cell death.

## 4.2 **Objectives**

Bearing in mind the importance of controlled drug release, we aimed to develop hybrid organic-inorganic mesoporous materials in which cargo release could be triggered by the action of intracellular enzymes. Specifically, our aim was:

- To design and synthesize a new organic-inorganic hybrid material using mesoporous silica nanoparticles as inorganic scaffold loaded with a dye and funcitonalized with a specific molecule able to act as a substrate for a specific enzyme.
- To design an analogous material being loaded with a chemotherapeutic drug.
- To characterize the new mesoporous organic-inorganic hybrid materials.
- To evaluate the uncapping ability of the enzyme, this is, the enzyme-driven controlled release.
- To study the internalization of the nanoparticles on cells and cargo delivery.

## 4.3 **Design of the system**

Two different mesoporous hybrid materials have been synthesized. As a proof-of-concept, mesoporous silica nanoparticles were loaded with Safranine O and the external surface was functionalized with *N*-(3-triethoxysilylpropyl)gluconamide

(**S1**). A second analogous solid was then prepared, whose pores were loaded with the anticancer agent camptothecin and the external surface was functionalized with the same alkoxysilane derivative (**S1-CPT)**.

Both materials were designed in such a way that the cargo is only released in the presence of the appropriate enzymes (peptidase, amidase). In case of **S1-CPT** the release of the cargo in the intracellular media causes cell death.

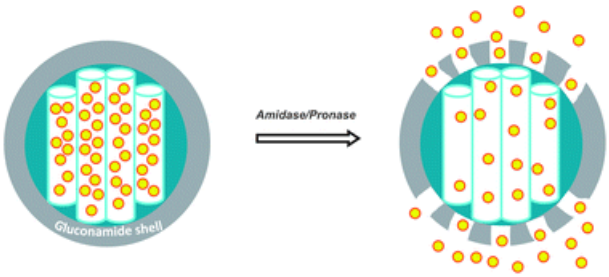


**Figure 4**. Schematic representation of the controlled released paradigm. The hydrolysis of the capping molecule in the presence of the appropriate enzyme induces cargo release. *[Nanoscale, 2012, 4, 7237–7245] - Reproduced by permission of The Royal Society of Chemistry.*

# *Antitumoral drug amidase-responsive controlled release on intracellular media using gluconamide-capped mesoporous silica nanoparticles.*

*Inmaculada Candel,[a,c] Elena Aznar,[c,a] Laura Mondragón,[a,b,c] Cristina de la Torre,[a,c] Ramón Martínez-Máñez,[a,b,c] Félix Sancenón,[a,b,c] M. Dolores Marcos,[a,b,c] Pedro Amorós,[e] Carmen Guillem,[e] Enrique Pérez-Payá,[f,g] Ana Costero,[a,d] Salvador Gil,[a,d] Margarita Parra[a,d]*

*a Centro de Reconocimiento Molecular y Desarrollo Tecnológico (IDM), Unidad Mixta UniversitatPolitècnica de València-Universitat de València, Spain.*

*b Departamento de Química, UniversitatPolitècnica de València, Camino de Vera s/n, 46022, Valencia, Spain.*

*c CIBER de Bioingeniería, Biomateriales y Nanomedicina (CIBER-BBN).*

*d Departamento de Química Orgánica, Facultad de Química, Universitat de València, 46100 Burjassot, Valencia, Spain.*

*eInstitut de Ciencia delsMaterials, Universitat de València, P. O. Box 22085, E-46071, Valencia, Spain.*

*fCentro de Investigación Príncipe Felipe, Laboratorio de Péptidos y Proteínas, Avd. Autopista al Saler, 16, E-46012, Valencia, Spain.*

*gIBV-CSIC, Jaime Roig, 11, E-46010, Valencia, Spain.*

**Received 30 Jul 2012, Accepted 24 Sep 2012**
**First published on the web 02 Oct 2012**

*Nanoscale, 2012, **4**, 7237–7245*
*(Reproduced with permission of the Royal Society of Chemistry)*

***ABSTRACT***

MCM-41 silica nanoparticles were used as inorganic scaffolding to prepare a nanoscopic-capped hybrid material **S1**, which was able to release an entrapped cargo in the presence of certain enzymes, whereas in the absence of enzyme, a zero release system was obtained. **S1** was prepared by loading nanoparticles with safranine O dye and was then capped with a gluconamide derivative. In the absence of enzyme, the release of the dye from the aqueous suspensions of **S1** was inhibited as a result of the steric hindrance imposed by the bulky gluconamide derivative, the polymerized gluconamide layer and the formation of a dense hydrogen-bonded network around the pore outlets. Upon the addition of amidase and pronase enzymes, delivery of safranine O dye was observed due to the enzymatic hydrolysis of the amide bond in the anchored gluconamide derivative. **S1** nanoparticles were not toxic for cells, as demonstrated by cell viability assays using HeLa and MCF-7 cell lines, and were associated with lysosomes, as shown by confocal microscopy. Finally, the **S1-CPT** material loaded with the cytotoxic drug camptothecin and capped with the gluconamide derivative was prepared. The HeLa cells treated with **S1-CPT** underwent cell death as a result of material internalization, and of the subsequent cellular enzyme-mediated hydrolysis and aperture of the molecular gate, which induced the release of the camptothecin cargo.

**INTRODUCTION**

The preparation of hybrid functional materials in an attempt to mimic objects that perform active tasks in living organisms is a fertile multidisciplinary research area.[1] Nature uses simple molecules (amino acids, saccharides, nucleobases and certain inorganic compounds) to design functional structures (channels, pumps, gates) of a nanometric size. Chemists, inspired by these biological systems, have started to develop nanometric functional materials that work similarly to these complex structures in living organisms.[2]

One of the most appealing concepts in nature is related with channels that act as gates and control mass transport on-command. Inspired by this concept, researchers have recently been involved in the design of “molecular gates”.[3] A

molecular gate can be defined as a nanoscopic system in which mass transport (or delivery) can be triggered by a target external stimulus, which is able to control the state of the gate (closed or open) at will. In general, an abiotic gated material is composed of two subunits: (i) a suitable inorganic support and (ii) certain organic molecules, usually grafted on the external surface, which are the responsible for mass transport/delivery control.

In most prepared gated materials, silica mesoporous supports of the MCM-41 family have been used as inorganic scaffolds. This is due to the special properties of these materials, such as large load capacity, biocompatibility, high thermal stability, homogeneous porosity, inertness, and tunable pore sizes with a diameter of ca. 2-10 nm. In addition, the existence of well-known surface functionalization procedures makes these scaffoldings suitable to develop molecular gated systems.

Since the first example of a gate-like ensemble based on mesoporous materials was described by Fujiwara et al.,[4] many different molecular gated organic-inorganic hybrid materials using a wide range of different chemistries have been reported.[5] Following this pioneering work, several research groups have demonstrated that it is possible to design gated materials capable of achieving "zero release", which can be fully opened by applying certain external stimuli. Both physical and chemical triggers, such as pH,[6] temperature,[7] redox potential,[8] light[9] or reaction with chemical species,[10] have been reported. Most systems have been designed for drug delivery applications, although sensing protocols using molecular gated supports have also been described.[10b,c,d]

Despite the fact that molecular gated devices have been studied over the last few years, the use of silica mesoporous gated-like devices involving biomolecules like caps or stimuli to deliver the cargo has not been fully explored. For instance, a few examples using specific drugs as cargo,[11] biomolecules as capping agent,[12] or enzymes as external stimuli[13] have been described. In particular, very few examples using enzymes have been reported and most cases have focused on peptide-capped nanocontainers capable of releasing their cargo in the presence of the appropriate peptidase.[13e,f] The development of enzyme-responsive bio-gated mesoporous silica nanoparticles

is appealing taking into account the wide range of available enzymes able to selectively catalyse a large number of different chemical reactions. In particular, the possibility of prepare tailor-made sequences, that may provide fine selectivity in the design of advanced gate-opening devices, opens new perspectives of applicability for drug delivery systems using mesoporous nanoscopic gated systems.

The use of molecular gated devices based on mesoporous silica nanoparticles as drug containers offers very promising applications in the field of medicine as they would allow the controlled and specific deliver of the drug in the target organ, thus avoiding degradation of the drug by other physiological agents.[14] The application of these concepts in antitumoral medicine has become an area of great interest.[15] Thus, the research community is making great efforts to develop new, innovative mass transport devices capable of delivering anticancer drugs on tumour cells.

Bearing in mind the fact that there are very few examples of gated materials based on the enzymatic hydrolysis of capping groups and taking into account the potential applications of such systems to develop nanodevices showing a "zero release" before the presence of target enzymes, we report herein the design of new and simple capped nanoparticles displaying enzyme-induced delivery. Mesoporous silica nanoparticles were used as inorganic scaffolding while their external surface was functionalized with a gluconamide derivative capable of being hydrolyzed in the presence of the corresponding specific amidases both *in vitro* and on intracellular media. Materials' efficiency was tested using dye molecules as the cargo to prove both the delivery profiles and the non toxicity of the silica nanoparticles in cells. Moreover, camptothecin-(CPT) loaded nanoparticles were proved to cause cell death in several cancer cell lines.

## *RESULTS AND DISCUSSION*

### Design and synthesis of gated materials

Application of supramolecular chemistry principles to design gate-like

ensembles based on mesoporous scaffoldings allows the development of nanoscopic devices for mass transport and controlled release applications. As stated in the Introduction, most developed gated materials employ molecular/supramolecular interactions for the fine control of cargo delivery. In contrast, relatively few examples use biomolecules for capping or uncapping protocols. Following our interest in applying biological interactions, as triggered for control delivery, here we paid attention to using enzymes as "biological-keys".

Our aim was to design biocompatible easy-to-prepare capping systems in order to synthesize simple gated scaffoldings capable of being used efficiently in delivery applications. With this approach, silica mesoporous MCM-41 nanoparticles were selected as inorganic scaffolds. Scheme 1 shows the proposed enzyme-driven gate-opening mechanism for the new gated material **S1**. In order to prepare the designed material, the pores of the MCM-41-type nanoparticulated scaffolding were loaded with safranine O. Then the external surface was functionalized with *N*-(3-triethoxysilylpropyl)gluconamide to yield the final hybrid material **S1**. This organic compound has been selected bearing in mind the presence of an amide hydrolysable group and five hydroxyl groups, which were expected to result in a dense hydrogen-bonded network around the pore outlets, which should avoid cargo delivery. In the presence of the appropriate amidase, the amide bond is hydrolyzed with the subsequent reduction in size of the attached capping molecule and, consequently, the delivery of the cargo. In order to completely block the drug inside the mesopores in the absence of amidase (to favor a selective drug release), we used a higher proportion of *N*-(3-triethoxysilylpropyl)gluconamide compared to previous works of our group (*vide infra*). Under these conditions, and together with the direct silica surface functionalization (by the interaction of the silanol groups with the triethoxy moieties of the silane), a certain polymerization of the silane on the silica surface was expected (in this last case, by using a limited number of silanol groups to maintain the interaction with the support). Thus, this strategy guarantees the formation of a thicker shell around the mesoporous silica nanoparticles. However, regardless of the nature of the incorporated silanes (directly functionalized or polymerized), the

enzyme was expected to be able to cut the organic arms inducing the drug release.

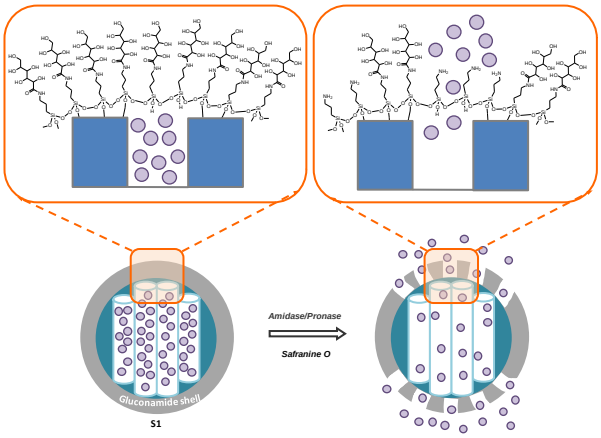


**Scheme 1** Schematic representation of the synthesis procedure and the gate-opening mechanism of **S1** in the presence of the appropriate enzyme.

The silica nanoparticulated material (a calcined MCM-41-like solid) was prepared by following well-known procedures using TEOS as the hydrolysable inorganic precursor and the surfactant hexadecyltrimethylammonium bromide (CTABr) as the porogen species.[16] Moreover *N*-(3-triethoxysilylpropyl)gluconamide is a commercially available alkoxysilane derivative, which was selected and used as the molecular gate.

In order to ensure the correct functionality of the final hybrid material, we followed a two-step synthetic procedure which we and others have previously used to prepare gated structures containing a loaded cargo on the pores and suitable switchable ensembles on the pore outlets.[6e] In the first step, the efficient loading of pores was achieved by stirring a highly concentrated Safranine O solution in the presence of the mesoporous nanoparticles. Then in a second step, the gluconamide derivative was added to the same mixture to functionalize the external surface of the siliceous material. Following this protocol, the anchoring reaction of *N*-(3-triethoxysilylpropyl)gluconamide occurred on the nanoparticles containing pores filled with safranine O in a

suspension which still contained a high concentration of the dye, thus inhibiting dye diffusion from the inner pores to the bulk solution and, at the same time, hampering as much as possible the entrance of *N*-(3-triethoxysilylpropyl)gluconamide into the porous network.

Following this protocol, the final **S1** material should contain the gluconamide derivative, mainly as a shell on the external surface (*vide infra* for a more detailed comment), whereas safranine O should be located inside the mesopores. Finally, the violet/pinkish solid **S1** was filtered, washed with water and dried at 40°C for 12 h.

A second solid, **S1-CPT**, was prepared following the same procedure as cited above. In this case, mesopores were filled with the anticancer agent campthotecin, and the uptake was performed in acetonitrile-ethanol mixtures to favor drug dissolution. Then, *N*-(3-triethoxysilylpropyl)gluconamide was added to the suspension and the final material was isolated by filtration, washed with chloroform-methanol 3:4 v/v and dried at vacuum for 1 h.

**Characterization of solids**

The prepared material **S1** was characterized by standard techniques. Figure 1 shows the powder X-ray diffraction (XRD) patterns of solids MCM-41 as synthesized, MCM-41 calcined, **S1** and **S1-CPT**. The XRD of the mesoporous MCM-41 material as-synthesized (Figure 1, curve i) displayed the expected four peaks of a hexagonal ordered array indexed as (100), (110), (200), and (210) Bragg reflections. From the XRD data, an $a_0$ cell parameter of 41 Å ($d_{100}$ spacing of 36.05 Å) was calculated. In curve ii, corresponding to the MCM-41 calcined sample, a significant shift of the (100) reflection in the XRD is clearly observed. This displacement, together with the broadening of the (110) and (200) reflections, corresponds to an approximate cell contraction of *ca*. 6-8 Å due to the condensation of silanols groups in the calcination step. Figure 1 also depicts the XRD patterns for solids **S1** and **S1-CPT**. For these materials, reflections (110) and (200) were lost, most likely due to a reduced contrast as the result of the loading and functionalization process. Yet the presence of the $d_{100}$ peak in the XRD patterns in both **S1** and **S1-CPT** suggested that the pore

loading (with Safranine O dye or with the campthotecin drug) and functionalisation process did not modify the mesoporous MCM-41 scaffolding.

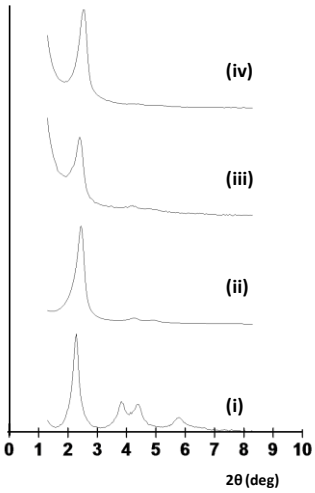


**Fig. 1** XRD Patterns for the nanoparticulated MCM-41 as-synthesized (i), calcined MCM-41 nanoparticles (ii), **S1** (iii) and **S1-CPT** (iv).

Preservation of the mesoporous structure in the final functionalized solid **S1** was also confirmed by the Transmission Microscopy (TEM) images. Figure 2 shows the morphology of the prepared mesoporous materials. MCM-41 scaffolding was obtained as spherical particles showing a mean diameter of 80-100 nm. From the images, it is apparent that the loaded and functionalized derivative **S1** maintains the initial MCM-41 matrix morphology. A similar result was obtained for **S1-CPT** (data not shown). In all the samples, the characteristic channels of a mesoporous matrix were observed as alternate black and white lines.

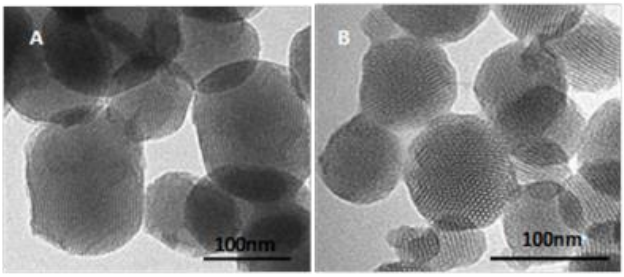


**Fig. 2** Representative Transmission Electron Microscopy (TEM) image of the calcined MCM-41 nanoparticles (A) and the loaded and functionalized mesoporous silica nanoparticles (**S1**) (B).

Further DLS (Dynamic Light Scattering) studies showed particles with a mean diameter of 100 nm. The studies also shown that the size of the nanoparticles was not modified throughout the loading and functionalization processes (figure 3). Signals at *ca*. 500 nm suggested that a small proportion of the nanoparticles were aggregated.

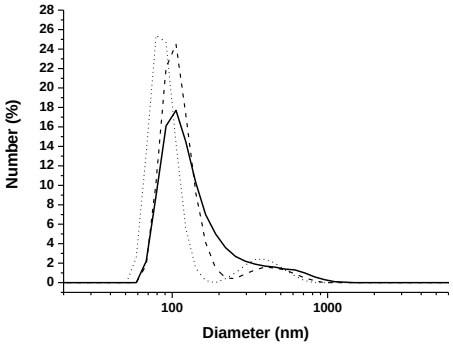


**Fig. 3** Statistical representation of particle size obtained by DLS (Dynamic Light Scattering) studies. The average size of nanoparticles of calcined MSN (straight), **S1** (dash) and **S1-CPT** (dot) was found to be *ca*. 100 nm.

The $N_2$ adsorption-desorption isotherms of the nanoparticulated MCM-41 calcined material are shown in Figure 4. A typical curve for this mesoporous support, consisting of an adsorption step at an intermediate $P/P_0$ value (0.1-0.3), is observed. This curve matches a type IV isotherm in which the observed step deals with nitrogen condensation inside the mesopores. The narrow BJH

pore distribution and the absence of a hysteresis loop in this interval suggest the existence of uniform cylindrical mesopores (pore diameter of 2.40 nm and pore volume of 0.71 $cm^3$ $g^{-1}$ calculated by using the BJH model on the adsorption branch of the isotherm). Application of the BET model resulted in a value of 963.3 $m^2$ $g^{-1}$ for the total specific surface. From the XRD, porosimetry and TEM studies, the $a_0$ cell parameter (4.1 nm), the pore diameter (2.40 nm), and the wall thickness value of 1.7 nm were calculated. In addition to this adsorption step, a second feature is observed in the isotherm at a high relative pressure ($P/P_0$ 0.8), which corresponds to the filling of the large voids among the particles (0.39 $cm^3$ $g^{-1}$ calculated by the BJH model) and must be considered a textural-like porosity. In this case, the curves show a characteristic H1 hysteresis loop and a wide pore size distribution. The $N_2$ adsorption-desorption isotherm of **S1** is typical of mesoporous systems with practically filled mesopores (see Figure 4). Consequently, relatively low $N_2$ adsorbed volume (BJH mesopore volume (0.03 $cm^3$ $g^{-1}$) and surface area (45.6 $m^2$ $g^{-1}$) values were calculated, thus indicating effective pore blocking and the subsequent absence of appreciable mesoporosity. BET-specific surface values, mesopore volumes and mesopore sizes were calculated from the $N_2$ adsorption-desorption isotherms for MCM-41 and **S1** and are listed in Table 1.

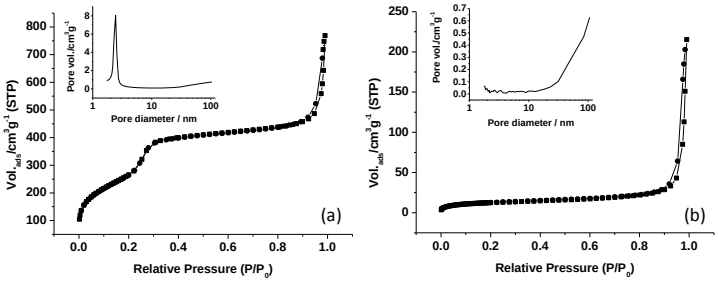


**Fig. 4** Nitrogen adsorption-desorption isotherms for (a) the MCM-41 mesoporous nanoparticles (b) **S1.** Insets: Pore size distribution of each material.

**Table 1** BET-specific surface values, pore volumes and pore sizes (associated with intraparticle mesopores) calculated from the $N_2$ adsorption-desorption isotherms for each material.

| | **Mesopore Size (nm)** | **Mesopore Volume ($cm^3/g$)** | **Large pore Volume ($cm^3/g$)** | **BET surface area ($m^2/g$)** |
|---|---|---|---|---|
| MCM-41 | 2.40 | 0.71 | 0.39 | 963.3 |
| **S1** | - | < 0.03 | 0.23 | 45.6 |

**Table 2.** Contents of the alcoxysilane derivative and cargo found on **S1** and **S1-CPT.**

| | **Alcoxysilane derivative (mmol/g $SiO_2$)** | **Safranine O Content (mmol/g $SiO_2$)** | **CPT content (mmol/g $SiO_2$)** |
|---|---|---|---|
| **S1** | 3.47 | 0.25 | - |
| **S1-CPT** | 1.35 | - | 0.27 |

The contents of *N*-(3-triethoxysilylpropyl)gluconamide and Safranine O dye or camptothecin in solid **S1** and solid **S1-CPT** respectively were determined by elemental and thermogravimetric analyses and are shown in Table 2. The amount of CPT present in **S1-CPT** before the functionalization with the gluconamide groups was *ca*. double of the final content (data not shown). The high content of the organosilane groups incorporated into **S1** indicates that functionalization was not restricted to only direct interactions between silanol groups and the triethoxy moieties of the silanes on the external surface. Then, incorporation of the silanes anchored onto the internal surfaces (mesopore entrances), and even external polymerization, cannot be discarded (according to the experimental conditions used). The capability of the organo-silanes to modify the internal surface of mesopores, even in the case of materials with filled mesopores (with guest species), has been previously described.[17] In fact, effective anchoring of the silanes inside mesopores of up to 8-10 nm deep has

been usually observed. Then, besides the external surface of the MCM-41 particles (*ca.* 70 $m^2/g$) (determined from the $N_2$ adsorption isotherms on the as-synthesized material), an extra surface of *ca.* 178 $m^2/g$ of the internal mesopores should be considered as being accessible for the gluconamide containing silanes (this last value has been roughly estimated from the internal surface (963 $m^2/g$) by assuming an average particle diameter of 100 nm, and a maximum of 10 nm in deep functionalization, and by also bearing in mind that each mesopore has two entrances). In short for **S1**, we obtained an average total surface of 248 $m^2/g$ for organosilane incorporation.

By taking into account that the normal density of the silanol groups in silica materials is *ca.* 6 Si-OH $nm^2$ and that the gluconamide derivative has three reactive ethoxy groups, the maximum density of the gluconamide groups directly anchored onto hybrid solids should be expected to be *ca.* 2-3 molecules/$nm^2$. By assuming our anchoring model and the available 278 $m^2/g$ surface, only 0.82 mmol of the functional groups could be admitted by our MCM-41. Then, a significant amount of the *N*-(3-triethoxysilylpropyl)gluconamide groups are necessary incorporated through polymerization around the silica particles to form an organosilane shell. This assembling model is supported by NMR data. The $^{29}Si$ NMR spectra of MCM-41 and **S1** are shown in Figure 5. The evolution of the $Q^2+Q^3$ sites from 28% (MCM-41) to 23% (**S1**) indicates that most of the silanol groups inside the mesopores remain unaltered. This fact is compatible with our model, where the *N*-(3-triethoxysilylpropyl)gluconamide groups can be connected on a maximum silica surface of *ca.* 248 $m^2/g$. In fact, a maximum estimated percentage of *ca.* 7% of the $Q^2+Q^3$ sites is accessible on this surface. Together with this decrease in the silanol groups, the T sites significantly increase (from 0 to 28%) after functionalization. Obviously, this high proportion of T sites is not compatible only with a direct polymerization of silanes on the external silica surface. Therefore, the presence of such a large amount of gluconamide moieties can be associated only with a significant polymerization of the *N*-(3-triethoxysilylpropyl)gluconamide groups around the silica particles, which require a limited number of silanol groups to preserve the connection with the

support. Moreover, this model is in accordance with the relatively low condensation of the organosilane network (T3:T2= 19:9).

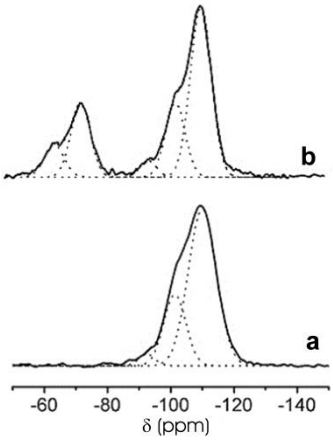


**Fig.5** [29] Si-NMR of the MCM-41 as synthesized (a) and **S1** (b) showing the evolution of the $Q^2$+$Q^3$and T sites through the loading and functionalization process.

**Functional enzyme-driven controlled release**

In this section, several experiments were carried out in order to study the enzyme-responsive controlled-release protocol using capped materials in detail. The controlled release behavior of **S1** was studied in aqueous media in the presence of two different enzymes (pronase, a non specific peptidase from *Streptomyces griseus* at pH 8.3; an amidase from *Citrus sinensis* at pH 7.5). The selected pHs are those at which the enzymes presented their optimal activity. In a first experiment, solid **S1** (2.5 mg) was suspended in 25 mL of an aqueous solution (pH 8.3) containing pronase and the final suspension was stirred. The uncapping and subsequent delivery of the dye was easily detected by monitoring the safranine O emission band centered at 580 nm (excitation at 520 nm). As a control experiment, dye release was also measured using suspensions of **S1** under similar conditions, but in the absence of pronase. The difference in dye delivery in both experiments is displayed in Figure 6. Each point in the figure was determined using the above-described protocol, the suspension was filtered at a certain time and the emission of safranine O in the solution was measured. In the absence of the pronase enzyme, a flat baseline was found, indicating that the safranine O

cargo remained in the nanoparticles without release. In contrast, in the presence of pronase, delivery of safranine O was observed as increased dye fluorescence in terms of time (see Figure 6).

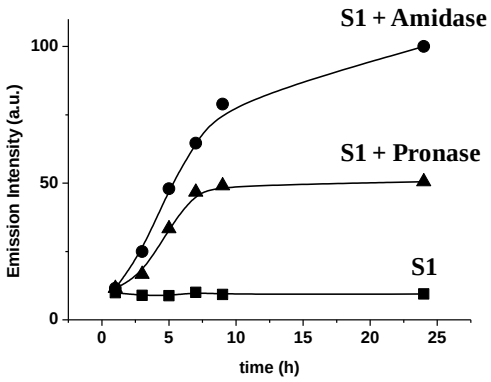


**Fig. 6** Release profiles in the absence and the presence of pronase from *Streptomyces griseus* and peptide amidase from *Citrus sinensis*. The release of Safranine O was monitored via the fluorescence emission band centred at 580 nm ($\lambda_{exc}$ = 520 nm).

The maximum delivery of safranine O dye from final material **S1** amounted to 0.28 % in weight was determined by suspending a certain amount of **S1** in water at pH 8.3 containing pronase and by allowing a complete dye delivery for at least 48 h. Under similar conditions, but in the absence of an enzyme, the maximum safranine O dye delivery from **S1** was less than 0.01% in weight. This enzyme-induced release was ascribed to the hydrolysis of the amide bond located in the anchored derivative, which resulted in both the reduced size of the appended groups and the destruction of the dense hydrogen bond network provided by the attached gluconamide.

In spite of the considerable size reduction upon the hydrolysis of the amide bond, the dye release was slow and a constant cargo delivery was observed by at least 10 h. This low delivery rate may be ascribed to the location of the amide bond, which was deep inside the thread and close to the inorganic scaffolding surface. This position of the hydrolysable group hampers fast hydrolysis in the presence of pronase or amidase, and suggests that it is possible to modulate the release kinetics by locating amide moieties in

different parts of the molecular threads.

Pronase is a mixture of proteinases that is able to induce the hydrolysis of the amide bond and the release of safranine O to the solution. In order to study the cargo delivery in more detail, some other enzymes were also tested. Figure 6 also displays the delivery profile found in the presence of amidase from *Citrus sinensis* at pH 7.5 using similar experimental conditions to those previously studied in the presence of pronase. Moreover at pH 7.5, and in the absence of an enzyme, a flat curve was found, thus confirming the selective rupture of the amidase bond only in the presence of enzyme. As observed in the figure, greater delivery in this case was obtained when compared with pronase, which is most probably due to the different active concentration of both enzymes. In a final experiment, the cargo delivery from **S1** was also tested in the presence enzyme esterase from porcine liver; as expected, no delivery was observed under these conditions. During another experiment, it was also verified that the safranine O cargo remained in the **S1** nanoparticles when the solid was in DMEM supplemented with 10% of FCS, which simulates typical cell culture conditions and indicates that no delivery was found using a medium with high salt concentrations.

It should be noted that we previously prepared mesoporous nanoparticles functionalized with gluconamide groups on the external surface. In our previous example, a significant cargo delivery was observed when nanoparticles were suspended in water in the absence of enzymes.[10b,13d] However, as previously explained, a "zero release" was found in this new prepared **S1** material. This different behavior can be explained by the different degree and type of gluconamide functionalization in these solids. Thus, whereas our previous material contained 0.07 g of the gluconamide derivative per g of $SiO_2$ (mainly anchored directly onto the silica surface), in **S1,** functionalization was larger and the final solid contained 0.81 g of gluconamide/g $SiO_2$ (combining direct functionalized groups and polymerized ones to form a relatively thick organosilane shell). It is apparent from these data that a simple control of the amount of capping molecule attached to nanoparticles allows the design of systems that either only tune the entrapped cargo delivery rate (our previously reported system) or show a remarkable inhibition of dye delivery (the system reported herein).

**Delivery of Gated Materials in Intracellular Media**

Having demonstrated the *in vitro* enzyme-controlled aperture of the gated material, cellular uptake of **S1** and cargo release experiments were carried out. Our main objective was to validate these nanoparticles as drug reservoirs for on command release once inside the cells. For these experiments, two different tumorigenic cell lines, HeLa and MCF-7, were used. Firstly, cell viability studies were done to rule out any toxic effect due to the nanoparticles themselves or to the nature of the molecular gate. Briefly, cells were treated with **S1** for 24 h before adding the WST-1 reagent. This yellow reagent can be reduced by metabolically active cells by mitochondrial enzymes to give a reduced orange soluble product. By measuring absorbance at 450 nm and the subsequent normalization of these measures at 690 nm, the innocuous effect of **S1** on cells was proved at the concentrations tested (see Figure 7). To complement this cell viability assay, confocal microscopy internalization studies were also carried out by taking advantage of Safranine O **S1**-associated fluorescence (see Figures 7A and 7B for further details). In the images obtained, cells were also stained with DNA-associated dye Hoechst 33342 and the plasma membrane marker wheat germ agglutinin Alexa Fluor 647. A dotted pattern associated with **S1** can be observed, which is comparable with that obtained by lysosomes staining, indicating that the possible internalization mechanism of the nanoparticle is endocytosis (Figures 7A and 7B).

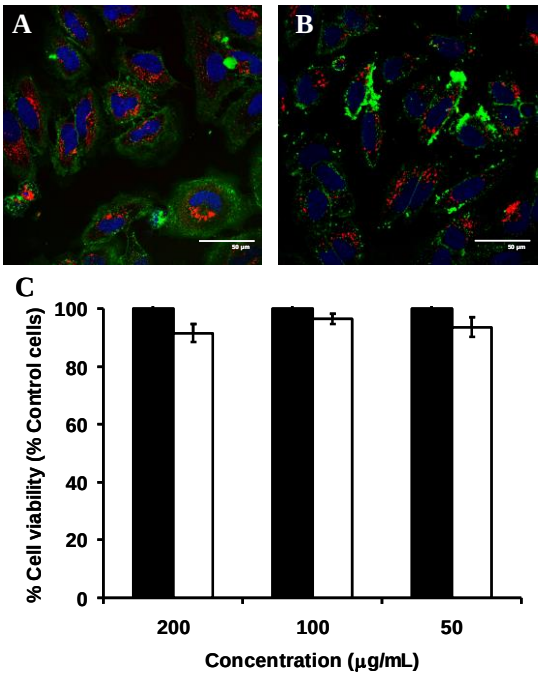


**Fig. 7** **S1** Cellular internalization and WST-1 cell viability assay. HeLa and MCF-7 cells were treated with **S1** at concentrations of 200, 100 and 50 µg/mL for 24 h. Then, the confocal microscopy studies of the **S1** cellular uptake in HeLa (A) and MCF-7 (B) at the 100 µg/mL concentration were performed by Safranine O-**S1-**associated fluorescence (red) in the presence of DNA marker Hoechst 33342 (blue) and plasma membrane marker WGA Alexa Fluor 647 (green). For the cell viability studies, (C) HeLa (black bars) and MCF-7 (white bars) cells were incubated for 24 h with **S1** at the concentrations stated before, while cell viability was quantified by employing the WST-1 reagent. Two independent experiments were performed and the data are represented as (mean ± SE).

Having tested the biocompatibility of the **S1** solid, a new nanoparticulated material containing the chemotherapeutic agent camptothecin (CPT) was synthesized (**S1-CPT**). As stated above, **S1-CPT** was prepared by following a similar procedure to that followed for **S1,** which consists in mesoporous nanoparticles loaded with CPT and capped with the gluconamide derivative. CPT is a quinoline alkaloid employed in the treatment of different cancer types given its ability to inhibit DNA polymerase I, thus disrupting DNA replication processes and inducing cell death. However, its low solubility prevents its application in patients.[18] In this case, HeLa cells were employed to demonstrate the possible cellular

internalization of **S1-CPT,** the possible release of the cargo molecule after lysosomal localization and the subsequent uncapping by lysosomal enzymes. Therefore, cells were treated with these new nanoparticles for 48 h at different concentrations before performing the confocal microscopy and flow cytometry analyses. The confocal microscopy results obtained are shown in Figure 8. The cytotoxic effect of **S1-CPT** is clearly noted when compared to MCM-41-treated cells. CPT release induced cell death and detached cells showing membrane blebbing are observed (Figure 8).

For the flow cytometry studies, quantification of CPT-associated cell death was performed by using propidium iodide (PI) and Annexin V (Ann V) markers, which stain dead cells and cells undergoing cell death, respectively. After 48 h of treatment, the **S1-CPT**-treated cells presented an increment in dead cells (ca. 20%) and cells undergoing cell death when compared to the MCM-41-treated cells. This fact proves the release of the cargo molecule inside the cell, this confirming the possible use of **S1** as a drug-carrier of CPT. The main reason behind the relatively low percentage of cell death after 48 h of treatment was most likely due to the relatively low loading of CPT into the mesopores. According to the thermogravimetric and elemental analysis the **S1-CPT** solid contains 0.27 mmoles CPT per gram of $SiO_2$ (vide ante). This is a lower value to that found in some other capped mesoporous supports containing CPT (for instance 0.43 mmol of CPT / g $SiO_2$ were determined in reference 13h) which resulted in a lower percentage of cell death.[13h]

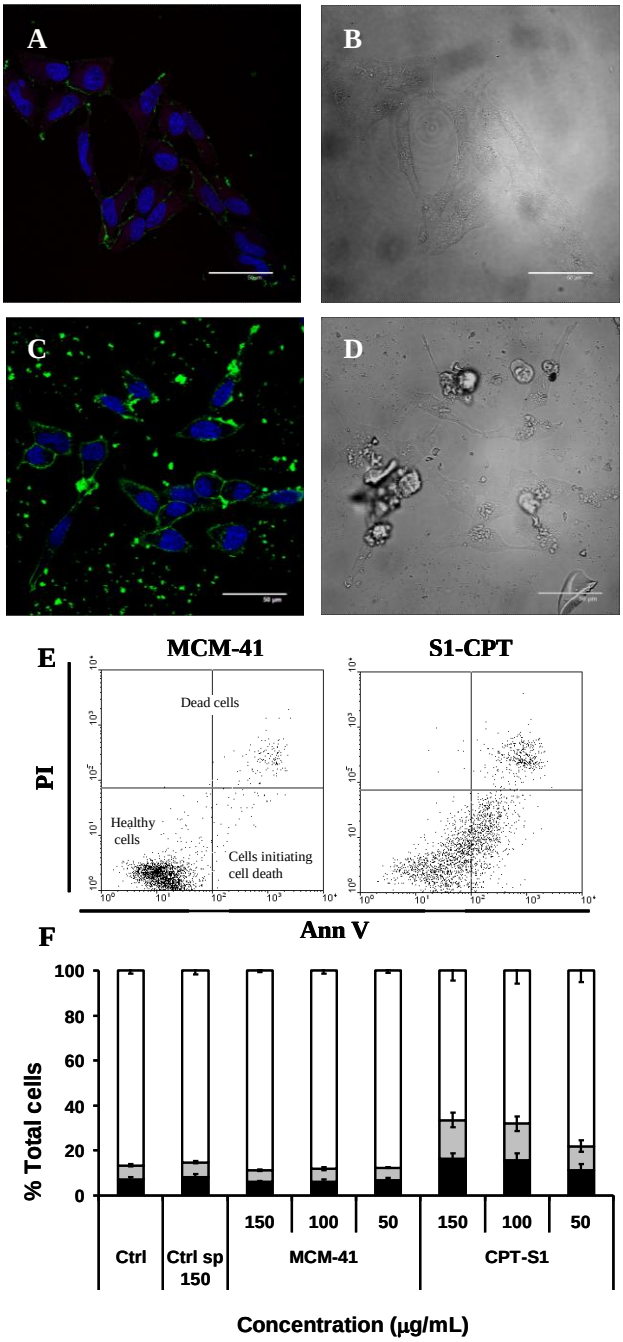


**Fig. 8 S1-CPT** cell internalization induces cell death. HeLa cells were treated with control MCM-41 (A, B) or **S1-CPT** (C, D) at 150 μg/mL, and cells were further incubated for 48 h. MCM-41-treated cells presented normal morphology and remained attached to the plate (A) in the confocal microscopy analysis (B), in which the plasma membrane was stained with WGA Alexa Fluor 647 (green). In contrast, **S1-CPT**-treated cells presented a phenotype associated with cell death (C) and a cell diffuse

pattern of CPT-associated fluorescence (blue) due to CPT release and subsequent cell death induction. Quantification of cell viability and cell death (E, F) was performed by flow cytometry by means of PI and Ann V stainings, respectively. The percentage of dead cells (black), cells undergoing cell death (gray) and healthy cells (white) are shown after 48 h of treatment. Three independent experiments containing triplicates were performed and the data are reported as (mean ± SE).

Finally, in order to test that CPT release in cells was a consequence of the enzymatic hydrolysis of the gate, controlled release experiences with **S1-CPT** in a hydrophobic solvent (DMSO) were carried out. These experiences, developed in the absence of enzyme, showed that after 24 hours the amount of CPT release was negligible.

**CONCLUSIONS**

The efficiency of a new gated material to deliver its cargo in a controlled manner in the presence of certain enzymes has been proved. In this work, a new "zero-release" system based on the gated nanomaterial **S1** has been prepared. This hybrid solid was composed of a nanoparticulated mesoporous scaffolding whose pores were loaded with safranine O dye and whose outer surface was covered with a gluconamide derivative. In the presence of pronase and amidase enzymes, the amide linkage in the gluconamide threads was hydrolyzed with the subsequent safranine O release. This study demonstrates that it is possible to use relatively simple molecules containing enzyme-hydrolyzable groups to design capped materials that can be opened at will. The present work also proves that gluconamide-functionalized nanoparticles are efficiently taken up by tumoral cells. The cellular uptake of nanoparticles probably occurs via endocytosis by targeting them to autolysosomes, where the molecular gate is degraded by lysosomal enzymes and the cargo is released. Finally, the possible application of gluconamide-functionalized nanoparticles as suitable delivery systems in the cells of chemotherapeutic agents, such as CPT, has been demonstrated, and a significant reduction of cell viability has been observed in the cells treated with solid **S1-CPT**.

**ACKNOWLEDGEMENTS**

We thank the Spanish Government (Project MAT2009-14564-C04 and SAF2010-15512) and the Generalitat Valenciana (Project PROMETEO/2009/016and /2010/005) for support. I. C. thanks the Universitat Politècnica de València for her fellowship. We thank the Confocal Microscopy service of CIPF and the Electronic Microscopy service of UPV for their technical support.

**EXPERIMENTAL SECTION**

**Synthesis. General Methods**

XRD, TGA, elemental analysis, TEM, $^{29}$Si-NMR and $N_2$ adsorption-desorption techniques were employed to characterize synthesized materials. Powder X-ray measurements were taken in a Philips D8 Advance diffractometer using Cu Kα radiation. Thermogravimetric analyses were carried out on a TGA/SDTA 851e Mettler Toledo balance using an oxidant atmosphere (air, 80 mL/min) with a heating program consisting of a heating ramp of 10 °C per minute from 393 to 1273 K and an isothermal heating step at this temperature for 30 min. TEM images were obtained with a 100 kV Philips CM10 microscope. Dynamic Light Scattering (DLS) studies were conducted at 25 °C using a Malvern Zetasizer Nano ZS equipped with a 4 mW He-Ne solid-state laser operating at 633 nm. Back-scattered light was detected at 173°, and the mean particle diameter was calculated from the quadratic fitting of the correlation function over 12 runs of 10 s duration. All measurements were performed in triplicate on previously sonicated highly dilute aqueous dispersions. $N_2$ adsorption-desorption isotherms were recorded with a Micromeritics ASAP2010 automated sorption analyzer. Samples were degassed at 70 °C in vacuum overnight. Specific surface areas were calculated from the adsorption data in the low pressure range using the BET model. Pore size was determined following the BJH method. $^{29}$Si MAS NMR spectra were recorded using a BrukerAvance 3 instrument 400 MHz operating at 400 MHz and a magic angle spinning speed of 10.0 kHz. Fluorescence spectroscopy was carried out with a Felix 32 Analysis, version 1.2 (Build 56) PTI

(Photon Technology International). Live cellular internalization studies were performed with a Cytomics FC 500 (Beckman Coulter Inc.) and a confocal Leica microscope was handled with a TCS SP2 system equipped with an acoustic optical beam splitter (AOBS). Cell viability measurements were carried out with a Wallac 1420 workstation.

**Chemicals**

Chemicals tetraethylorthosilicate (TEOS), *n*-cetyltrimethylammonium bromide (CTABr), sodium hydroxide (NaOH), safranine O, pronase from *Streptomyces griseus*, peptide amidase from *Citrus sinensis* and esterase from porcine lpiver were provided by Aldrich. *N*-(3-triethoxysilylpropyl)gluconamide was supplied by Fluorochem. Camptothecin was provided by Sequoia Research Products. D-MEM with L-glutamine, fetal calf serum (FCS), trypan blue solution (0.4%), cell culture grade, trypsin, wheat germ agglutinin (WGA) Alexa Fluor 647, and Hoechst 33342 were acquired from Gibco-Invitrogen. The cell proliferation reagent WST-1 was obtained from Roche Applied Science. Annexin V-FITC (AnnV) was supplied by Immunostep and propidium iodide (PI) came from BD Dickinson. All the products were used as received.

**Synthesis of the Mesoporous MCM-41 Nanoparticles**

The MCM-41 mesoporous nanoparticles were synthesized by the following procedure: *n*-cetyltrimethylammoniumbromide (CTABr, 1.00 g, 2.74 mmol) was first dissolved in 480 mL of deionized water. NaOH (aq) (2.00 M, 3.5 mL) was added to the CTABr solution after adjusting the solution temperature to 80°C. TEOS (5 mL, $2.57 \cdot 10^{-2}$ mol) was then added dropwise to the surfactant solution. The mixture was allowed to stir for 2 h to give a white precipitate. The solid product was centrifuged, and was washed with deionized water and ethanol. Finally, the solid was dried at 60°C (MCM-41 as-synthesized). To prepare the final porous material (MCM-41), the as-synthesized solid was calcined at 550°C using an oxidant atmosphere for 5 h to remove the template phase.

**Synthesis of S1**

In a typical synthesis, 0.340 g of templated-free MCM-41 and safranine O dye (0.036 g, 0.1mmol) were suspended in 90 mL of acetonitrile in a round-bottomed flask. To remove the adsorbed water, 10 mL of acetonitrile were distilled in a Dean-Stark set-up. After stirring 24 h at room temperature, an excess of the alkoxysilane derivative *N*-(3-triethoxysilylpropyl)gluconamide (50% ethanol) (2.86 mL, 3.4 mmol) was added and the final mixture was stirred for 24 h at room temperature. Finally, solid **S1** was filtered off, washed with 800 mL of acetonitrile (200mL four times) and dried at 38°C overnight.

**Synthesis of S1-CPT**

In a typical synthesis, 0.100 g of templated-free MCM-41 and the a solution of the corresponding amount of camptothecin (56 mg, 0.16 mmol / 5mL ethanol) were suspended in 20 mL of anhydrous acetonitrile. After stirring for 24 h, the corresponding amount of *N*-(3-triethoxysilylpropyl)gluconamide (50% Ethanol) was added (0.974 mL, 1.15 mmol) and the mixture was stirred for 24 h at room temperature. Finally, solid **S1-CPT** was filtered. In order to eliminate the non reacted reagents, a suspension of **S1-CPT** in 200 mL of a chloroform-methanol mixture 3:4 (v/v) was stirred overnight. After filtering the solid, it was dried at vacuum for 1 h and kept in inert atmosphere.

**Dye release studies**

In a typical experiment, 2.5 mg of **S1** were suspended on 25 mL of water. pH must be previously adjusted to optimum enzyme conditions (pH=7.5 for amidase from *Citrus sinensis*, pH=8.3 for pronase from *Streptomyces griseus*). Then 50 µL of peptide amidase from *Citrus sinensis* were added, whereas to evaluate the Pronase and Esterase effects, 3 mg of **S1** were suspended on 25 mL of a solution of pronase from *Streptomyces griseus* or esterase from porcine liver, respectively (0.12 mg/mL). These suspensions were used to evaluate the gate-like effect by studying the dye release from the pore voids of the functionalized material. The delivery of safranine O dye from the pore voids to the solution was easily monitored by the fluorescent emission band of the dye centered at 580 nm (excitation at 520 nm).

**Cell Culture Conditions**

The HeLa human cervix adenocarcinoma and the MCF-7 human breast adenocarcinoma were purchased from the German Resource Centre for Biological Materials (DSMZ) and were grown in D-MEM and Medium 199 supplemented with 10% of FCS. Cells were maintained at 37°C in an atmosphere of 5% carbon dioxide and 95% air, and they underwent passage twice a week.

**WST-1 Cell Viability Assay**

Cells were cultured in sterile 96-well microtiter plates at a seeding density of $2.5x10^3$ and $3x10^3$ cells/well for HeLa and MCF-7, respectively, and they were allowed to settle for 24 h. **S1** in DMSO was added to cells at the final concentrations of 200, 100 and 50 μg/mL. After 23 h, WST-1 (7 μL of a 5 mg/mL solution) was added to each well. Cells were further incubated for 1 h (a total of 24 h of incubation was therefore studied), and absorbance was measured at 450 nm and normalized versus absorbance at 690 nm in a Wallac 1420 workstation.

**Live Confocal Microscopy S1 Cellular Internalization**

HeLa and MCF-7 cells were seeded in 24 mm ϕ glass coverslips in 6-well plates at a seeding density of $5{\cdot}10^4$ cells/well. After 24 h, cells were treated when indicated with **S1** or **S1-CPT** at a final concentration of 150 μg/mL. After 24 h of incubation, cells were stained with 10 ng/mL of Hoechst 33342 and 5 mg/mL WGA Alexa Fluor 647 for 30 min in PBS containing 10% FCS or by keeping the medium for the **S1-DOX** treatments. Slides were visualized under a confocal microscope. Two independent experiments were done and contained triplicates with similar results.

**Cytofluorometry Studies Employing S1**

To carry out the cytofluorometry studies, HeLa cells were seeded at $5x10^4$ cells/well in a 12-well plate. After 24 h, cells were treated with **S1-CPT** at the following concentrations for 48 h: 150, 100 and 50 μg/mL. Then, cells were stained with PI and Ann V according to the manufacturer's protocol (BD

Pharmingen). Quantification of PI-positive and AnnV-positive staining was done by the WinMDI program, version 2.9. Three independent experiments were done and contained triplicates with analogous results.

## NOTES AND REFERENCES


1 (a) G. A. Ozin, *Adv. Mater*., 1992, **4**, 612. (b) E. Katz, I. Willner, *Angew. Chem. Int. Ed*., 2004, **43**, 6042.

2 *The supramolecular chemistry of organic-inorganic hybrid materials*, (R. Martínez-Máñez, K. Rurack Ed.), 2010, J. Wiley & Sons, Hoboken.

3 A. B. Descalzo, R. Martínez-Máñez, F. Sancenón, K. Hoffmann, K. Rurack, *Angew. Chem. Int. Ed.*, 2006, **46**, 5924.

4 N. K.. Mal, M. Fujiwara, Y. Tanaka, *Nature* 2003, **421**, 350.

5 (a) E.Aznar, R. Martínez-Máñez, F. Sancenón,*Expert Opin. Drug Deliv.*2009, **6**, 643. b) K. Cotí, M. E. Belowich, M. Liong, M. W. Ambrogio, Y. A. Lau, H. A. Khatib, J. I. Zink, N. M. Khashab, J. F. Stoddart, *Nanoscale*, 2009, **1**, 16.

6 (a) R. Casasús, M.D. Marcos, R. Martínez-Máñez, J.V. Ros-Lis, J. Soto, L.A. Villaescusa, P. Amorós, D. Beltrán, C. Guillem, J. Latorre, *J. Am. Chem. Soc.* 2004, **126**, 8612. (b) Q.Yang, S.Wang,P.Fan, L.Wang, Y.Di, K.Lin, F.-S.Xiao, *Chem. Mater.* 2005, **17**, 5999. (c)T. D. Nguyen, K.C.-F. Leung, M.Liong, C. D.Pentecost,J. F.Stoddart,J. I. Zink,. *Org. Lett.*2006, **8**, 3363. (d) C.Park, K.Oh, S. C.Lee, C.Kim, *Angew. Chem., Int. Ed.* 2007, **46**, 1455. (e) R. Casasús, E. Climent, M.D. Marcos, R. Martínez-Máñez, F. Sancenón, J. Soto, P. Amorós,J. Cano, E. Ruiz,*J. Am. Chem. Soc.*2008, **130**, 1903. (f) N.Knežević, B.G. Trewyn, V.-Y. Lin, *Chem. Eur. J.*2011, **17**, 3338. (g) R.Liu, P.Liao, J.Liu, P.Feng, *Langmuir*2011, **27**, 3095. (h) F.Muhammad, M. Guo, W.Qi, F.Sun, A.Wang, Y.Guo, G.Zhu, *J. Am. Chem.Soc.*2011, **133**, 8778. (i) A.Schlossbauer, C.Dohmen, D.Schaffert, E.Wagner, T.Bein, *Angew. Chem., Int. Ed.* 2011, **50**, 6828. (j) K.Zhou, Y.Wang, X.Huang, K.Luby-Phelps, B.D.Sumer, J.Gao, *Angew. Chem., Int. Ed.* 2011, **50**, 6109.

7 (a) Q. Fu,G. V. R.Rao, L. K.Ista, Y. Wu, B. P.Andrzejewski,L. A.Sklar, T. L.Ward,G. P. López, *Adv. Mater.* 2003, **15**, 1262.(b)C.R. Thomas, D.P. Ferris, J.-H. Lee, E. Choi, M.H. Cho, E.S. Kim, J.F. Stoddart, J.-S. Shin, J. Cheon, J.I. Zink, *J. Am. Chem. Soc.*2010, **132**, 10623. (c) E. Ruiz-Hernández, A. Baeza, M. Vallet-Regí, *ACSNano* 2011, **5**, 1259. (d) E. Aznar, L. Mondragón, J.V. Ros-Lis, F. Sancenón, M.D. Marcos, R. Martínez-Máñez, J. Soto, E. Pérez-Payá, P. Amorós, *Angew. Chem. Int. Ed.*2011, **50**, 11172. (e) A. Baeza,E. Guisasola, E. Ruiz-Hernández, M. Vallet-Regí, *Chem. Mater.* 2012, **24**, 517.(f) J. Croissant, J. I. Zink, *J. Am. Chem. Soc.* 2012, **134**, 7628.

8 (a)C.-Y. Lai, B. G.Trewyn, D. M. Jeftinija, K.Jeftinija, S.Xu, S.Jeftinija, V.S.-Y.Lin, *J. Am.Chem. Soc.* 2003, **125**, 4451. (b) R. Hernandez, H.-R. Tseng, J. W. Wong, J. F.Stoddart, J. I. Zink, *J. Am. Chem. Soc.*2004, **126**, 3370. (c) Y.Zhao, B. G.Trewyn, I. I.Slowing,V.S.-Y. Lin, *J. Am. Chem. Soc.* 2009, **131**, 8398. (d) M. Fujiwara, S. Terashima, Y. Endo, K. Shiokawa, H. Ohue, *Chem. Commun.* 2006, 4635.(e) B. G.Trewyn, S. Giri, I. I.Slowing,V. S.-Y. Lin, *Chem.Commun.* 2007, 3236. (f) R. Liu, Y. Zhang, P.Feng,

*J. Am. Chem. Soc.* 2009, **131**, 15128. (g) F. Porta, G.E.M. Lamers, J.I. Zink, A.Kros, *J. Phys. Chem. C* 2011, **13**, 9982. (h) Z. Luo, K. Cai, Y. Hu, L. Zhao, P. Liu, L.Duan, W.Yang, *Angew. Chem., Int. Ed.* 2011, **50**, 640.

9 (a) E. Aznar, R. Casasús, B. García-Acosta, M. D. Marcos, R. Martínez-Máñez, F. Sancenón, J. Soto, P. Amorós, *Adv. Mater.* 2007, **19**, 2228. (b) N. G. Liu, Z.Chen, D. R. Dunphy, Y. –B.Jiang, R. A.Assink,C. J. Brinker, *Angew. Chem. Int. Ed.* 2003, **42**, 1731. (c) J. Lu, E. Choi, F. Tamanoi, J. I. Zink, *Small*2008, **4**, 421. (d) E. Aznar, M.D. Marcos, R. Martínez-Máñez, F. Sancenón, J. Soto, P. Amorós, C. Guillem,*J. Am. Chem. Soc.* 2009, **131**, 6833. (e) X. Yang, X. Liu , Z. Liu , F. Pu , J. Ren , X. Qu, *Adv. Mater.*2012, **24**, 2890.

10 (a) C. Coll, R. Casasús, E. Aznar, M. D. Marcos, R. Martínez-Máñez, F. Sancenón, J. Soto, P. Amorós, *Chem. Commun.* 2007, 1957; (b) E. Aznar, C. Coll, M. D. Marcos, R. Martínez-Máñez, F. Sancenón, J. Soto, P. Amorós, J. Cano, E. Ruiz, *Chem.Eur. J.* 2009, **15**, 6877. (c) E. Climent, M. D. Marcos, R. Martínez-Máñez, F. Sancenón, J. Soto, K. Rurack, P. Amorós, *Angew. Chem., Int. Ed.* 2009, **48**, 8519. (d) I. Candel, A. Bernardos,E. Climent, M. D. Marcos, R. Martínez-Máñez, F. Sancenón, J. Soto, A. Costero, S. Gil, M. Parra, M. *Chem. Commun.* 2011, **47**, 8313. (e) J.Lee, J. Lee, S.Kim, C.-J. Kim, S.Lee, B.Min, Y. Shin, C.Kim, *Bull. Korean Chem. Soc.* 2011, **32**, 1357.

11 See for example: (a) H.Tanga, J.Guoa, Y.Sunb,B. Changa,Q. Renb, W.Yang, *International Journal of Pharmaceutics* 2011, **421**, 388.(b) N. Singh, A. Karambelkar, L. Gu, K. Lin, J.S. Miller, C.S. Chen, M.J. Sailor, S.N. Bhatia, *J. Am. Chem. Soc.*, 2011, **133**, 19582. (c) Q. He, J. Shi, *J. Mater. Chem.*, 2011, **21**, 5845.

12 (a) E. Climent, A. Bernardos, R. Martínez-Máñez, A. Maquieira, M. D. Marcos, N. Pastor-Navarro, R. Puchades, F. Sancenón, J. Soto, P. Amorós, *J. Am. Chem. Soc.*2009, **131**, 14075.(b) E. Climent, R. Martínez-Máñez, F. Sancenón, M. D. Marcos, J. Soto, A. Maquieira, P. Amorós, *Angew. Chem., Int. Ed.* 2010, **49**, 7281. (c) C.-L. Zhu, C.-H. Lu, X.-Y. Song, H.-H.Yang, X.-R. Wang, *J. Am. Chem. Soc.* 2011, **133**, 1278. (d) C. Chen, J. Geng, F. Pu, X. Yang, J. Ren,X. Qu, *Angew. Chem. Int. Ed.* 2011, **50**, 882. (e) Y.L. Choi,J.H. Lee, J. Jaworski, J.H. Jung, *J. Mater. Chem.*, 2012, **22**, 9455.

13 (a) K. Patel, S. Angelos, W. R.Dichtel, A. Coskun, Y.-W. Yang, J. I.Zink, J. F.Stoddart, *J. Am. Chem. Soc.* 2008, **130**, 2382. (b) A.Schlossbauer, J.Kecht, J. Bein, *Angew. Chem., Int. Ed.* 2009, **48**, 3092. (c) C. Park, H. Kim, S. Kim, C. Kim, *J. Am. Chem. Soc.* 2009, **131**, 16614. (d) A. Bernardos, L. Mondragón, E. Aznar, M. D. Marcos, R. Martínez-Máñez, F. Sancenón, J. Soto, J. M. Barat, E. Pérez-Payá, C. Guillem, P. Amorós, *ACSNano* 2010, **4**, 6353. (e) P. D. Thornton, A. Heise; *J. Am. Chem. Soc.* 2010, **132**, 2024. (f) C. Coll, L. Mondragón, R. Martínez-Máñez, F. Sancenón, M. D. Marcos, J. Soto, P. Amorós, E. Pérez-Payá, *Angew. Chem., Int. Ed.*2011, **50**, 2138. (g) J. Liu, X. Du, X. Zhang, *Chem.-Eur. J.* 2011, **17**, 810. (h) A. Agostini, L. Mondragón, C. Coll, E. Aznar, M.D. Marcos, R. Martínez-Máñez, F. Sancenón, J. Soto, E. Pérez-Payá, P.Amorós, *ChemistryOpen*, 2012, **1**, 17.

14 (a) A. Bernardos, E. Aznar, C. Coll, R. Martínez-Máñez, J. M. Barat, M. D. Marcos, F. Sancenón, A. Benito, J. Soto,*Journal of Controlled Release* 2008**, 131**, 181; (b) S-H. Cheng, W-N Liao, L-M Chen, C-H. Lee, *J. Mater. Chem.*, 2011, **21**, 7130. (c) Y. Zhu, J. Shi, W. Shen, X. Dong, J. Feng, M.

Ruan, Y. Li, *Angew. Chem. Int. Ed.* 2005, **44**, 5083. (d) Y. -F. Zhu, J. -L. Shi, Y. -S. Li, H. –R. Cheng, W. -H. Shen, X. –P. Dong, *Micropor. Mesopor. Mater.* 2005, **85**, 75.

15 (a) S-H. Wu,Y. Hung, C-Y. Mou, *Chem Commun*2011, **47**, 9972. (b) Y.-W. Yang, *Med. Chem. Commun.*, 2011, **2**, 1033. (c) P. Yang ,S. Gai, J. Lin, *Chem. Soc. Rev.*, 2012,**41**, 3679.

16 (a) S. Cabrera, J.El Haskouri, J. Guillem, J. Latorre, A. Beltrán, D. Beltrán, M. D. Marcos, P. Amorós, *Solid State Sci*. 2000, **2**, 405. (b) D.R. Radu, C-Y.Lai, K.Jeftinija, E.W. Rowe, S.Jeftinija, V.S.Y Lin, *J. Am. Chem. Soc.*2004, **126**, 13216.

17 N. Gartmann,D.Brühwiler, *Angew. Chem., Int. Ed.***2009**, *48*, 6354.

18 (a) Y. Pommier, *Chem. Rev.*, 2009, **109**, 2894. (b) Q. –Y. Li, Y. –G. Zu, R. –Z. Shi, L. –P. Yao, *Curr. Med. Chem.*, 2006, **13**, 2021.

# 5. CONCLUSIONS.

The development of functional hybrid organic-inorganic materials is a relatively young field of research and has gained great interest in the last years, among others, in areas such as controlled release and sensing of chemical species. The present PhD thesis is intended to contribute to the expansion of these branches of research.

In the general introduction, the principles, perspectives and recent developments in supramolecular chemistry were described. On the other hand, the synthesis, functionalization and applications of mesoporous materials were also reported. The concept of molecular gated systems was developed and examples of their behaviour in the presence of target external stimuli as some of their applications were shown.

In the first chapter, organic-inorganic hybrid materials acting as probes were developed. In this case silica nanoparticles were functionalised with two different molecules, i.e. a binding site able to interact with anions and a signalling unit (a fluorophore). These molecules were anchored on the silica support in such a way that the interaction between the anions and the binding unit induced some change on the emission properties of the signalling unit. Following this concept two solids were developed, in both cases the signalling unit was rhodamine B whereas an imidazolium group or a guanidinium derivative were used as binding units. In both cases a modulation of the fluorescent emission was found in the presence of certain anions. Nanoparticles functionalized with imidazolium were specifically responsive to iodide and benzoate whereas the material functionalized with guanidinium moieties was able to selectively respond to hydrogen sulfate. Moreover the guanidinium functionalised nanoparticles aggregated in the presence of dihydrogenphophate anions.

In the second chapter, organic-inorganic hybrid materials were used for sensing and removal of nerve gases simulants. The first part of this chapter dealt with the application of a gated material for signalling the presence of nerve gases mimics. A mesoporous silica material (MCM-41) was used as inorganic scaffold. The pores

were loaded with a dye which acted as an indicator of the process whereas the external surface was functionalized with HET (3-[Bis(2-hydroxyethyl)amino]propyltriethoxysilane) able to interact with nerve agents. The presence of the neurotoxic agents mimics in acetonitrile suspensions of the hybrid material induced pore opening and therefore dye release that can be noticed to the naked eye. In the second part of this chapter silica mesoporous materials were used to enhance the hydrolysis of nerve agent simulants via the formation of silanol groups on the materials by a basic treatment. It was proven that mesoporous materials by themselves were not able to accelerate the degradation of these compounds, however, in the presence of certain bases an enhancement of the degradation of the DCNP (diethyl cyanophosphonate) simulant was observed. Particularly, mesoporous nanoparticles-$K_2CO_3$/DABCO/$Et_3N$ mixtures were studied and it was found that in the presence of $K_2CO_3$ or DABCO a hydrolysis of 95 % and 90 % of DCNP was achieved respectively in a lapse of time of 60 min. On the contrary, in the presence of $Et_3N$ the hydrolysis of DCNP was much lower (ca. 30 %) in the same period of time. Moreover the solid MSN-1 (prepared by treating mesoporous nanoparticles with $K_2CO_3$) was found to act similarly to the mixture mesoporous nanoparticles-$K_2CO_3$ whereas MSN-2 (prepared by treating mesoporous nanoparticles with DABCO) was found to have a much lower hydrolytic ability. Finally, based on kinetic studies, a catalytic mechanism was proposed. This consisted of three steps dealing with the water assisted addition of DCNP to the silanolate moieties that gave an active intermediate phosphate species anchored to the silica surface that allowed the final formation of diethyl phosphoric acid or formation of tetraethylpyrophosphate via reaction with another DCNP molecule.

Finally, in the third and last chapter, organic-inorganic hybrid materials were used for an application which has gained an increasing interest in the latest years: controlled release. A “zero release” material was developed based on a molecular gated system. In this case, the pores of the mesoporous material were loaded with safranine O dye and the external surface was functionalized with a gluconamide derivative. In a suspension of this material in the presence of suitable enzymes (pronase and amidase) the amide bonds were cleaved inducing

the release of the dye. This system was also applied for delivering the anticancer drug camptothecin in intracellular media.